Geometric Control of Quantum Mechanical and Nonlinear Classical Systems

by

Richard Joseph Nelson

B.S., Brigham Young University, 1992
S.M.M.E., Massachusetts Institute of Technology, 1995

Submitted to the Mechanical Engineering Department
in partial fulfillment of the requirements for the degree of

Doctor of Philosophy in Mechanical Engineering

at the

MASSACHUSETTS INSTITUTE OF TECHNOLOGY

September 1999

Author .....
Mechanical Engineering Department
June 14, 1999

Certified by .....
Seth Lloyd
Associate Professor of Mechanical Engineering
Thesis Supervisor

Accepted by .....
Ain A. Sonin
Chairman, Committee on Graduate Students

Geometric Control of Quantum Mechanical and Nonlinear Classical Systems

by

Richard Joseph Nelson

Submitted to the Mechanical Engineering Department
on June 14, 1999, in partial fulfillment of the
requirements for the degree of
Doctor of Philosophy in Mechanical Engineering

Abstract

Geometric control refers to the judicious use of the non-commuting nature of inputs and natural dynamics as the basis for control. The last few decades in control system theory have seen the application of differential geometry in proving several important properties of systems, including controllability and observability. Until recently, however, the results of this mathematical geometry have rarely been used as the basis for designing and implementing an actual controller. This thesis demonstrates the application of a judicious selection of inputs, so that if the system is proven to be controllable using geometric methods, one can design input sequences using the same geometry. A demonstration of this method is shown in simulating the attitude control of a satellite: a highly non-linear, non-holonomic control problem. Although not a practical method for large re-orientations of a typical satellite, the approach can be applied to other nonlinear systems.

The method is also applied to the closed-loop performance of a quantum mechanical system to demonstrate the feasibility of coherent quantum feedback—something impossible using a conventional controller. Finally, the method is applied in the open-loop control of a quantum mechanical system: in this case, the creation of Greenberger-Horne-Zeilinger correlations among the nuclei of an ensemble of alanine molecules in a nuclear magnetic resonance spectrometer. In each case, the data demonstrate the usefulness of a geometric approach to control. In addition to demonstrations of geometric control in practice, the quantum mechanical experiments also demonstrate for the first time peculiar quantum correlations, including GHZ correlations, that have no classical analog. The quantum experiments further establish nuclear magnetic resonance as a viable and accessible testbed of quantum predictions and processes.

Thesis Supervisor: Seth Lloyd
Title: Associate Professor of Mechanical Engineering

Acknowledgments

To write a dissertation is a difficult thing, and I could not have done it alone. Superlative credit goes to my thesis advisor, Professor Seth Lloyd, whose rare coupling of vast scientific understanding and unpretentious nature ensured that my research was a validating experience. Equally priceless was the assistance of Professor David Cory, whose trustworthy mentoring extended well beyond the potential pitfalls of NMR spectroscopy to professional and collegial development. For challenging my methods and madness I also owe Professor Jean-Jacques Slotine a debt of gratitude.

In addition, I have received from time to time sound and wise scientific guidance from countless sources; unfortunately space-time considerations allow only abbreviated annotations at best, and a token of blanket appreciation otherwise. I esteem as considerable the aid proffered by Dr. Tim Havel, Dr. Yehuda Sharf, Dr. Shyamal Somaroo, and Dr. Lorenza Viola, who have greatly contributed to my understanding. The unique insights of my friends Michael Quintana, Sean Warnick, and David Robinson have at times caused me great reflection—sometimes scientifically—for which I am greatful. Sincere thanks also goes to Dr. Ching-Hua Tseng, Mark Price, Grum Teklemariam, Yaakov Weinstein, Evan Fortunato, Marco Pravia, and other associates who work in Prof. Cory's laboratory at the Massachusetts Institute of Technology. I also express my appreciation to the myriad of wonderful leaders, friends, and acquaintances who saw me through my graduate days at MIT.

Finally, no words exist to express my deepest thankfulness to my family. Every brother and sister has encouraged me, including the families of my wife's siblings (Gordon and Katherine, Greg and Miriam, Andrea, and Benjamin) as well as my own (Kevin and Angela, Clint and Ginger, Scott and Trina, and Darcy). The faith and trust of my in-laws Dr. Boyd Bauer and Alice Bauer, and the constant encouragement of Dr. Edith Bauer cannot be overlooked. Of supreme importance in my life has been the perpetual attention of my parents, Richard E. Nelson and Bonnie Jo M. Nelson, whose undying faith in my abilities and concern for my welfare have engendered in me a quest for excellence and a desire for eternal propinquity. Finally, the selfless love and unending support of my wonderful wife Elizabeth are immeasurable; to her and my two beautiful daughters, Melanie Jane and Rebecca Joelle, I dedicate this thesis.

Contents

List of Figures

List of Tables

Chapter 1

Introduction

1.1 Overview

All control methods use actuators as inputs that augment the natural dynamics of the system to be controlled. The direct application of an actuator (in the presence of the natural dynamics of the system to be controlled) provides a "push" along a certain direction, or degree of freedom, in the configuration space of the system. For controllability at a point in configuration space, one must be able to "push" in all directions at that point. However, it is not always necessary to have the same number of independent actuators as there are degrees of freedom: if the application of two different inputs does not commute, then it is possible to "push" in a third direction. *Geometric control* refers to control systems that take advantage of, or at least address, the inherent geometry in a system's dynamics through the judicious use of the non-commuting nature of inputs and natural dynamics.

The origins of geometric control are found in the mathematical application of differential geometry, especially the application of Lie groups and Lie algebras to nonlinear control theory, including the works of such notable mathematicians and theoreticians as W. Chow [1], K. Chen [2], R. Brockett [3], A. Bloch [4], H. Hermes [5], H. Sussmann [6], and V. Jurdjevic [7]. The result of such applications has been a set of theorems whose aim is to characterize the accessibility [8] and controllability [9, 10] of a nonlinear control system, especially in the ubiquitous fields of robotic control, non-holonomic motion planning, and, in general, nonlinear control problems (see, for example, [11-13]). In all these cases, establishing the *a priori* controllability of the nonlinear classical control system using these differential geometric methods has become standard practice before the task of finding and

implementing an actual control strategy.

Quantum control refers to the theory and application of control to systems whose dynamics obey the laws of quantum physics. Formal quantum control principles have been established over the last two decades [14-20], accompanied by experiments using atoms, solid state systems, and lasers. In general, open quantum systems (quantum systems that interact with a large or even infinite degree-of-freedom environment) have nonlinear dynamics. Even for closed quantum systems that obey a linear evolutionary state equation (the Schrödinger equation), the problems of measurement and implementation preclude the possibility of wholesale adoption of linear control theory directly to the quantum control problem. In any case, for most problems of practical interest, the number of actuators available is much smaller than the number of degrees of freedom in the quantum system to be controlled, thus necessitating the use of geometric methods.

The contributions of this thesis address the application of control to quantum mechanical and classical nonlinear systems using the results of geometric control theory as a framework. The rest of this chapter introduces the concept of geometric effects in linear systems (specifically, a closed quantum mechanical system) by expanding the time evolution of the system in terms of commutation relations; then, a simple method for producing motion in the direction of a specific commutator at a desired order is presented. The main contributions of the dissertation are then presented in the following three chapters.

Chapter 2 extends the linear model of closed-system quantum mechanics (*i.e.*, systems governed by the Schrödinger equation) to classical systems. Some specific mathematical tools are developed that make it possible to apply many of the geometric ideas developed for the quantum case directly to the classical mathematics. The control scheme using geometric control in the classic case is then applied to a non-linear, non-holonomic system: attitude control of a satellite using gyroscopes.

Chapter 3 contains a theoretical and experimental demonstration of novel concept: closed-loop quantum feedback that preserves quantum coherence. Although this experimental work is a new application of existing technology, the results are important to emerging fields, such as quantum information processing. In addition to constructing the world's smallest man-made feedback loop, the experiment also reconfirms the usefulness of NMR as a convenient and accessible system for demonstrating quantum dynamics.

Chapter 4 describes an open-loop quantum control experiment. In addition to highlight-

ing the usefulness of geometric control to generate a pulse sequence in a nuclear magnetic resonance (NMR) spectrometer, the experiment serves to demonstrate—for the first time—the peculiar and uniquely quantum mechanical Greenberger-Horne-Zeilinger correlations that have no classical analog.

1.2 Geometric Effects in Quantum Systems

Geometric effects emerge in systems when the order of dynamic operators is important. The dynamics of quantum systems typically includes a natural Hamiltonian that governs the uncontrolled evolution of the system, and other "control" Hamiltonian terms that can be added at the discretion of the control engineer. Based on the important work of J. Waugh on average Hamiltonian theory [21], the resultant dynamics can be used to drive the system in directions not possible under the natural Hamiltonian alone; for example, control Hamiltonians can be used to average undesirable terms in the natural Hamiltonian to zero at the end of a specified time period. The genesis of geometric effects in closed quantum systems is presented below.

Consider the Hamiltonian evolution of a quantum system under the Schrödinger equation:

$$\frac{\partial}{\partial t}|\Psi\rangle = -\frac{i}{\hbar}\mathcal{H}\,|\Psi\rangle\ , \tag{1.1}$$

where $|\Psi\rangle$ is the wave function (or "state vector"), and where $\mathcal{H}$ is the Hamiltonian that describes the system dynamics. If the Hamiltonian is constant over the time interval $0 < t \leq \Delta t$, then the formal solution to the linear, time-invariant (LTI) version of Eq. 1.1 is

$$|\Psi(\Delta t)\rangle = e^{-\frac{i}{\hbar}\mathcal{H}\,\Delta t}\,|\Psi(0)\rangle\ . \tag{1.2}$$

To be specific, the wave function—or state—of the system is given by an exponential operator operating on the initial state, where the exponential operator is a shorthand for the formal Taylor series expansion:

$$e^{-\frac{i}{\hbar}\mathcal{H}\,\Delta t} = \sum_{k=0}^{\infty}\frac{1}{k!}\left(\frac{-i}{\hbar}\right)^{k}\mathcal{H}^{k}\,(\Delta t)^{k}\ . \tag{1.3}$$

Suppose in the present case that only one input ($\mathcal{A}$) is available. The control $\mathcal{A}$ allows

input along one direction only: we can only "push" the system in either the direction of $\mathcal{A}$ (or $-\mathcal{A}$), but in no other direction. In quantum systems the inputs are typically applied potentials that make the system affine in the control; that is, the system dynamics can be decomposed into the sum of natural Hamiltonian ($\mathcal{H}_0$) and control Hamiltonians. Thus, in this case, the complete Hamiltonian for the system over the time period in question is:

$$\mathcal{H} = \mathcal{H}_0 + \mathcal{A} \,, \tag{1.4}$$

and the lowest order terms in the exponential expansion of the trajectory are:

$$\begin{aligned} |\Psi(\Delta t)\rangle &= e^{-\frac{i}{\hbar}(\mathcal{H}_0+\mathcal{A})\,\Delta t}\,|\Psi(0)\rangle \\ &= \left\{\mathbf{1} - \frac{i}{\hbar}\,(\mathcal{H}_0+\mathcal{A})\,\Delta t - \frac{1}{2\hbar^2}\,(\mathcal{H}_0+\mathcal{A})^2\,(\Delta t)^2 + ...\right\}|\Psi(0)\rangle \,. \end{aligned} \tag{1.5}$$

If the system begins at equilibrium (*i.e.*, $\mathcal{H}_0|\Psi(0)\rangle = 0$), then to first order in time Δt the dynamics take the state to $-\frac{i}{\hbar}\mathcal{A}\,|\Psi(0)\rangle$—that is, in the direction of $\mathcal{A}$.

Now suppose that it is possible to change the dynamics of the system to $\mathcal{H}_{new}$ (by changing the input) over the time interval $\Delta t < t \leq 2\,\Delta t$. It is simple to show that the new state of the system is now

$$\begin{aligned} |\Psi(2\,\Delta t)\rangle &= e^{-\frac{i}{\hbar}\mathcal{H}_{new}\,\Delta t}\,|\Psi(\Delta t)\rangle \\ &= e^{-\frac{i}{\hbar}\mathcal{H}_{new}\,\Delta t}\,e^{-\frac{i}{\hbar}\mathcal{H}\,\Delta t}\,|\Psi(0)\rangle \,. \end{aligned} \tag{1.6}$$

If the "new" Hamiltonian is $\mathcal{H}_{new} = \mathcal{H}_0 - \mathcal{A}$ so that the dynamics evolve according to

$$\mathcal{H} = \begin{cases} \mathcal{H}_0 + \mathcal{A} & 0 < t \leq \Delta t \\ \mathcal{H}_0 - \mathcal{A} & \Delta t < t \leq 2\,\Delta t \end{cases} \,, \tag{1.7}$$

then application of Eq. 1.6 shows that the end state is

$$\begin{aligned} |\Psi(2\,\Delta t)\rangle &= e^{-\frac{i}{\hbar}(\mathcal{H}_0-\mathcal{A})\,\Delta t}\,e^{-\frac{i}{\hbar}(\mathcal{H}_0+\mathcal{A})\,\Delta t}\,|\Psi(0)\rangle \\ &= \left\{\mathbf{1} - \frac{i}{\hbar}2\mathcal{H}_0\,\Delta t - \frac{1}{2\hbar^2}\left(2\mathcal{H}_0^2 + [\mathcal{H}_0,\mathcal{A}]\right)\,(\Delta t)^2 + ...\right\}|\Psi(0)\rangle \,, \end{aligned} \tag{1.8}$$

where

$$[\mathcal{H}_0,\mathcal{A}] = \mathcal{H}_0\,\mathcal{A} - \mathcal{A}\,\mathcal{H}_0 \tag{1.9}$$

is the commutator between $\mathcal{H}_0$ and $\mathcal{A}$. Note that if the system begins at equilibrium, to lowest order the motion is along $[\mathcal{H}_0, \mathcal{A}]$, which in general is altogether different from the direction $\mathcal{A}$ (unless, of course, $\mathcal{A}$ satisfies the general eigenvalue problem $\mathcal{H}_0\mathcal{A} = \lambda\mathcal{A}$); in addition, the system does not return to its equilibrium $|\Psi(0)\rangle$ unless $\mathcal{H}_0$ and $\mathcal{A}$ commute.

As a specific example, consider a single quantum particle with only two eigenstates (such as a spin-$\frac{1}{2}$ particle in an external magnetic field). Suppose that the natural Hamiltonian is $\mathcal{H}_0 = \sigma_z$, and the only input available is $\mathcal{A} = \sigma_x$, where $\{\mathbf{1}, \sigma_x, \sigma_y, \sigma_z\}$ are the usual Pauli spin operators that generate $SU(2)$. In addition to possible motions along σ_z and σ_x, motion along σ_y is also possible since $[\sigma_z, \sigma_x] = 2i\sigma_y$. In the classical world, this example is analogous to the fact that one needs the ability to rotate around only 2 of the 3 normal Cartesian axes that span $SO(3)$ in order to move any unit vector to any location on the unit sphere [22].

1.3 How to Produce Bracket Directions

The previous section suggested how it is possible to move the state in a direction given by the commutator between two matrices (if the higher order terms are negligible). If motion in the direction of a particular commutator is necessary, one specifies the input control law to produce such motion. This dissertation considers only discontinuous step inputs, valid for applications in which the controller switching time is much shorter than the fastest time constant of the natural dynamics.

To produce the zero order bracket $\mathcal{A}$, the control input is applied for a time Δt, where $\Delta t \ll 2\hbar\|\mathcal{A}\|/\|(\mathcal{H}_0 + \mathcal{A})\mathcal{A}\|$. As seen in the previous section, it is possible to produce the first order bracket $[\mathcal{H}_0, \mathcal{A}]$ by applying $\mathcal{A}$ for a time Δt and then applying $-\mathcal{A}$ for another time Δt. In this case, the second period of evolution serves to "undo" the first order effects, leaving second order effects as the lowest order terms (in addition to the natural Hamiltonian). This pattern can be extended to higher order brackets when the control term appears an *odd* number of times in the desired bracket: applying the "inverse" sequence (*i.e.* the same sequence in reverse order and with opposite sign on the control—or equivalently, the same sequence run "backward" in time) will cancel the previous "odd" bracket and leave the next higher-order term as the lowest-order response. For example, for "simple" brackets of the form $[(\cdot), [(\cdot), [...[(\cdot), (\cdot)]...]]]$, where the $(\cdot)$ can represent either $\mathcal{H}$ or $\mathcal{A}$, the kth order

brackets can be produced by using 2^k periods of evolution, during which the control inputs during the last $2^{(k-1)}$ evolution periods repeat, in reverse order and with opposite signs, the control inputs during the first $2^{(k-1)}$ evolution periods. Examples can be seen in Table 1.1.

Table 1.1: **Producibility of Some Simple Brackets.**

bracket	operator	expansion
$\mathcal{A}$	$e^{(\mathcal{H}_0+\mathcal{A})\Delta t}$	$= \mathbf{1} + (\mathcal{H}_0 + \mathcal{A})\,\Delta t + \frac{1}{2}\left(\mathcal{H}_0^2 + \mathcal{H}_0\mathcal{A} + \mathcal{A}\mathcal{H}_0 + \mathcal{A}^2\right)\,(\Delta t)^2 + \ldots$
$[\mathcal{H}_0, \mathcal{A}]$	$e^{(\mathcal{H}_0-\mathcal{A})\Delta t}e^{(\mathcal{H}_0+\mathcal{A})\Delta t}$	$= \mathbf{1} + 2\mathcal{H}_0\,\Delta t + \left(\mathcal{H}_0^2 + [\mathcal{H}_0, \mathcal{A}]\right)(\Delta t)^2 + \left(\frac{4}{3}\mathcal{H}_0^3 + [\mathcal{H}_0, \mathcal{A}]\mathcal{H}_0 + \mathcal{H}_0[\mathcal{H}_0, \mathcal{A}] - \frac{1}{3}[\mathcal{A}, [\mathcal{H}_0, \mathcal{A}]]\right)(\Delta t)^3 + \ldots$
$[\mathcal{H}_0, [\mathcal{H}_0, \mathcal{A}]]$	$\left[e^{(\mathcal{H}_0+\mathcal{A})\Delta t}e^{(\mathcal{H}_0-\mathcal{A})\Delta t} e^{(\mathcal{H}_0-\mathcal{A})\Delta t}e^{(\mathcal{H}_0+\mathcal{A})\Delta t}\right]$	$= \mathbf{1} + 4\mathcal{H}_0\,\Delta t + 8\mathcal{H}_0^2\,(\Delta t)^2 + \left(\frac{32}{3}\mathcal{H}_0^3 + 2\,[\mathcal{H}_0, [\mathcal{H}_0, \mathcal{A}]] - \frac{2}{3}[\mathcal{A}, [\mathcal{H}_0, \mathcal{A}]]\right)(\Delta t)^3 + \left(\frac{32}{3}\mathcal{H}_0^4 + 4\,[\mathcal{H}_0, [\mathcal{H}_0, \mathcal{A}]]\mathcal{H}_0 + 4\,\mathcal{H}_0[\mathcal{H}_0, [\mathcal{H}_0, \mathcal{A}]] - \frac{4}{3}\mathcal{H}_0[\mathcal{A}, [\mathcal{H}_0, \mathcal{A}]] - \frac{4}{3}[\mathcal{A}, [\mathcal{H}_0, \mathcal{A}]]\mathcal{H}_0\right)(\Delta t)^4 + \ldots$

However, brackets with an even number of $\mathcal{A}$ terms cannot be canceled this way.

In general, finding a sequence of control operations that yield the desired lowest-order bracket direction is difficult. To date, symplectic methods and application of the Campbell-Baker-Hausdorff formula [2] have been the tools of geometric control. In addition, heuristic methods using a digital computer can reveal a suitable if not optimal sequence. For example, it is simple to show that the sequences

$$e^{(\mathcal{H}_0-\mathcal{A})\,\Delta t}e^{(\mathcal{H}_0+\mathcal{A})\,\Delta t}\quad,$$

$$e^{\mathcal{H}_0\,\Delta t}e^{(\mathcal{H}_0-\mathcal{A})\,\Delta t}e^{\mathcal{H}_0\,\Delta t}e^{(\mathcal{H}_0+\mathcal{A})\,\Delta t}\quad,\quad\text{and}$$

$$e^{(\mathcal{H}_0-\mathcal{A})\,\Delta t}e^{\mathcal{H}_0\,\Delta t}e^{(\mathcal{H}_0+\mathcal{A})\,\Delta t}e^{\mathcal{H}_0\,\Delta t}$$

all have motion along $[\mathcal{H}_0, \mathcal{A}]$ as the lowest order response, but the last two operators take twice as long to implement.

Use of the computer coupled with analytic methods to find suitable sequences seems

particularly useful, since computers need only add and multiply—things a computer does well (instead of, say, differentiate). For example, to produce motion in the direction $[[\mathcal{H}_0, \mathcal{A}], [\mathcal{H}_0, \mathcal{B}]]$ from equilibrium with two inputs $\{\mathcal{A}, \mathcal{B}\}$ available, and knowledge that $[\mathcal{A}, [\mathcal{H}_0, \mathcal{A}]] = [\mathcal{B}, [\mathcal{H}_0, \mathcal{B}]] = 0$, a simple program finds the operator

$$
\begin{aligned}
&e^{(\mathcal{H}_0+\mathcal{B})\,\Delta t} e^{(\mathcal{H}_0-\mathcal{B})\,\Delta t} e^{(\mathcal{H}_0+\mathcal{A})\,\Delta t} e^{(\mathcal{H}_0-\mathcal{A})\,\Delta t} e^{(\mathcal{H}_0-\mathcal{B})\,\Delta t} e^{(\mathcal{H}_0+\mathcal{B})\,\Delta t} e^{(\mathcal{H}_0-\mathcal{A})\,\Delta t} e^{(\mathcal{H}_0+\mathcal{A})\,\Delta t} \times \\
&e^{(\mathcal{H}_0-\mathcal{B})\,\Delta t} e^{(\mathcal{H}_0+\mathcal{B})\,\Delta t} e^{(\mathcal{H}_0-\mathcal{A})\,\Delta t} e^{(\mathcal{H}_0+\mathcal{A})\,\Delta t} e^{(\mathcal{H}_0+\mathcal{B})\,\Delta t} e^{(\mathcal{H}_0-\mathcal{B})\,\Delta t} e^{(\mathcal{H}_0+\mathcal{A})\,\Delta t} e^{(\mathcal{H}_0-\mathcal{A})\,\Delta t} \times \\
&e^{(\mathcal{H}_0-\mathcal{B})\,\Delta t} e^{(\mathcal{H}_0+\mathcal{B})\,\Delta t} e^{(\mathcal{H}_0-\mathcal{A})\,\Delta t} e^{(\mathcal{H}_0+\mathcal{A})\,\Delta t} e^{(\mathcal{H}_0+\mathcal{B})\,\Delta t} e^{(\mathcal{H}_0-\mathcal{B})\,\Delta t} e^{(\mathcal{H}_0+\mathcal{A})\,\Delta t} e^{(\mathcal{H}_0-\mathcal{A})\,\Delta t} \times \\
&e^{(\mathcal{H}_0+\mathcal{B})\,\Delta t} e^{(\mathcal{H}_0-\mathcal{B})\,\Delta t} e^{(\mathcal{H}_0+\mathcal{A})\,\Delta t} e^{(\mathcal{H}_0-\mathcal{A})\,\Delta t} e^{(\mathcal{H}_0-\mathcal{B})\,\Delta t} e^{(\mathcal{H}_0+\mathcal{B})\,\Delta t} e^{(\mathcal{H}_0-\mathcal{A})\,\Delta t} e^{(\mathcal{H}_0+\mathcal{A})\,\Delta t},
\end{aligned}
\tag{1.10}
$$

since the expression has a Taylor series expansion equal to:

$$
\begin{aligned}
\mathbf{1} \;+\;& 32\,\mathcal{H}_0\,\Delta t + 512\,\mathcal{H}_0^2\,(\Delta t)^2 \\
&+ \left(\frac{16384}{3}\mathcal{H}_0^3 - \frac{8}{3}[\mathcal{A},[\mathcal{H}_0,\mathcal{A}]] - \frac{8}{3}[\mathcal{B},[\mathcal{H}_0,\mathcal{B}]]\right)(\Delta t)^3 \\
&+ \Big(\frac{131072}{3}\mathcal{H}_0^4 - 4\,[[\mathcal{H}_0,\mathcal{A}],[\mathcal{H}_0,\mathcal{B}]] \\
&\quad - 40\,[\mathcal{A},[\mathcal{H}_0,\mathcal{A}]]\mathcal{H}_0 - \frac{136}{3}\mathcal{H}_0[\mathcal{A},[\mathcal{H}_0,\mathcal{A}]] \\
&\quad - 40\,[\mathcal{B},[\mathcal{H}_0,\mathcal{B}]]\mathcal{H}_0 - \frac{136}{3}\mathcal{H}_0[\mathcal{B},[\mathcal{H}_0,\mathcal{B}]]\Big)(\Delta t)^4 \\
&+ \Big(\frac{4194304}{15}\mathcal{H}_0^5 - 64\,\mathcal{H}_0[[\mathcal{H}_0,\mathcal{A}],[\mathcal{H}_0,\mathcal{B}]] - 64\,[[\mathcal{H}_0,\mathcal{A}],[\mathcal{H}_0,\mathcal{B}]]\mathcal{H}_0 \\
&\quad + 512\,[\mathcal{H}_0,[\mathcal{H}_0,[\mathcal{H}_0,[\mathcal{H}_0,\mathcal{A}]]]] + 512\,[\mathcal{H}_0,[\mathcal{H}_0,[\mathcal{H}_0,[\mathcal{H}_0,\mathcal{B}]]]] \\
&\quad + \frac{106}{15}[\mathcal{A},[\mathcal{H}_0,[\mathcal{H}_0,[\mathcal{H}_0,\mathcal{A}]]]] + \frac{106}{15}[\mathcal{B},[\mathcal{H}_0,[\mathcal{H}_0,[\mathcal{H}_0,\mathcal{B}]]]] \\
&\quad - \frac{7568}{15}[\mathcal{H}_0,[\mathcal{H}_0,[\mathcal{A},[\mathcal{H}_0,\mathcal{A}]]]] - \frac{7568}{15}[\mathcal{H}_0,[\mathcal{H}_0,[\mathcal{B},[\mathcal{H}_0,\mathcal{B}]]]] \\
&\quad - \frac{2}{15}[\mathcal{A},[\mathcal{A},[\mathcal{A},[\mathcal{H}_0,\mathcal{A}]]]] - \frac{2}{15}[\mathcal{B},[\mathcal{B},[\mathcal{B},[\mathcal{H}_0,\mathcal{B}]]]] \\
&\quad + 4\,[\mathcal{B},[\mathcal{H}_0,[\mathcal{H}_0,[\mathcal{H}_0,\mathcal{A}]]]] + 4\,[\mathcal{A},[\mathcal{H}_0,[\mathcal{H}_0,[\mathcal{H}_0,\mathcal{B}]]]] \\
&\quad - 4\,[\mathcal{H}_0,[\mathcal{B},[\mathcal{H}_0,[\mathcal{H}_0,\mathcal{A}]]]] - 4\,[\mathcal{H}_0,[\mathcal{A},[\mathcal{H}_0,[\mathcal{H}_0,\mathcal{B}]]]] \\
&\quad - \frac{4096}{3}\mathcal{H}_0[\mathcal{A},[\mathcal{H}_0,\mathcal{A}]]\mathcal{H}_0 - \frac{256}{3}[\mathcal{H}_0,[\mathcal{A},[\mathcal{H}_0,\mathcal{A}]]]\mathcal{H}_0 \\
&\quad - \frac{4096}{3}\mathcal{H}_0[\mathcal{B},[\mathcal{H}_0,\mathcal{B}]]\mathcal{H}_0 - \frac{256}{3}[\mathcal{H}_0,[\mathcal{B},[\mathcal{H}_0,\mathcal{B}]]]\mathcal{H}_0\Big)(\Delta t)^5 + \ldots
\end{aligned}
\tag{1.11}
$$

Since the "even" brackets ($[\mathcal{A},[\mathcal{H}_0,\mathcal{A}]]$ and $[\mathcal{B},[\mathcal{H}_0,\mathcal{B}]]$) are zero, motion from equilibrium

has $-4[[\mathcal{H}_0, \mathcal{A}], [\mathcal{H}_0, \mathcal{B}]](\Delta t)^4$ as the lowest order response.

In summary, once a control system has been shown to be controllable by examining the system's geometry, motion in the necessary bracket directions is accomplished by application of a sequence that produces the bracket as the lowest order response, and over a time scale small enough to keep higher order effects at acceptably low levels. The following chapters discuss examples of how the accumulated knowledge about the geometric properties of the system can be used as the basis for a control algorithm.

Chapter 2

Classical Control Using Geometric Methods

2.1 Introduction

One of the most important questions regarding any control system is the question of controllability [23]: can the controller drive the system to be controlled from an arbitrary initial state to a desired final state? The question is easily answered in the affirmative if independent and arbitrarily large inputs are available for all possible directions in the configuration space, although rarely is this the case. For the so-called under-actuated systems, a large body of literature exists on the subject, using differential geometry as the basis for determining the controllability of the system in question [1-7]. Of particular import is Sussmann's general theorem on local controllability [10], which is reviewed below. Establishing controllability via the theorem requires computing the Lie brackets of the control system vector fields.

Once it is determined that the control system in question is indeed controllable, the question of algorithm arises: what inputs (or control law) will drive the system to be controlled from an arbitrary initial state to a desired final state? General strategies for computing such an algorithm using the Lie brackets as a basis do exist for dynamic systems without natural dynamic terms [24]; otherwise, rarely are the Lie brackets used directly to implement a control algorithm. This chapter shows how it is possible to construct a control strategy that successfully drives the initial state in the direction of the final state by

directly using the Lie brackets. The strategy is then applied to the attitude control of an under-actuated satellite using two single-gimbaled control moment gyroscopes, where the initial and final states lie on the equilibrium manifold of the control system.

2.2 Classical Formalism

2.2.1 Small time local controllability

Consider a general affine control system defined by the dynamic equation

$$\dot{\mathbf{x}} = \mathbf{f}(\mathbf{x}) + \sum_k u_k(t)\, \mathbf{g}_k \ , \tag{2.1}$$

where $\mathbf{x}(t) = [x_1(t),\ x_2(t),\ ...,\ x_n(t)]^T$ is the vector of state variables (or, simply, the state), $\mathbf{f} = [f_1(\mathbf{x}),\ F_2(\mathbf{x}),\ ...,\ f_n(\mathbf{x})]^T$ are the natural dynamics (or "drift"), the $\mathbf{g}_k$ are available control vector directions, and the u_k are the control inputs. Let the vector fields $(\mathbf{f},\ \mathbf{g}_1,\ ...,\ \mathbf{g}_m)$ be appropriately defined on the set M of allowable states, which is locally a subset of $\mathbf{R}^n$; in addition, let $\mathbf{x}_r(\mathbf{x}_0, t)$ denote the set of reachable states from initial state $\mathbf{x}_0$ in exactly time t. The following preparatory definitions are standard [25]:

Accessibility: The system in Eq. 2.1 is accessible at $\mathbf{x}_0$ if, for any time $t_f > 0$, $\cup_{t \le t_f} \mathbf{x}_r(\mathbf{x}_0, t)$ has a non-void interior with respect to M. If this holds for every $\mathbf{x}_0$ in M, then the system is called accessible.

Small Time Local Controllability: The system in Eq. 2.1 is said to be small time locally controllable (STLC) at $\mathbf{x}_0$ if, for any $t_f > 0$, $\mathbf{x}_0$ is an interior point of $\cup_{t < t_f} \mathbf{x}_r(\mathbf{x}_0, t)$.

Lie Bracket of Two Vector Fields: The Lie bracket of two vector fields $\mathbf{f}_1(\mathbf{x})$ and $\mathbf{f}_2(\mathbf{x})$ is

$$[\mathbf{f}_1,\ \mathbf{f}_2] = \frac{\partial \mathbf{f}_2}{\partial \mathbf{x}}\, \mathbf{f}_1 - \frac{\partial \mathbf{f}_1}{\partial \mathbf{x}}\, \mathbf{f}_2 \ . \tag{2.2}$$

The Lie bracket is itself a vector field, and iterated Lie brackets can found by repeating the differentiation and multiplication in Eq. 2.2. The order of a Lie bracket is the sum of the number of times each vector field appears in the bracket. In general, Lie brackets represent directions in which the system can be "pushed"; the specific control sequence to obtain motion in a given bracket direction is presented in later subsections.

Establishment of small time local controllability consists of tests on the vector fields ($\mathbf{f}$, $\mathbf{g}_1$, ..., $\mathbf{g}_m$) and iterated Lie brackets between them: the Lie algebra for the system. Following Sussmann [10], let $L_r(\mathbf{x})$ denote the smallest Lie algebra of vector fields containing ($\mathbf{f}$, $\mathbf{g}_1$, ..., $\mathbf{g}_m$), and let L be any bracket in $L_r(\mathbf{x})$. Furthermore, let ($n_{\mathbf{f}}$, $n_{\mathbf{g}1}$ ... $n_{\mathbf{g}m}$) denote the number of occurrences of the vector fields ($\mathbf{f}$, $\mathbf{g}_1$, ... $\mathbf{g}_m$), respectively, in bracket L. Finally, denote as "bad" brackets all those Lie brackets that have both $n_{\mathbf{f}}$ odd and all $n_{\mathbf{g}k}$ even. Using these definitions, the small time local controllability theorem is:

The system defined in Eq. 2.1 is STLC if:

1. its dynamics are accessible; and
2. every "bad" bracket at $\mathbf{x}$ can be expressed as a linear combination of brackets of lower order at $\mathbf{x}$.

Establishing accessibility is equivalent to demonstrating that $\text{Rank}(L_r) = \text{Dim}(M)$ for every $\mathbf{x} \in M$, a condition known as the Lie algebra rank condition (LARC) [25]. Proof of the STLC theorem can be found in [10]. Simply put, controllability of a system (at least for small times) indicates that the available inputs and input directions allow motion in all directions in the configuration space of the system, and that any undesirable motions ("bad" bracket directions) can be canceled out by lower order effects. Note that the lowest order "bad" bracket is $\mathbf{f}$ itself (*i.e.*, the "drift" term), which can never be expressed by lower order brackets; consequently, controllability for systems with drift is necessarily restricted to the equilibrium manifold where $\mathbf{f} = 0$.

2.2.2 Trajectory expansion using the exponential operator

While demonstrating controllability via application of the STLC theorem reduces to computing and performing tests on Lie brackets, it does not directly address how motion in the direction of the Lie brackets may be accomplished. In the quantum mechanical case (in Chapter 1), motion along a desired commutator direction could be achieved as the lowest-order response when constant control inputs were applied for a time, and then switched. The same is possible for classical systems that have autonomous dynamics, as shown below.

This section shows how expansion of the state trajectory for autonomous systems that have analytic dynamics is conveniently written in terms of the exponential operator. As in

the quantum mechanical case, the formal exponential operator represents the formal Taylor series of the operators in the exponential argument. (Similar results can be found in the literature [26, 27].) In this case, the argument is the covariant derivative, defined similar to the Lie derivative as follows:

Covariant Derivative: For two vector-valued functions of the state, $\mathbf{f}(\mathbf{x})$ and $\mathbf{g}(\mathbf{x})$, appropriately defined on some region $M \subset \mathbf{R}^n$, the covariant derivative of $\mathbf{f}$ with respect to $\mathbf{g}$ is given by

$$D_{\mathbf{g}}\mathbf{f}(\mathbf{x}) = \nabla\mathbf{f} \cdot \mathbf{g} = \left[\sum_k \frac{\partial f_j}{\partial x_k} g_k\right]_{(j)} . \tag{2.3}$$

Higher order covariant derivatives can be defined iteratively, as in the case of ordinary Lie derivatives, provided that the appropriate order of derivatives of both $\mathbf{f}$ and $\mathbf{g}$ exist. In addition, define $D^0_{\mathbf{g}}\mathbf{f} = 0$.

The covariant derivative operator $D_{\mathbf{g}}$ simply takes the Lie derivative of each component of its vector argument and stacks them into a new vector. It is possible to write the Lie bracket of two vector fields as

$$[\mathbf{f},\ \mathbf{g}] = D_{\mathbf{f}}\mathbf{g} - D_{\mathbf{g}}\mathbf{f} . \tag{2.4}$$

In addition, if $\mathbf{g} = \mathbf{g}_1 + \mathbf{g}_2$, we have

$$D_{\mathbf{g}_1+\mathbf{g}_2} = D_{\mathbf{g}_1}\mathbf{f} + D_{\mathbf{g}_2}\mathbf{f} = \left(D_{\mathbf{g}_1} + D_{\mathbf{g}_2}\right)\mathbf{f} . \tag{2.5}$$

Finally, the commutator $[D_{\mathbf{g}_1},\ D_{\mathbf{g}_2}]$ of two covariant derivative operators is a simple extension of the Jacobi identity [27]; *i.e.*, provided that each of the vector fields is of the appropriate dimension, we have

$$\begin{aligned} [D_{\mathbf{g}_1},\ D_{\mathbf{g}_2}]\,\mathbf{f} &= \nabla\mathbf{f} \cdot (\nabla\mathbf{g}_2 \cdot \mathbf{g}_1 - \nabla\mathbf{g}_1 \cdot \mathbf{g}_2) + \left[\mathbf{g}_2{}^T \cdot \nabla(\nabla\mathbf{f}) \cdot \mathbf{g}_1 - \mathbf{g}_1{}^T \cdot \nabla(\nabla\mathbf{f}) \cdot \mathbf{g}_2\right] \\ &= \nabla\mathbf{f} \cdot [\mathbf{g}_1,\ \mathbf{g}_2] = D_{[\mathbf{g}_1,\ \mathbf{g}_2]}\mathbf{f} , \end{aligned} \tag{2.6}$$

where the bracketed expression in the first line is identically zero because of the symmetry $\left(\frac{\partial^2 f}{\partial x_j \partial x_k} = \frac{\partial^2 f}{\partial x_k \partial x_j}\right)$. It is important to note the order of the vector multiplication in Eq. 2.6, since in general covariant derivative operators do not commute.

Eq. 2.6 shows that the commutator operator is equivalent to the Lie bracket between the operator fields; in fact, the reason for defining the covariant derivative in this manner is

to facilitate a clear parallelism between the quantum and classical formalisms. Specifically, during a period of time in which the input to the system is constant, the dynamics in Eq. 2.1 can be written

$$\dot{\mathbf{x}} = \mathbf{F}(\mathbf{x}) \ . \tag{2.7}$$

For the states of physical systems whose state variables are analytic functions of time, $\mathbf{x}(t)$ may be expanded in a convergent Taylor series about the initial state for times less than the escape time of the system ($\Delta t < t_{esc}$):

$$\mathbf{x}(\Delta t) = \mathbf{x}(0) + \dot{\mathbf{x}}(0)\Delta t + \frac{1}{2}\ddot{\mathbf{x}}(0)\Delta t^2 + ... + \frac{1}{k!}\mathbf{x}^{(k)}(0)\Delta t^k + ... \ , \tag{2.8}$$

where the terms are to be evaluated after the appropriate number of derivative operations. If $\mathbf{F}$ is of class $\mathbf{C}^\infty$, Eq. 2.7 and the chain rule allow the time derivatives to be written as

$$\begin{aligned} \dot{\mathbf{x}} &= \mathbf{F} = \nabla\mathbf{x}\cdot\mathbf{F} = D_{\mathbf{F}}\mathbf{x} \\ \ddot{\mathbf{x}} &= \frac{d\mathbf{F}}{dt} = \frac{\partial\mathbf{F}}{\partial\mathbf{x}}\dot{\mathbf{x}} = \nabla\mathbf{F}\cdot\mathbf{F} = D_{\mathbf{F}}^2\mathbf{x} \\ \mathbf{x}^{(k)} &= D_{\mathbf{F}}^k\mathbf{x} \ . \end{aligned} \tag{2.9}$$

The right side of Eq. 2.8 can then be written as a convergent Taylor series of the vector field $\mathbf{F}$ in the neighborhood of $\mathbf{x}(0)$ and for small times ($\Delta t < t_{esc}$) as:

$$\begin{aligned} \mathbf{x}(\Delta t) &= \left[\left(D_{\mathbf{F}}^0\Delta t^0 + D_{\mathbf{F}}^1\Delta t^1 + \frac{1}{2}D_{\mathbf{F}}^2\Delta t^2 + \ ... + \frac{1}{k!}D_{\mathbf{F}}^k\Delta t^k + \ ...\right)\mathbf{x}\right]\Big|_{\mathbf{x}(0)} \\ &= \left(e^{D_{\mathbf{F}}\Delta t}\mathbf{x}\right)\Big|_{\mathbf{x}(0)} \end{aligned} \tag{2.10}$$

where the vertical bar is written as a reminder that all the operations must be performed considering the state as a variable before evaluating the expression at the specific initial state. The notation $e^{D_{\mathbf{F}}\Delta t}$ for the Taylor series expansion of the state in terms of covariant derivatives is henceforth denoted the exponential operator.

Note that Eq. 2.10 reduces to the familiar form if the system is linear: a linear time-invariant system automatically satisfies the Lipschitz condition for all $\Delta t \geq 0$, and if in addition the input is constant over time Δt, then $\mathbf{F}(\mathbf{x}) = \mathbf{A}\mathbf{x}$; hence,

$$\mathbf{x}(\Delta t) = \left[\left(\mathbf{1} + D_{\mathbf{A}\mathbf{x}}\Delta t + \ ... + \frac{1}{k!}D_{\mathbf{A}\mathbf{x}}^k\Delta t^k + \ ...\right)\right]\Big|_{\mathbf{x}(0)}$$

$$
\begin{aligned}
&= \left[\mathbf{x} + \nabla\mathbf{x}\cdot\mathbf{A}\mathbf{x}\Delta t + \ \ldots + \frac{1}{k!}\nabla\left(\ldots\left(\nabla\mathbf{x}\cdot\mathbf{A}\mathbf{x}\right)\ldots\right)\cdot\mathbf{A}\mathbf{x}\Delta t^k + \ \ldots\right]\Big|_{\mathbf{x}(0)} \\
&= \mathbf{x}(0) + \mathbf{A}\mathbf{x}(0)\Delta t + \ \ldots + \frac{1}{k!}\mathbf{A}^k\mathbf{x}(0)\Delta t^k + \ \ldots \\
&= e^{\mathbf{A}\Delta t}\mathbf{x}(0)\ ,
\end{aligned}
$$

as expected. It is important to note that the operator $D_{\mathbf{F}} \neq \mathbf{A}$, even for linear $\mathbf{F}$; indeed, although the domains of the operators $D_{\mathbf{F}}$ and $\mathbf{A}$ may be the same, $D_{\mathbf{F}}\mathbf{g} \neq \mathbf{A}\mathbf{g}(\mathbf{x})$ for arbitrary $\mathbf{g}$, and it is necessary to derive the exponential operator in terms of $\mathbf{A}$ from the relation $\mathbf{F} = \mathbf{A}\mathbf{x}$.

2.2.3 Trajectory expansion with different dynamic intervals

The expression in Eq. 2.10 is valid for short times during which the autonomous dynamics (including the input) are given by $\mathbf{F}$. Consider now the system given by

$$
\dot{\mathbf{x}}(t) = \begin{cases} \mathbf{F}\left(\mathbf{x}(t)\right) & 0 \leq t < \Delta t \\ \mathbf{G}\left(\mathbf{x}(t)\right) & t \geq \Delta t \end{cases} \ . \tag{2.11}
$$

It would be convenient to express the state for $t \geq \Delta t$ as a Taylor expansion near the initial state $\mathbf{x}(0)$, although in general this is formidable and perhaps unenlightening except in the special case when $t = 2\,\Delta t$. If $\mathbf{F}$ and $\mathbf{G}$ are of class C^ω on regions containing $\mathbf{x}(0)$ and $\mathbf{x}(\Delta t)$ (*i.e.*, if $\mathbf{F}$ and $\mathbf{G}$ are analytic at these points), and if $\mathbf{F}$ and $\mathbf{G}$ are autonomous, then Eq. 2.10 indicates

$$
\begin{aligned}
\mathbf{x}(\Delta t) &= \left(e^{D_{\mathbf{F}}\,\Delta t}\mathbf{x}\right)\Big|_{\mathbf{x}(0)} \\
\mathbf{x}(2\,\Delta t) &= \left(e^{D_{\mathbf{G}}\,\Delta t}\mathbf{x}\right)\Big|_{\mathbf{x}(\Delta t)}
\end{aligned} \tag{2.12}
$$

for small enough Δt such that the system is locally Lipschitz. Since $\mathbf{G}$ is analytic at $\mathbf{x}(0)$, the second line in Eq. 2.12 can be further expanded in a Taylor series about the point $\mathbf{x}(0)$:

$$
\begin{aligned}
\mathbf{x}(2\,\Delta t) &= \left[\left(\sum_{j=0}^{\infty} D_{\mathbf{G}}^j \Delta t^j\right)\mathbf{x}\right]\Big|_{\mathbf{x}(\Delta t)} \\
&= \sum_{j=0}^{\infty}\frac{1}{j!}\left\{\sum_{k=0}^{\infty}\nabla^k\left(D_{\mathbf{G}}^j\mathbf{x}\right)\Big|_{\mathbf{x}(0)}\cdot\left[\sum_{m=0}^{\infty}\frac{1}{m!}\left(D_{\mathbf{F}}^m\mathbf{x}\right)\Big|_{\mathbf{x}(0)}(\Delta t)^m\right]^k\right\}(\Delta t)^j
\end{aligned}
$$

$$= \sum_{j=0}^{\infty}\sum_{k=0}^{\infty}\sum_{m_1=1}^{\infty} \cdots \sum_{m_k=1}^{\infty} \frac{1}{j!}\frac{1}{m_1!\,\ldots\,m_k!} \left(\nabla^k D_{\mathbf{G}}^j D_{\mathbf{F}}^{m_1} \,\ldots\, D_{\mathbf{F}}^{m_k}\right)\Big|_{\mathbf{x}(0)} (\Delta t)^{(j+m_1+\,\ldots\,m_k)}$$

$$= \left(e^{D_{\mathbf{F}}\,\Delta t}\, e^{D_{\mathbf{G}}\,\Delta t}\,\mathbf{x}\right)\Big|_{\mathbf{x}(0)} \tag{2.13}$$

where the last line follows by grouping like orders of Δt.

The last line of Eq. 2.13 is the main result for the expansion of the system trajectory for small times and in the vicinity of the initial state. The order of the operators is important, since in general $[\mathbf{F},\ \mathbf{G}] \neq \mathbf{0}$. Although the order of the exponential operators may seem reversed in this formalism, it is correct given the definition of the covariant derivative in Eq. 2.3 and a straightforward application of Taylor's theorem for analytic functions [26]. For example, it is simple to verify Eq. 2.13 in the LTI case where $\mathbf{F} = \mathbf{A}\mathbf{x}$ and $\mathbf{G} = \mathbf{B}\mathbf{x}$; in this case,

$$\begin{aligned}
\mathbf{x}(2\,\Delta t) &= \left(e^{D_{\mathbf{A}\mathbf{x}}\,\Delta t}\, e^{D_{\mathbf{B}\mathbf{x}}\,\Delta t}\,\mathbf{x}\right)\Big|_{\mathbf{x}(0)} \\
&= \left[e^{D_{\mathbf{A}\mathbf{x}}\,\Delta t}\,\left(\mathbf{x} + \mathbf{B}\mathbf{x}\Delta t + \frac{1}{2}\mathbf{B}^2\mathbf{x}\,\Delta t^2 + \,\ldots\, \frac{1}{j!}\mathbf{B}^j\mathbf{x}\,\Delta t^j + \,\ldots\,\right)\right]\Big|_{\mathbf{x}(0)} \\
&= \left[\mathbf{x} + (\mathbf{A}+\mathbf{B})\,\mathbf{x}\,\Delta t + \left(\frac{1}{2}\mathbf{A}^2 + \mathbf{B}\mathbf{A} + \frac{1}{2}\mathbf{B}^2\right)\Delta t^2 + \,\ldots\,\right]\Big|_{\mathbf{x}(0)} \\
&= e^{\mathbf{B}\,\Delta t}\, e^{\mathbf{A}\,\Delta t}\,\mathbf{x}(0)
\end{aligned}$$

as expected.

Finally, it is now possible to take advantage of the linear structure of the quantum control scheme developed in the preceding chapters by generalizing Eq. 2.13 to multiple dynamic periods. Thus, if $\{\mathbf{F}_1,\ \mathbf{F}_2,\ \ldots\,\mathbf{F}_N\}$ are all autonomous vector fields of class C^ω in the vicinity of initial state $\mathbf{x}(0)$, and if the dynamics of the system can be written as $\mathbf{x}(t) = \mathbf{F}_j\,(\mathbf{x}\,(t))$ during time interval $(j-1)\,\Delta t \leq t < j\,\Delta t$ for $\Delta t < \min_j\,(t_{esc,j})\,,\ j = 1,\ 2,\ \ldots\,N$, then the state of the system at time $t = N\,\Delta t$ is given by

$$\mathbf{x}\,(N\,\Delta t) = \left(e^{D_{\mathbf{F}_1}\,\Delta t}\, e^{D_{\mathbf{F}_2}\,\Delta t}\,\ldots\, e^{D_{\mathbf{F}_N}\,\Delta t}\right)\Big|_{\mathbf{x}(0)}\,. \tag{2.14}$$

As in the example of the quantum system in Chapter 1, it is possible to construct motions in the desired bracket direction by applying an (exponential) operator for some time, and then reversing the order and sign of the operator to cancel lower order effects. Moving in any desired direction, then, is performed by building up small motions in the bracket

directions. Since the vector fields are analytic, the higher order "error" terms in the Taylor series expansion can theoretically be made as small as necessary by making Δt small.

2.3 Satellite Attitude Control: A Case Study

Geometric control theory has found particular applications in non-holonomic systems, such as the attitude control of space platforms, or satellites [28-33]. After the system is shown to be controllable, various control schemes are presented, motivated by sliding mode control [33], energy considerations [28, 29], or others [31, 32]. Satellite attitude control usually involves gas jets (as in [34]), control moment gyroscopes (as in [35]), or some other momentum exchange device through which the input torques are applied to the system. Typical configurations for attitude control systems that use single gimbaled control moment gyroscopes include four gyroscopes, with the major axes arranged in a pyramid style, in order to maintain controllability of the satellite around three independent directions in the event that one of the gyroscopes should become inoperable [35]. The simulation provided below explores whether a "fault-mode" operation requiring only two non-collinear single-gimbal control moment gyroscopes is possible while still maintaining controllability of the satellite.

2.3.1 The satellite dynamics

A detailed state-space model for a satellite equipped with two identical, non-collinear single-gimbal control moment gyroscopes is supplied in Appendix A. Considering only the orientation of the system (the attitude), there are at most 18 degrees of freedom: three angular measures and three rotation rates for each of the two gyroscopes and for the platform. Holonomic constraints include the fixed mounts that secure the gyroscopes to the rigid platform, reducing the number of degrees of freedom for each gyroscope to two: the rotation angle of the gimbal (σ), measured with respect to the platform, and the angular rate of rotation of the gimbal ($\dot{\sigma}$). The orientation of the platform is conveniently represented by three Euler angles (ψ, θ, ϕ), and the angular rotation rates (ω_1, ω_2, ω_3) are measured around axes that coincide with the principal moments of inertia. Using "a" and "b" subscripts as labels for the two gyroscopes, the state can then be written as

$$\mathbf{x} = [\psi,\, \theta,\, \phi,\, \sigma_a,\, \sigma_b,\, \omega_1,\, \omega_2,\, \omega_3,\, \dot{\sigma}_a,\, \dot{\sigma}_b]^T \tag{2.15}$$

with configuration space

$$M = \left\{ \mathbf{x} | -\pi < (\psi,\, \phi) \leq \pi,\, -\frac{\pi}{2} < (\theta,\, \sigma_a,\, \sigma_b) \leq \frac{\pi}{2},\, (\omega_1,\, \omega_2,\, \omega_3,\, \dot{\sigma}_a,\, \dot{\sigma}_b) \in \mathbf{R} \right\} . \quad (2.16)$$

Torques on the gimbal axes are the only inputs to the system. The model assumes that the rotational inertia of the gyroscopes is much smaller than that of the platform, and that the rate of rotation of the gyroscopes is always much greater than the platform. Appendix A derives the model and shows that the system can be written in the form of Eq. 2.1.

Since no external torques are applied to this system, the equations of motion must also satisfy conservation of angular momentum; these constraints are non-holonomic, indicating that they cannot be integrated *a priori* to reduce the number of state variables. Consequently, not all of the state variables are independent: the state is constrained to evolve on a 7 degree-of-freedom manifold M' ($M' \subset M$, $\mathrm{Dim}(M') = 7$). Note that the equilibrium manifold ($\dot{\mathbf{x}} = \mathbf{0}$) is a sub-manifold of M', and requires that the natural dynamics ($\mathbf{f}$) be zero everywhere on the sub-manifold. Physically, the platform and gyroscopes must be at rest at equilibrium, although the orientation angles of the platform may take on any valid values. Since the net angular momentum for the system must be zero at equilibrium, the gyroscopic moments of the control moment gyroscopes point in opposite directions on the equilibrium sub-manifold. It is assumed that the initial state of the system is an equilibrium position, which without loss of generality can be set to the origin in configuration space; thus the controllability of the system at the origin represents the controllability of the system at any point on the equilibrium sub-manifold.

The small time local controllability theorem can be applied to the system by computing elements of the Lie algebra. Significantly, the vector fields ($\mathbf{f}$, $\mathbf{g}_1$, $\mathbf{g}_2$) are analytic at the origin. Calculating the necessary Lie brackets is efficiently done using a digital computer; however, the length and complexity of even low-order brackets make displaying the general results impractical. Of import are the pertinent brackets evaluated at the origin, which, for the parameters used in the simulation (see Table 2.2) are:

$$\mathbf{g}_1(0) = 10^{-6}\,[0,\, 0,\, 0,\, 0,\, 0,\, 0,\, -0.001,\, 0,\, 0.002,\, 0]^T \quad (2.17)$$

$$\mathbf{g}_2(0) = 10^{-6}\,[0,\, 0,\, 0,\, 0,\, 0,\, -0.001,\, 0,\, 0,\, 0,\, 0.002]^T \quad (2.18)$$

$$[\mathbf{f},\, \mathbf{g}_1]\,(0) = 10^{-6}\,[0,\, 0.001,\, 0,\, -2.00,\, 0,\, 1.00,\, 0,\, 0,\, 0,\, 0]^T \quad (2.19)$$

$$[\mathbf{f},\, \mathbf{g}_2]\,(0) \;=\; 10^{-6}\,[0,\, 0,\, 0.001,\, 0,\, -2.00,\, 0,\, 1.00,\, 0,\, 0,\, 0]^T \tag{2.20}$$

$$[\mathbf{f},\, [\mathbf{f},\, \mathbf{g}_1]]\,(0) \;=\; 10^{-6}\,[0,\, 0,\, -1.00,\, 0,\, 0.17,\, 0,\, 0.42,\, 0,\, -1.00,\, 0]^T \tag{2.21}$$

$$[\mathbf{f},\, [\mathbf{f},\, \mathbf{g}_2]]\,(0) \;=\; 10^{-6}\,[0,\, -0.83,\, 0,\, -0.17,\, 0,\, 0.50,\, 0,\, 0,\, 0,\, -0.83]^T \tag{2.22}$$

$$[[\mathbf{f},\, \mathbf{g}_1],\, [\mathbf{f},\, \mathbf{g}_2]]\,(0) \;=\; 10^{-6}\,[-1.75,\, 0,\, 0,\, 0,\, 0,\, 0,\, 0,\, 0,\, 0,\, 0]^T \tag{2.23}$$

These seven brackets constitute seven independent directions; thus, the LARC is satisfied, and the dynamics are accessible on M'. Restricting attention to the equilibrium sub-manifold, the "bad" brackets are found to be identically zero:

$$\mathbf{f}(0) \;=\; 0\,, \tag{2.24}$$

$$[\mathbf{g}_1,\, [\mathbf{f},\, \mathbf{g}_1]]\,(0) \;=\; 0\,, \tag{2.25}$$

$$[\mathbf{g}_2,\, [\mathbf{f},\, \mathbf{g}_2]]\,(0) \;=\; 0\,, \tag{2.26}$$

Thus the requirements for controllability are satisfied for small times on the equilibrium manifold.

The remaining problem is to specify the control inputs (the torques to the the gimbal axes) that will bring about maneuvers in the 7 independent bracket directions. Here the parallelism between the Lie bracket in nonlinear differential geometric control theory and and commutator in linear control (as introduced in Chapter 1) greatly simplifies the task. In fact, using the formalism in the previous section, the sequence of torque inputs to "push" in any of the independent bracket directions given in Eqs. 2.17–2.23 was presented in Chapter 1. In light of Eq. 2.14, simple reversal of the time ordering of the comparable operation from Chapter 1 will produce the desired motion. Specifically, compare the brackets in Eqs. 2.17–2.22 with the entries in Table 1.1, substituting $\mathbf{f}$ for $\mathcal{H}_0$ and $\mathbf{g}_1$ or $\mathbf{g}_2$ for $\mathcal{A}$. Moving in the direction of $\mathbf{g}_1$ (or $\mathbf{g}_2$) requires applying a torque to the gimbal axis of gyroscope "a" (or to gyroscope "b") while maintaining zero torque on the other gimbal axis. To bring about $[\mathbf{f},\, \mathbf{g}_1]$ or $[\mathbf{f},\, \mathbf{g}_2]$ as the lowest-order response at equilibrium, apply the sequence of operators as in the production of $[\mathcal{H}_0,\, \mathcal{A}]$—although in reverse time order. A sequence for "pushing" in the direction of the brackets in Eq. 2.21 and Eq. 2.22 is ascertained in like manner. Finally, motion in the direction of $[[\mathbf{f},\, \mathbf{g}_1],\, [\mathbf{f},\, \mathbf{g}_2]]$ from an equilibrium position can be found by reversing the order of operators in Eq. 1.10.

Table 2.1 summarizes the sequence input operations that yield the desired bracket direc-

tion from equilibrium as the lowest-order term in the Taylor series response of the system. The right column indicates the order in which the constant torque input of magnitude $|u|$ should be applied to the gimbal of the subscripted gyroscope for time Δt while the torque on the complementary gyroscope is zero.

Table 2.1: **How to Produce Bracket Directions from Equilibrium.**

Bracket	Sequence of Inputs (each for time Δt)
$\mathbf{g}_1$	$+u_a$
$\mathbf{g}_2$	$+u_b$
$[\mathbf{f}, \mathbf{g}_1]$	$-u_a, +u_a$
$[\mathbf{f}, \mathbf{g}_2]$	$-u_b, +u_b$
$[\mathbf{f}, [\mathbf{f}, \mathbf{g}_1]]$	$+u_a, -u_a, -u_a, +u_a$
$[\mathbf{f}, [\mathbf{f}, \mathbf{g}_2]]$	$+u_b, -u_b, -u_b, +u_b$
$[[\mathbf{f}, \mathbf{g}_1], [\mathbf{f}, \mathbf{g}_2]]$	$+u_b, -u_b, -u_a, +u_a, -u_b, +u_b, +u_a, -u_a,$ $-u_b, +u_b, +u_a, -u_a, +u_b, -u_b, -u_a, +u_a,$ $-u_b, +u_b, +u_a, -u_a, +u_b, -u_b, -u_a, +u_a,$ $+u_b, -u_b, -u_a, +u_a, -u_b, +u_b, +u_a, -u_a$

From equilibrium, motion in any direction that also leads to an equilibrium state is possible. It is not possible to move from one equilibrium state to another without leaving the equilibrium set in the interim; errors are therefore possible in returning to the set of equilibrium states. The errors incurred in using the above sequences of inputs are represented by higher order terms in the Taylor series expansion of the system dynamics. In theory the error in moving from one equilibrium state to another can be kept within arbitrary bounds by reducing the time step (Δt). Control of the satellite from one orientation to another is thus possible by decomposing the displacement vector from the origin to the desired equilibrium position in terms of the above independent brackets, and then weighting the terms in the input sequence to produce those brackets.

2.3.2 Simulation

This section provides simulations of the motion of the state variables in moving in the 7 independent directions elucidated above. It can be verified that motion in all seven independent bracket directions is possible by directly simulating the actual dynamics in a regime where

1. the inputs (torques) are small enough so that the assumptions made in the model derivation are satisfied; and

2. the time per operation is small enough so that contributions due to higher order effects are negligible. For the simulation, errors of less than 1% from the predicted bracket direction for each state variable were considered acceptable.

The simulations used the model derived in Appendix A with parameter values as given in Table 2.2.

Table 2.2: **Parameter Values in the Attitude Control Simulation.**

Parameter	Symbol	Simulation Value
Platform inertia around $\mathbf{e}_1$	I_1	1000 kg m^2
Platform inertia around $\mathbf{e}_2$	I_2	1200 kg m^2
Platform inertia around $\mathbf{e}_3$	I_3	2000 kg m^2
Inertia of gyroscopes ("a" and "b")	I_g	10 kg m^2
Angular speed of gyroscopes ("a" and "b")	ω_g	1000 rad/s

The results of the simulation for each bracket direction are shown in Figs. 2-1–2-7. In each case, the sequence in Table 2.1 drove the state in the direction of the desired bracket: the values of the state variables at the end of the input sequence are proportional to the brackets in the table. The time for each sequence of input operations was set at $10\,\mu$s in order to satisfy the model assumptions (ω_g much smaller than the angular velocity of the platform), maintain acceptable error levels, and keep all dimensionless torque inputs $< \mathcal{O}(1)$. Note that in order to remain within the operating regime defined by the model assumptions and by the acceptible errors in the motion, only small displacements from the origin are possible. To illustrate, if the goal of the control system is to reorient the platform by changing the Euler angle ψ from its initial value (0) to (π), the control scheme applied to the simulation model would require approximately 10^{13} s to reorient the space craft. Although the control scheme works in theory, it may be practical only for very fine control near an equilibrium position.

2.4 Conclusions

The control scheme presented in this chapter demonstrated how a strategy to control nonlinear affine systems on equilibrium states can be created directly from the geometric con-

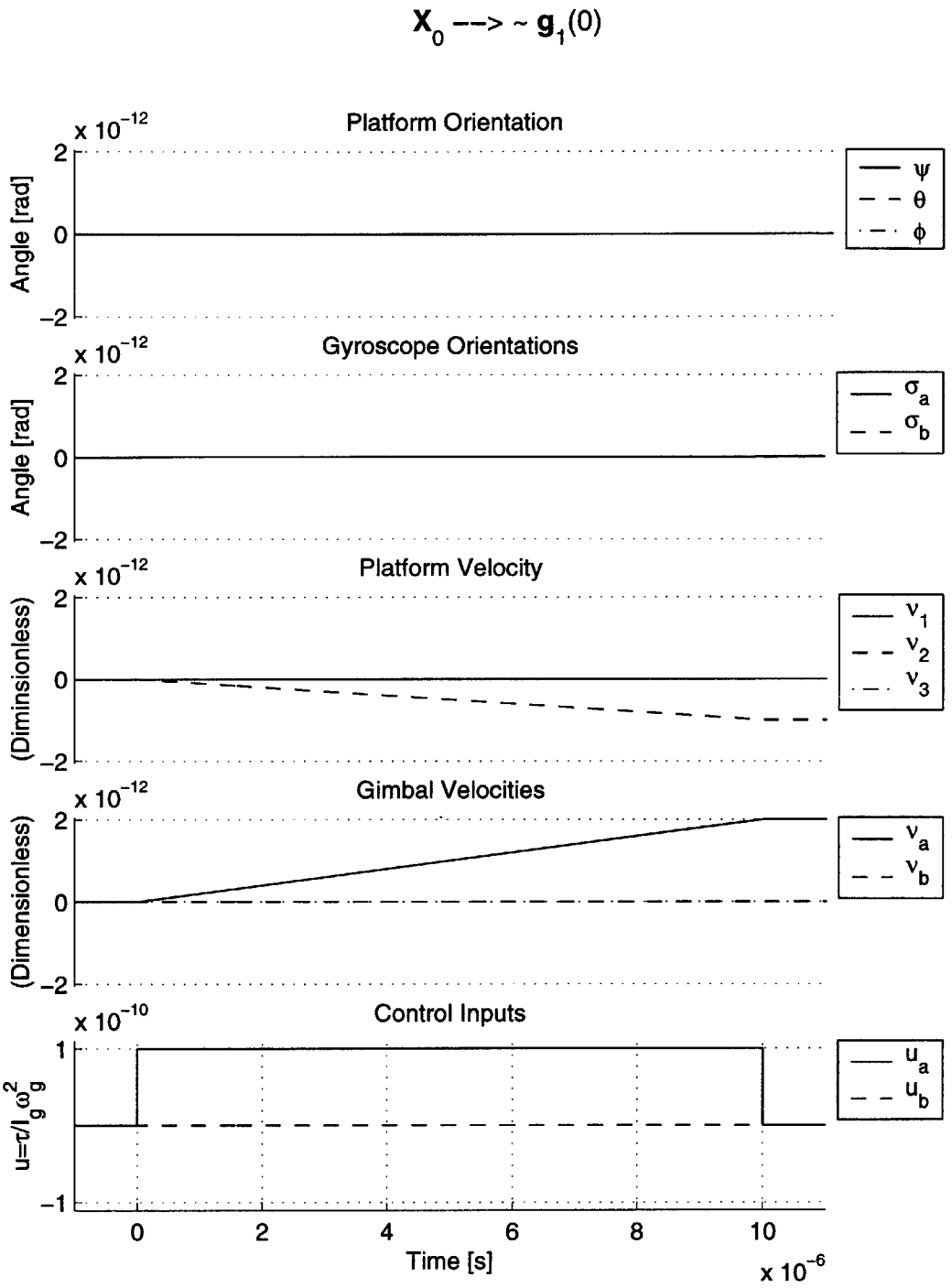

Figure 2-1: **Pushing in the Direction of g_1.** The final state (at 10 μs) after execution of the control sequence for this bracket (see Table 2.1) is proportional to the theoretical prediction in Eq. 2.17. Errors due to higher-order terms in the Taylor series expansion are less than 1% for each state variable. The same scale is used for the plots of all 7 brackets.

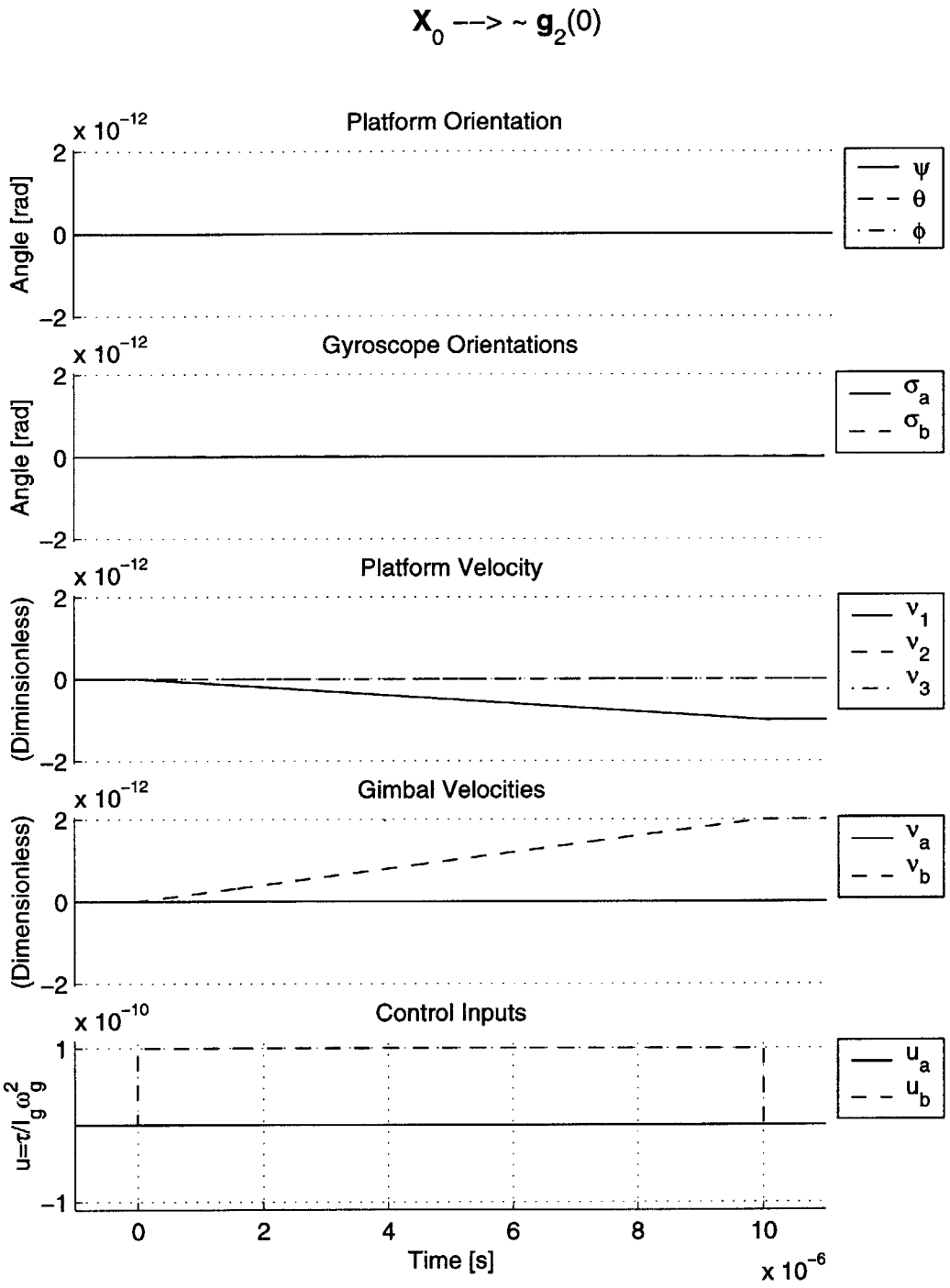

Figure 2-2: **Pushing in the Direction of g_2.** The final state (at $10\,\mu s$) after execution of the control sequence for this bracket (see Table 2.1) is proportional to the theoretical prediction in Eq. 2.18. Errors due to higher-order terms in the Taylor series expansion are less than 1% for each state variable. The same scale is used for the plots of all 7 brackets.

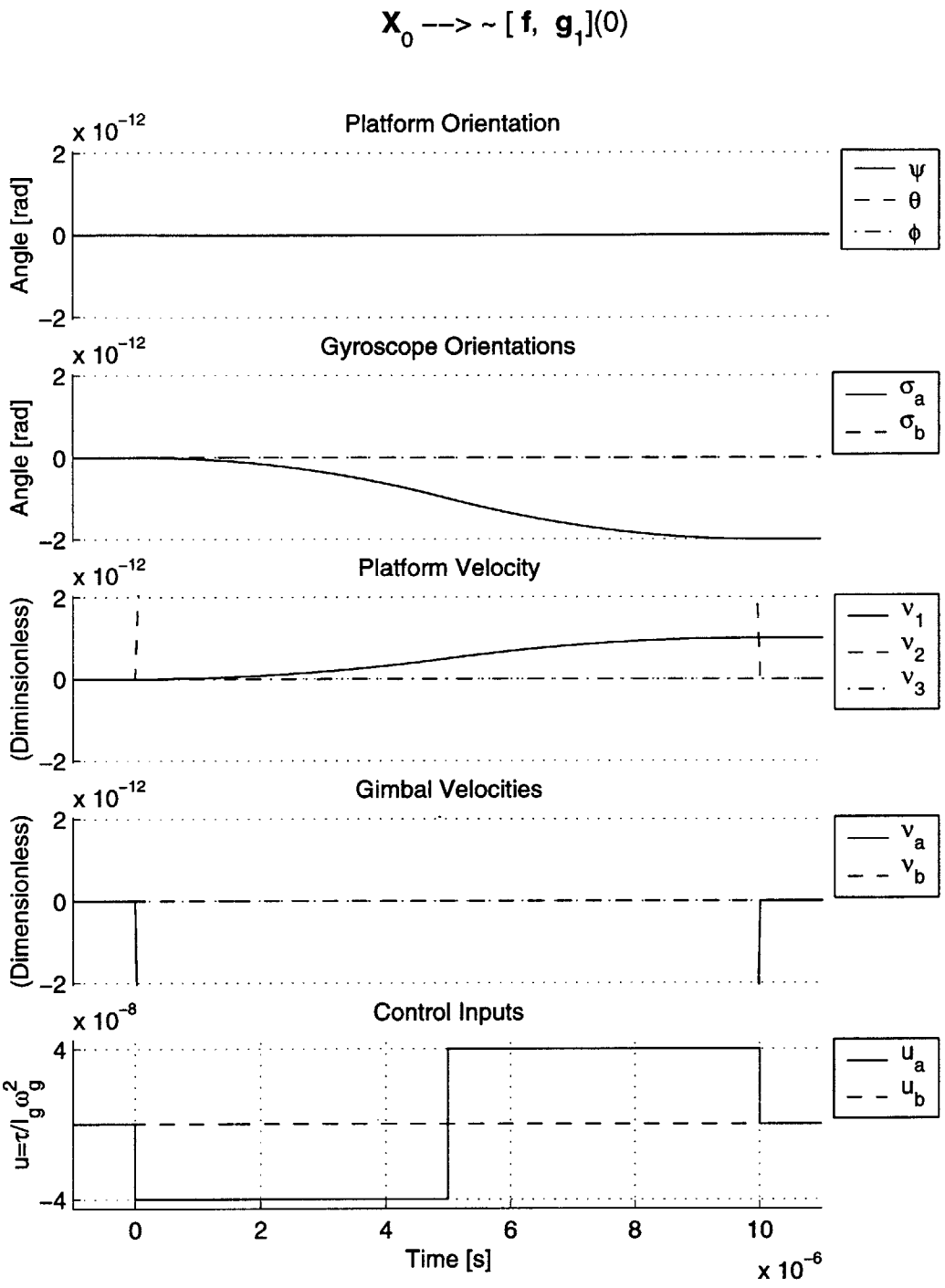

Figure 2-3: **Pushing in the Direction of $[\mathbf{f}, \mathbf{g}_1]$.** The final state (at 10 μs) after execution of the control sequence for this bracket (see Table 2.1) is proportional to the theoretical prediction in Eq. 2.19. Errors due to higher-order terms in the Taylor series expansion are less than 1% for each state variable. The same scale is used for the plots of all 7 brackets.

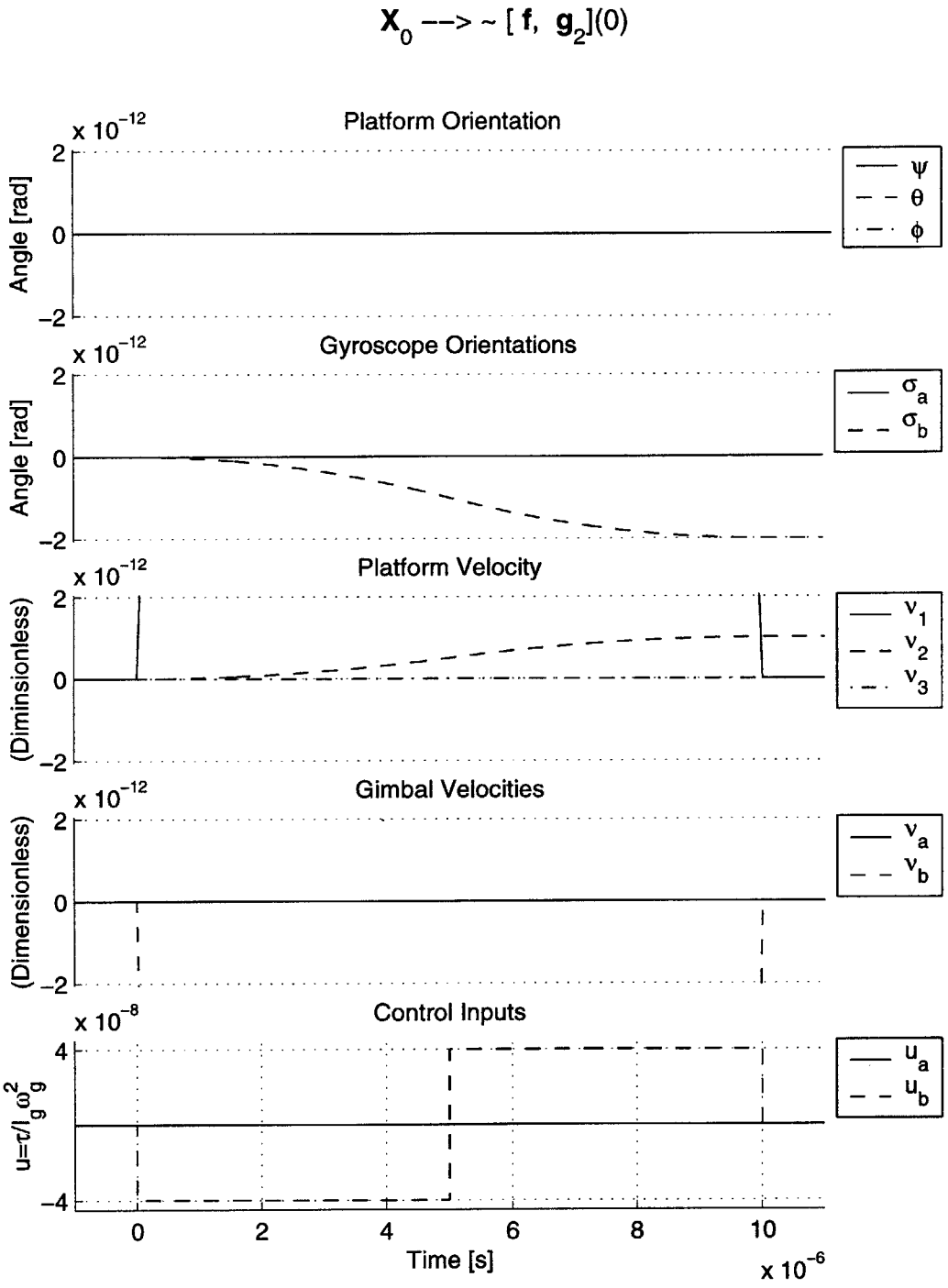

Figure 2-4: **Pushing in the Direction of** $[\mathbf{f}, \mathbf{g}_2]$. The final state (at $10\,\mu$s) after execution of the control sequence for this bracket (see Table 2.1) is proportional to the theoretical prediction in Eq. 2.20. Errors due to higher-order terms in the Taylor series expansion are less than 1% for each state variable. The same scale is used for the plots of all 7 brackets.

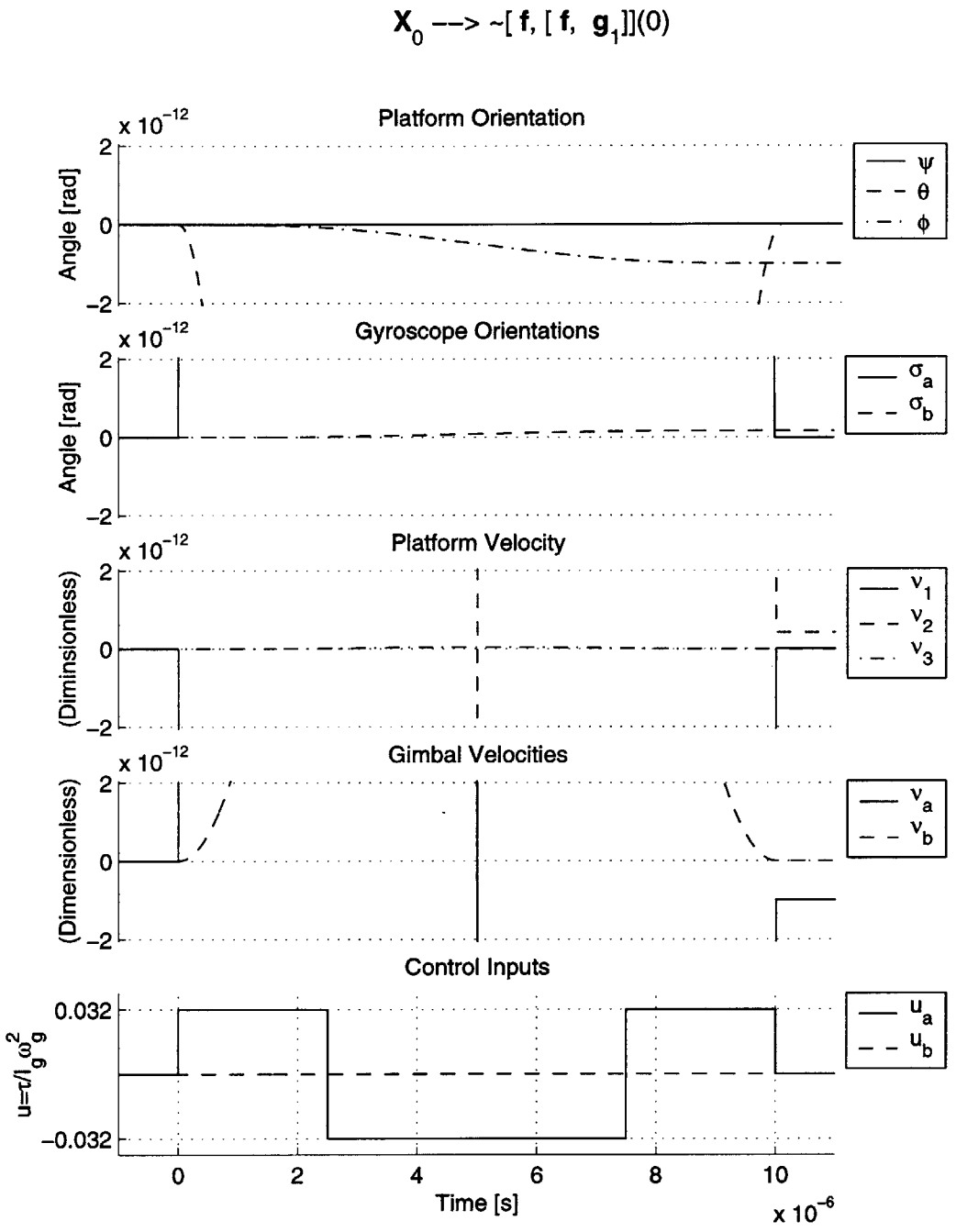

Figure 2-5: **Pushing in the Direction of $[\mathbf{f},[\mathbf{f},\mathbf{g}_1]]$.** The final state (at $10\,\mu$s) after execution of the control sequence for this bracket (see Table 2.1) is proportional to the theoretical prediction in Eq. 2.21. Errors due to higher-order terms in the Taylor series expansion are less than 1% for each state variable. The same scale is used for the plots of all 7 brackets.

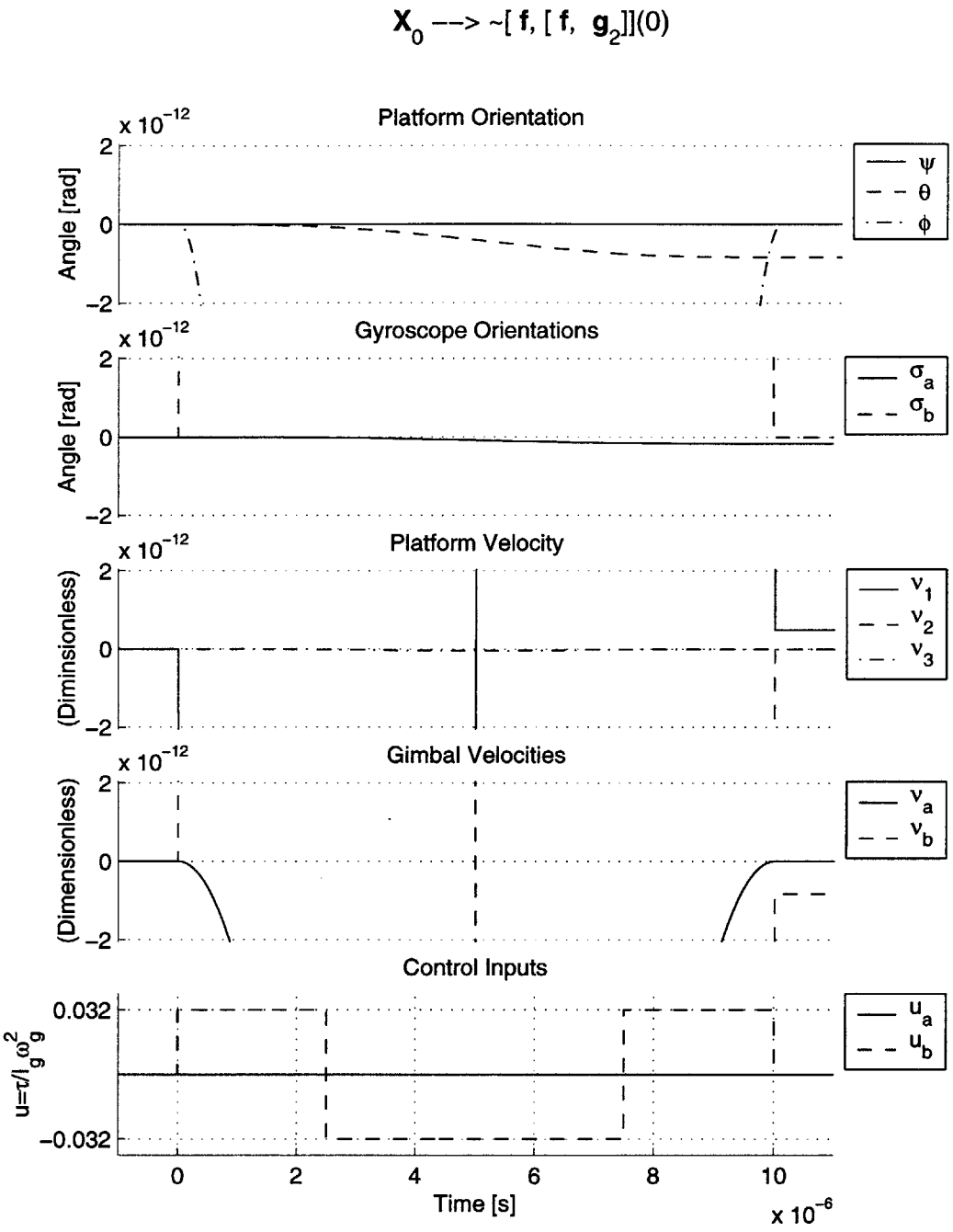

Figure 2-6: **Pushing in the Direction of** $[\mathbf{f},[\mathbf{f},\mathbf{g}_2]]$. The final state (at $10\,\mu$s) after execution of the control sequence for this bracket (see Table 2.1) is proportional to the theoretical prediction in Eq. 2.22. Errors due to higher-order terms in the Taylor series expansion are less than 1% for each state variable. The same scale is used for the plots of all 7 brackets.

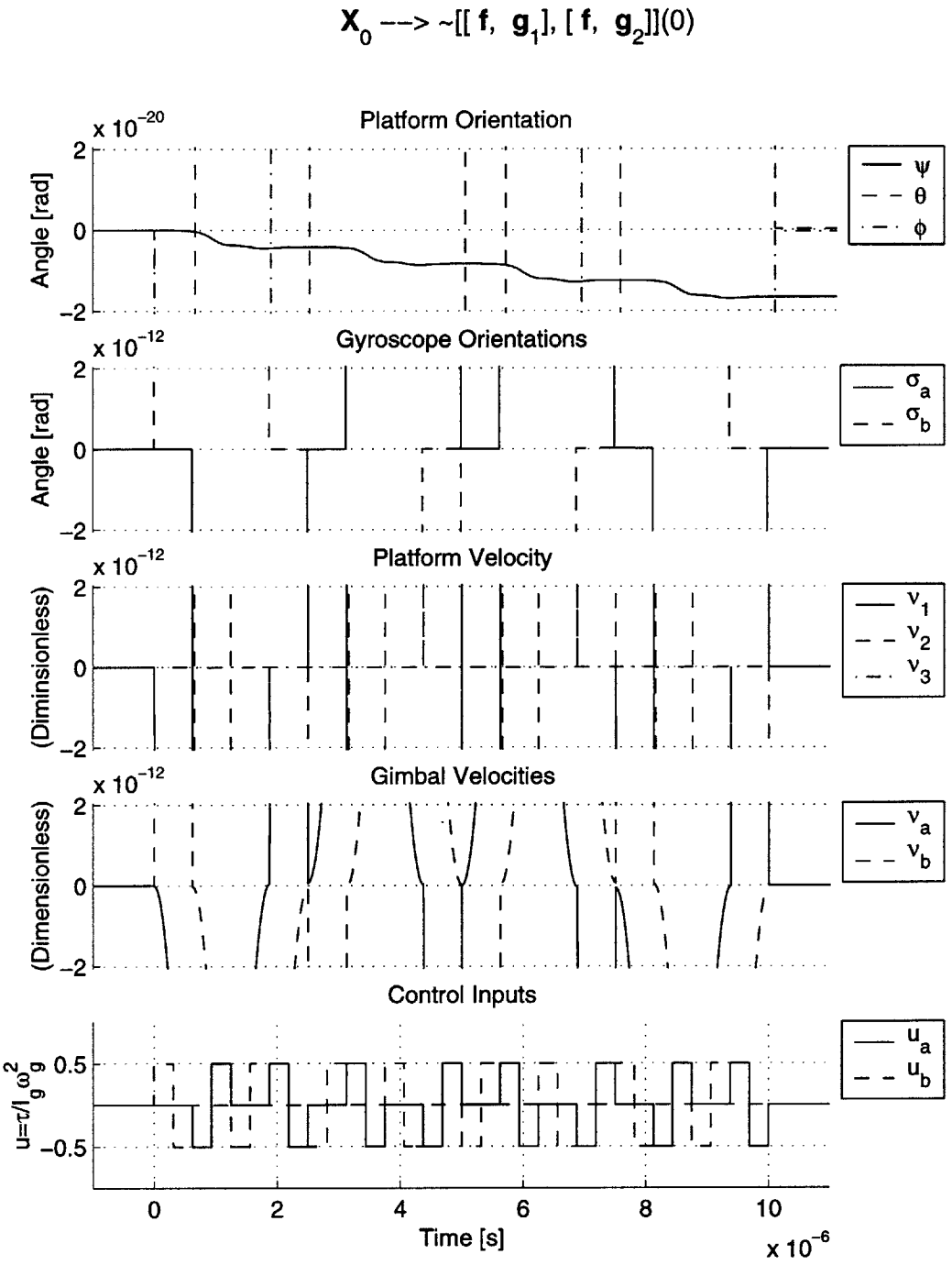

Figure 2-7: **Pushing in the Direction of** $[[\mathbf{f}, \mathbf{g}_1], [\mathbf{f}, \mathbf{g}_2]]$. The final state (at $10\,\mu$s) after execution of the control sequence for this bracket (see Table 2.1) is proportional to the theoretical prediction in Eq. 2.23. Errors due to higher-order terms in the Taylor series expansion are less than 1% for each state variable. The same scale is used for the plots of all 7 brackets, except for the Euler angles in this bracket.

trol algebra. Once controllability has been established by verifying the small-time local controllability of the system using the pertinent Lie brackets, sequences of inputs can be immediately designed that can move the system in any of the bracket directions. Theoretically the error in moving along the bracket directions can be made arbitrarily small by making the time step per input small.

Application of the control scheme to the attitude control of a space platform or satellite suggests that the system would be of practical use only very fine control near equilibrium positions given the scale of possible displacements. While larger motions may be possible with gyroscopes of rotational inertia comparable to that of the platform, or with greatly increased angular momentum, such scenarios are not practical.

Chapter 3

Coherent Feedback Control of a Quantum Mechanical System

3.1 Introduction

The objective of a control system is to drive a dynamic system from an unknown initial state to a desired final state. To accomplish this objective, a feedback controller gets information about a system and feeds it back to alter the system's behavior in a desired fashion. The resulting closed-loop system can exhibit better controllability, stability, and disturbance rejection than the open-loop system. Feedback control of *classical* dynamic systems involves measuring system variables, computing inputs, and applying those inputs back to the system to be controlled. These three main tasks are carried out by elements in the feedback loop usually called sensors, controller, and actuators, respectively. Traditionally, when this control scheme is applied to a *quantum mechanical* system, the result is a feedback loop that necessarily destroys quantum coherence because some or all of the elements are semi-classical [12, 14-16, 18-20, 36-44] For example, if the sensor is a semi-classical device that measures the spin state of a spin-1/2 quantum system, the measurement causes the wave function to collapse probabilistically to one of two possible eigenstates, irreversibly destroying the original wave function in the process. In addition, if the controller is a digital computer, then a von Neumann type (*i.e.*, wave function collapse–inducing) measurement must be made to digitize the measurement to classical data that can be processed by the

This chapter proposes and provides an experimental demonstration of a novel quantum

feedback technique in which sensors, controller, and actuators are all quantum systems that operate in a way that preserves quantum coherence. This method can be used to control quantum systems in ways that cannot be accomplished by "conventional" control of a quantum system using a classical feedback loop. In particular, the classical feedback loop cannot be used to transfer quantum information. As a result, a variety of quantum correlations cannot be transferred from one system to another using a classical feedback loop. For example, if two systems are entangled, then a quantum controller cannot be used to make measurements on one system and to transfer its entanglement with the second system to a third, initially uncorrelated system.

To demonstrate the potential of coherent quantum feedback, this chapter defines a class of intrinsically quantum correlations that cannot be transferred using a classical feedback loop. In fact, it is shown that two systems can be in state that is separable, *i.e.*, unentangled, and still possess correlations that cannot be transferred classically. The experiment reported on here created such states, and used a quantum feedback loop to transfer those non-classical correlations. In addition, the experiment is also another demonstration the accessibility of NMR as a convenient demonstration system for quantum dynamics.

3.2 Description of Coherent Quantum Feedback.

3.2.1 Classical *vs.* quantum coherent feedback

To distinguish between coherent control of a *quantum* system using a quantum feedback loop, and coherent control using a *classical* feedback loop, consider the following example of the latter. Monroe *et al.* employed classical feedback using optical measurements and laser as actuators to control coherently the $^2S_{1/2}$ hyperfine states

$$|F = 2, m_F = 2\rangle \equiv |\downarrow\rangle \ ,$$

$$|F = 1, m_F = 1\rangle \equiv |\uparrow\rangle \ ,$$

of a single $^9Be^+$ ion in an ion trap [45]. The ion is originally in an unknown superposition

$$|\psi_0\rangle = \alpha|\downarrow\rangle + \beta|\uparrow\rangle \ , \tag{3.1}$$

and the goal of the classical feedback loop is put the ion in the state

$$|\psi_d\rangle = |\uparrow\rangle \ . \tag{3.2}$$

The control loop begins by measuring the state of the ion by driving the cycling

$$|\downarrow\rangle \longrightarrow {}^2P_{3/2}|F = 3, m_F = 3\rangle$$

transition with $\sigma+$ polarized light and detecting the resulting ion fluorescence: fluorescence indicates that the ion is in the state $|\downarrow\rangle$. If the ion is found to be in the state $|\downarrow\rangle$, the controller (a classical digital computer) instructs the actuators (lasers) to effect a π pulse by driving a Raman transition through the virtual ${}^2P_{1/2}$ level to flip the atom into the $|\uparrow\rangle$ state. The net effect of the feedback loop is to put the ion in the state $|\uparrow\rangle$. The feedback loop is classical in the sense that the measurement provides a classical bit of information, and a classical controller decides on the basis of that bit whether or not to supply a Raman pulse to drive a coherent quantum transition in the ion.

The classical control scheme in the previous paragraph is pictorially represented in Fig. 3-1(a), where the single solid lines indicate the flow of classical information: information from the measured system is compared to desired values from the reference, and the resulting error is used as the basis for the input back to the system. Once the error is reduced to zero, the feedback ends; the system has been driven to the desired final state $|\psi_d\rangle$. If the goal of the control design includes "tracking", or following a desired time-varying state $|\psi_d(t)\rangle$, the feedback loop may be invoked repeatedly where the measurement of the system at each time τ is compared with the reference input $|\psi_d(\tau)\rangle$ to produce the updated error. Note that regulation of the system near a constant desired state (in the presence of disturbances that may cause evolution of the system away from $|\psi_d\rangle$) represents a special case of tracking. In any case, each instance of feedback requires comparison with a new reference.

Monroe's semi-classical control scheme is a method for controlling the spin of a proton in the nucleus of an ion using a classical feedback loop. Such a control scheme is clearly probabilistic: the initial measurement has a stochastic outcome; it is also destructive: the relative phase between α and β is irreversibly lost in the course of the measurement. The probabilistic, destructive nature of the classical feedback loop arises because the detector is a classical measuring device that irreversibly decoheres the quantum system in the course

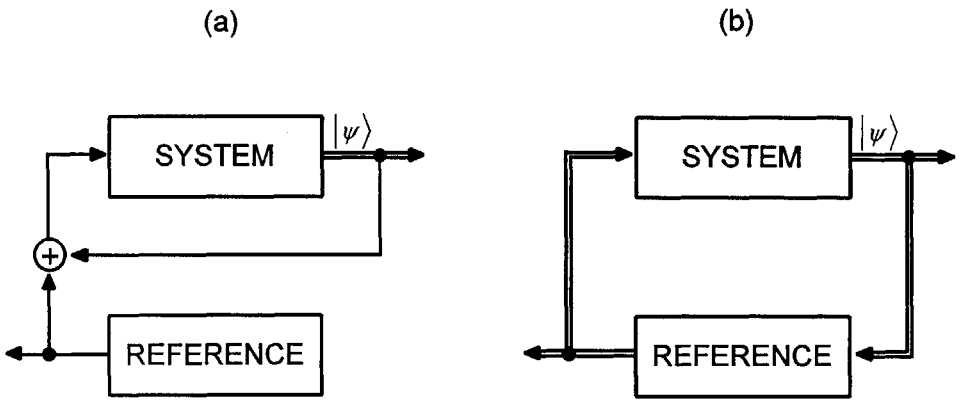

Figure 3-1: **Comparison of Feedback Systems.** (a) The standard picture of classical feedback involves transfer of classical information (the solid single line). First, a sensor measures the state of the system, destroying any quantum coherence in the process. The information is then compared with a reference state to produce an error signal (the difference between measured and desired states). The controller processes the information, using the error as the basis to act on the system (via actuators) that drives the system from an unknown initial state to the desired final state. The control system is clearly stochastic and irreversible due to the measurement that must be made in order to compare the states of the system and desired reference. (b) A fully-coherent feedback system transfers "quantum information", i.e., information about amplitudes and phases (the double solid lines). In this case, sensor, controller, and actuator are themselves quantum systems that interact with each other and with the system to be controlled in a coherent fashion. Although the reference state must change during implementation of the feedback loop in order to contain the information originally contained in the initial state of the system, the elements of sensor (to obtain information about the system), controller and actuator (to drive the system to the desired state based on the acquired information) are still present. In addition, fully-coherent quantum feedback can perform tasks impossible for the classical controller: transfer of quantum correlations.

of becoming correlated with it. This destructive feature of quantum measurement holds even for the least invasive type of measurement, a so-called "non-demolition" measurement [46-49]. For a quantum feedback loop to be non-destructive, the sensors must get information without making any measurements. Although this requirement sounds at first self-contradictory, it can be fulfilled if the sensor in the quantum feedback loop is itself a quantum system that interacts coherently with the quantum system to be controlled. Such a sensor can be thought of as obtaining "quantum information" that carries information about quantum phases as well as amplitudes. For the complete quantum feedback loop to preserve quantum coherence, the controller and actuator must also be quantum systems: the controller must process the quantum information obtained by the sensor in a coherent fashion, and the actuator must feed back that information into the system in a way that preserves quantum phases. Fig. 3-1(b) depicts a graphical representation of fully coherent quantum feedback.

At first, it might seem that a coherent quantum feedback loop requires a quantum controller capable of performing large-scale quantum computations, a technically difficult task [50-54]. In fact, a controller need not be complex to be effective: a useful classical controller can be constructed from a single operational amplifier, and as will be shown below, an effective quantum controller can consist of a single nuclear spin. The idea of using one nuclear spin to influence another in a controlled fashion is a familiar one in nuclear magnetic resonance (NMR), and has been used in double-resonance processes since the 1950's [55-57] to exchange or "swap" the states of two spins. Double-resonance swaps figure prominently in NMR quantum computation [52, 55, 58]: they can be used to realize the quantum information exchange process proposed by Feynman [59] and elucidated by Lloyd [52], Barenco *et al.* [60] and Zukowksi *et al.* [61]. In the experiment below, the use of a double-resonance "swap" is used to construct an experimental realization of a quantum feedback loop that performs a task that is not possible using a classical feedback loop. Like Monroe's classical feedback loop [45], the quantum feedback loop constructed here also controls the behavior of a proton in a nucleus, but uses nuclear magnetic resonance rather than optical techniques.

3.2.2 The "No Cloning" theorem and coherent control

It is perhaps not surprising that the fully coherent quantum feedback loop proposed and demonstrated in this paper uses a "swap" operation. In fact, if in addition to the initial state of the quantum system the desired reference state is also unknown, then a "swap" operation using fully coherent quantum feedback is the *only* method of control. This is true because it is impossible to characterize the unknown reference using the classical information required by the comparison step in the classical feedback algorithm—impossible because of the well-known "no cloning" theorem [62, 63]. For similar reasons it is not possible to regulate the system near an unknown desired reference state. Specifically, to preserve quantum coherence the information contained in the initial unknown state of the system must be contained in the final state of the quantum controller; therefore, the reference state after the feedback loop has been closed is no longer the desired reference state. Coherent regulation of the system near the desired state therefore requires multiple copies of the reference state, which, as noted, is prohibited if the desired reference state is unknown.

If instead the desired state is a known state, the system can still be controlled using the same "swap" operation that guides the unknown initial state of the system to the desired final state and stores the unknown initial state in another system. Furthermore, regulation of the system near the desired state is possible by repeated application of feedback. In this case, as in the classical case, each instance of feedback requires a fresh copy of the reference system. The inclusion of multiple copies of the reference in the controller does not therefore diminish the essential role of the quantum feedback loop as a system that must obtain quantum information and then act back on the system based on that information. Finally, the coherence-preserving quantum feedback loop can perform a control operation impossible for a classical feedback loop: transfer of quantum correlations.

3.2.3 Quantum correlations

It has been known since the work of Einstein, Podolsky and Rosen in the 1930's that quantum systems can exhibit types of correlation that are not permitted classically [64-68]. Such peculiar quantum correlations are of considerable importance in quantum communications and computation: they are required for quantum teleportation and in some schemes for quantum cryptography [69], and their systematic manipulation is the key for the exponen-

tial speed-up of computations such as factoring using quantum computers [70-73].

There are a variety of ways in which quantum systems can exhibit non-classical correlations [64-68]. The best known example of non-classical correlation is entanglement (see, for example, Eqs. 4.2 and 4.3); however, two quantum systems can be in a separable, *i.e.*, unentangled, state, and yet still exhibit intrinsically quantum mechanical correlations that cannot be transferred by means of a classical controller. When the density matrix for two systems B and C can be written in the form

$$\rho_{BC} = \sum_k a_k \rho_B^k \rho_C^k \tag{3.3}$$

where

$$\mathrm{Tr}\left(\rho_B^k \rho_B^{k'}\right) \propto \delta_{kk'} \ ,$$

then it is possible for a classical controller to transfer B's correlation with C to a third system, A, by making a measurement on B to determine which of the ρ_B^k states B is in, and preparing A in that state. Conversely, when the state for B and C cannot be written in the form of Eq. 3.3, any measurement that the controller makes on B necessarily destroys off-diagonal terms in the density matrix for B and C. Accordingly, the intrinsically quantum correlation between two systems whose state cannot be written as in Eq. 3.3 cannot be transferred by conventional feedback control of quantum systems using a classical controller. This correlation is non-classical, as any classical correlation can in principle be transmitted down a classical communications line. Note that if B and C are spins, Eq. 3.3 is equivalent to the condition that their density matrix is proportional to

$$\rho \propto \mathbf{1} + bI^B + cI^C + dI^B I'^C \tag{3.4}$$

for some generalized Pauli matrices I^B, I^C, and I'^C. As will be seen below, there exist states of the form of Eq. 3.4 that are separable: as a result, there are separable states that possess a form of non-classical correlation.

3.3 Using NMR to Demonstrate Quantum Dynamics

3.3.1 Density matrix description of the state

The spins in an NMR sample containing of order $\mathcal{O}(10^{18})$ molecules can to good approximation be treated as a macroscopic ensemble of isolated spins [56, 74]. Weakly-polarized macroscopic ensembles of spins in an NMR sample are conveniently described by an average density matrix (rather than a wave function, or "state vector"), which contains the same information with respect to measurement. In an external, z-oriented magnetic field at room temperature, the equilibrium Boltzmann distribution over an ensemble of homonuclear spins in a liquid NMR sample gives the average density matrix (per molecule) approximately proportional to

$$\rho_{tot} \propto \mathbf{1} + \sum_j \beta_j \sigma_z^j \ , \tag{3.5}$$

where

$$\beta_j = 2\mu_j \mathcal{B}_0 / k_B T = h\omega_j / k_B T \approx h\omega / k_B T \approx \beta \tag{3.6}$$

is the Boltzmann factor for the j'th spin. For a typical nuclear spin of interest, the Boltzmann factor is $<< 1$; for example, with $\omega \approx 100\,\mathrm{MHz}$ for $^{13}\mathrm{C}$ in a static magnetic field of $\mathcal{B}_0 = 9.6$ Tesla, the room-temperature ($T \approx 300\,\mathrm{K}$) Boltzmann factor is of order 10^{-6}. Higher order terms in the density matrix expansion can be neglected [56]. Only the deviation of the density matrix from unity, rescaled in the rest of this paper (at equilibrium, $\rho_{eq} = \sum \sigma_z^j$), represents surplus or deficit populations in energy levels whose transitions are observable in NMR. For the rest of the dissertation, "density matrix" shall refer to the rescaled deviation density matrix.

Evolution of the density matrix is conveniently expressed in the Heisenberg picture, where the Schrödinger equation (Eq. 1.1) becomes

$$\frac{\partial \rho}{\partial t} = \frac{i}{\hbar} [\mathcal{H}, \rho] \ . \tag{3.7}$$

For piecewise time-independent Hamiltonians, the solution to Eq. 3.7 is given by

$$\rho(t_k + \Delta t_k) = e^{\frac{i}{\hbar}\mathcal{H}_k \Delta t_k} \rho(t_k) e^{-\frac{i}{\hbar}\mathcal{H}_k \Delta t_k} \ . \tag{3.8}$$

Therefore, for a unitary operator $U = e^{\frac{i}{\hbar}\mathcal{H}_k}$, a new density matrix is found by applying U:

$\rho(t_k + \Delta t_k) = U\rho(t_k)U^{-1}$. For convenience, in all that follows $\hbar$ will be set to 1.

The equilibrium density matrix represents a highly mixed, thermal state. Techniques now exist whereby it is possible to create an *effective* pure state in a liquid sample of essentially non-interacting molecules at room temperature, meaning that the density matrix transforms under unitary operations exactly as a pure state density matrix [74, 75]. Since only the deviation density matrix, averaged over the whole sample, contains observable magnetization, the results obtained from unitary transformations on a pseudo-pure NMR state are identical to those that would be found were one to perform the same operations on a single quantum system. For example, the same unitary operator (*e.g.*, $\mathcal{U} = e^{i\frac{\pi}{4}\sigma_x^A\sigma_x^B\sigma_y^C}$) that transforms a pure state (*e.g.*, $|+++\rangle$) into a GHZ state (*e.g.*, $|\psi\rangle$) also transforms the deviation density matrix of an ensemble pseudo-pure state into a density matrix with the identical, non-classical correlations. (See Chapter 4 for details about this unitary operator and GHZ correlations.)

3.3.2 Experimental setup

Construction of the quantum feedback loop (and the verification of GHZ correlations in the following chapter) were performed on a Bruker AMX400 spectrometer. In our experimental setup, coils were available to provide a gradient in the z-oriented $\mathcal{B}_0$ across the sample. The result of a gradient is to introduce phase variations in the sample that vary spatially, which, when averaged over the whole sample, represent non-unitary operations on the ensemble density matrix. A gradient pulse produces a net loss of any bulk magnetic moment along the gradient direction by destroying phase coherence and thus removing the single-quantum coherence elements in the density matrix that are off the main diagonal.

In addition, another set of coils in the $x - y$ plane provided rf pulses that cause nearly unitary rotations of the density matrix. Selective pulses can be created using shaped pulses (*e.g.*, sinc or gaussian wave forms) whose net effect in the frequency domain is to rotate on-resonance spins. These selective pulses can be used to provide σ_x or σ_y rotations in the co-rotating reference frame. Similarly, unitary transformations that at a desired time average to zero unwanted terms in the Hamiltonian ($\mathcal{H}_0$) are possible by applying appropriately-named [π] refocusing pulses.

The rf coils were also used as pick-up coils to measure magnetization in the $x - y$ plane. For three spins (as in the demonstration below), the observable magnetization is the

spatially-averaged signal (S) during NMR signal acquisition, which is proportional to

$$S(t) = Tr\left[\rho(t)\sum_j \left(\sigma_x^j + i\sigma_y^j\right)\right] . \tag{3.9}$$

Other elements of the density matrix are unobserved. Correlations between spins can be read directly from the spectra produced by plotting the Fourier transform of the induction signal.

The sample used in the feedback loop demonstration was triply-labeled (^{13}C) alanine ($C_3H_7NO_2$). The principal terms in the Hamiltonian for the spin system are

$$\mathcal{H}_0 \approx \frac{1}{2}\omega_A\sigma_z^A + \frac{1}{2}\omega_B\sigma_z^B + \frac{1}{2}\omega_C\sigma_z^C + \frac{\pi}{2}J_{AB}\sigma_z^A\sigma_z^B + \frac{\pi}{2}J_{BC}\sigma_z^B\sigma_z^C \tag{3.10}$$

where ω_j is the Larmor precession frequency (including the effects of chemical shift) for spin j, and where J_{jk} is the usual scalar coupling between spins j and k. The experiment used ^{1}H decoupling to effectively remove (average to zero) the terms in the Hamiltonian that couple the hydrogen and carbon nuclei. The strengths of the coupling interactions between the carbon spins in alanine are $J_{AB} = 53.4\,\text{Hz}$ and $J_{BC} = 35.3\,\text{Hz}$. The scalar interaction between spins A and C is small ($J_{AC} = 1.4\,\text{Hz}$); this term in the Hamiltonian, and all other interactions (including the effects of diffusion and relaxation), can be neglected over the $\approx 160\,\text{ms}$ during which the entire experiment takes place. A typical spectrum is shown in Fig. 3-2.

Table 3.1: **Constants in the Alanine Experiments.**

Constant	Symbol	Value
Background magnetic field	$\mathcal{B}_0$	9.6 Tesla
Transmitter frequency	ω_f	100.617360 MHz
Resonant frequency of A spins (relative to ω_f)	ω_A	12580 Hz
Resonant frequency of B spins (relative to ω_f)	ω_B	0 Hz
Resonant frequency of C spins (relative to ω_f)	ω_C	-3442 Hz
Scalar coupling constant	J_{AB}	53.4 Hz
Scalar coupling constant	J_{BC}	35.3 Hz
Scalar coupling constant	J_{AC}	1.4 Hz
Relaxation time constant	T_1	$\approx$1 s
Decoherence time constant	T_2	$\approx$450 ms

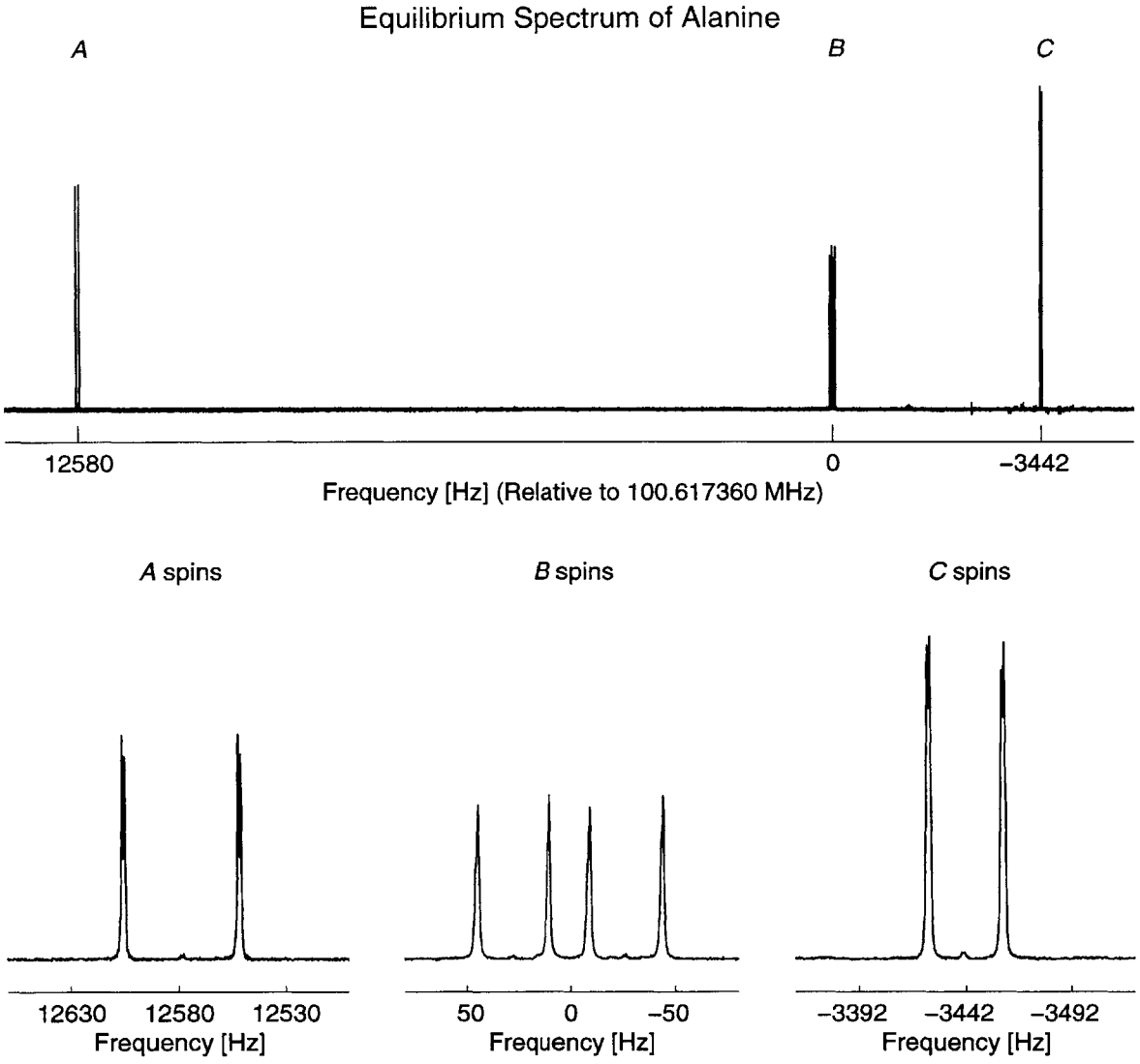

Figure 3-2: **NMR Spectrum of Alanine.** The spectrum is the Fourier transform of the free induction decay signal observed after each spin's magnetic moment is rotated into the transverse plane from equilibrium. The spectrum shows a multiplet of four lines for each of the three ^{13}C nuclei, each corresponding to an allowed energy transition, and plotted with frequency (or energy) increasing from right to left. The frequency of each of the four lines in a multiplet corresponds to the resonant frequency when the other two spins are either $|--\rangle$, $|-+\rangle$, $|+-\rangle$, or $|++\rangle$. For example, the spectrum for the B spins shows the four lines that correspond to the case when the A and C spins are, respectively (from left to right): $|-\rangle_A|-\rangle_C$, $|-\rangle_A|+\rangle_C$, $|+\rangle_A|-\rangle_C$, and $|+\rangle_A|+\rangle_C$.

3.4 Quantum Feedback Control

3.4.1 Controllability of closed-loop quantum systems

As in classical control, two important questions for any quantum control method concern controllability and observability [23]. For Hamiltonian quantum systems with dynamics of the form

$$\mathcal{H} = \sum_k \tau_k(t) \hat{\mathcal{O}}_k^A \hat{\mathcal{O}}_k^B \tag{3.11}$$

where $\hat{\mathcal{O}}^A$ and $\hat{\mathcal{O}}^B$ are Hermitian operators acting on the system (A) and the controller (B), respectively, and where the $\tau_k(t)$ are controls, S. Lloyd extended the classical measures of controllability and observability for fully coherent quantum systems [76]. It is assumed that at least one interaction between system and controller is non-trivial; that is, for some k, neither $\hat{\mathcal{O}}_k^A$ nor $\hat{\mathcal{O}}_k^B$ is the identity. Following the notion that a system is controllable if it can be driven from an arbitrary initial state to any desired final state, Lloyd proposes the following: a quantum system with Hamiltonian $\mathcal{H}$ is controllable by a quantum controller if and only if the algebra generated from $\{\mathcal{H}_0, \mathcal{O}_k\}$ by commutation is the full algebra of Hermitian operators for the system.

The dynamics for the control system presented here consists of the natural Hamiltonian ($\mathcal{H}_0$ in Eq. 3.10) and selective rf pulses (σ_x^A, σ_y^A, σ_x^B, σ_y^B, etc.) as described in the Experimental Setup section above. Note that the natural Hamiltonian contains the coupling term of the form $\sim J_{AB}\sigma_z^A\sigma_z^B$, (with fixed coupling constant J_{AB}). This term provides the coupling between the system and the controller, and can be "turned off," or averaged to zero, at a desired time t by applying refocusing [π] pulses on A and/or B such that the sign of the $\sigma_z^A\sigma_z^B$ term is (+) for net time $\frac{t}{2}$ and (−) for the other net time $\frac{t}{2}$. Given the usual commutation relations among the Pauli spin operators, the algebra generated by $\{\sigma_z^A, \sigma_z^B, \sigma_z^A\sigma_z^B, \sigma_x^A, \sigma_x^B\}$ easily satisfies Lloyd's controllability criteria, even without using σ_y^A and σ_y^B:

$$\begin{aligned}
\sigma_x^A &= \sigma_x^A \\
\sigma_x^B &= \sigma_x^B \\
\sigma_y^A &= \frac{i}{2}[\sigma_x^A, \sigma_z^A] \\
\sigma_y^B &= \frac{i}{2}[\sigma_x^B, \sigma_z^B]
\end{aligned}$$

$$
\begin{aligned}
\sigma_z^A &= \sigma_z^A \\
\sigma_z^B &= \sigma_z^B \\
\sigma_x^A\sigma_x^B &= \frac{1}{16}[[\sigma_x^A,\sigma_z^A],[[\sigma_x^B,\sigma_z^B],\sigma_z^A\sigma_z^B]]] \\
\sigma_x^A\sigma_y^B &= \frac{i}{8}[[\sigma_x^A,\sigma_z^A],[\sigma_x^B,\sigma_z^A\sigma_z^B]] \\
\sigma_x^A\sigma_z^B &= \frac{1}{4}[[\sigma_x^A,\sigma_z^A],\sigma_z^A\sigma_z^B] \\
\sigma_y^A\sigma_x^B &= \frac{-i}{8}[[\sigma_x^A,\sigma_z^A\sigma_z^B],[\sigma_x^B,\sigma_z^B] \\
\sigma_y^A\sigma_y^B &= \frac{1}{4}[[\sigma_x^A,\sigma_z^A\sigma_z^B],\sigma_x^B] \\
\sigma_y^A\sigma_z^B &= \frac{i}{2}[\sigma_x^A,\sigma_z^A\sigma_z^B] \\
\sigma_z^A\sigma_x^B &= \frac{1}{4}[[\sigma_x^B,\sigma_z^B],\sigma_z^A\sigma_z^B] \\
\sigma_z^A\sigma_y^B &= \frac{i}{2}[\sigma_x^B,\sigma_z^A\sigma_z^B] \\
\sigma_z^A\sigma_z^B &= \sigma_z^A\sigma_z^B
\end{aligned}
$$

Therefore, the quantum system is controllable via fully coherent quantum feedback.

3.4.2 Controlled-NOT: A geometric effect

An integral part of coherent feedback is coherently correlating spins; it is necessary for coherent sensing and actuation, and in general is required for all schemes in quantum information processing. Correlating spins can be accomplished using a C-NOT gate (similar to the XOR gate in digital logic) [74]. In effect, the C-NOT gate applies a unitary transformation that "flips" the state of one of the spins conditional on the state of another spin [77]. Specifically, application of

$$U_{\text{C-NOT}} = e^{\pm i\frac{\pi}{2}\sigma^A_{\alpha(\theta)}\frac{1}{2}(1-\sigma_z^B)} \tag{3.12}$$

rotates the A spins by $[\pi]$ about the axis $\alpha(\theta)$ (axis in the $x-y$ plane with phase θ) only if the B spins are in the state $|-\rangle_B$. The gate can be decomposed using unitary transformations that involve only scalar coupling terms in the natural Hamiltonian and selective rotations; using the algebraic rules of Ref. [77] produces:

$$U_{\text{C-NOT}} = e^{i\frac{\pi}{4}\sigma_z^A}e^{i\frac{\pi}{4}\sigma^A_{\alpha(\theta)}}e^{-i\frac{\pi}{4}\sigma_z^A\sigma_z^B}e^{-i\frac{\pi}{4}\sigma^A_{\alpha(\theta-90^\circ)}}\ . \tag{3.13}$$

Pulse sequences that implement this transformation are shown in the experiment below.

3.4.3 Experiment

The goal of the quantum feedback experiment is to control the state of a "system" spin (spin A) by constructing a quantum feedback loop via a "controller" spin (spin B). More specifically, the experiment sets up an initial quantum correlation between the controller spin and a third, "ancilla" spin (spin C). The ancilla spin is not part of the controller and does not participate in the feedback loop; it is coupled only weakly to the system spin and effectively does not interact with the system spin over the time scale that the feedback loop operates. A quantum feedback loop is then used to transfer the correlation from the controller spin to the system spin.

Since the scalar coupling between spins A and C is small (see Table 3.1), we identify the system with spin A, the sensor/controller/actuator with spin B, and the ancilla with spin C—all distinct ^{13}C nuclei in an alanine molecule. (See Fig. 3-2.) All spins are initially in the thermal state (Eq. 4.4); thus, the spins are initially uncorrelated.

The experimental procedure for setting up the entangled state and accomplishing the coherent quantum feedback is as follows:

I. *Quantum Correlation*: a correlated state is set up between the controller spin B and the ancilla spin C. The pulse sequence

$$\rho_{eq} \longrightarrow -\left[\frac{\pi}{2}\right]_y^{BC}\left[\frac{1}{4J_{BC}}\right]-[\pi]_x^A-\left[\frac{1}{4J_{BC}}\right]-\left[\frac{\pi}{2}\right]_x^B \longrightarrow \rho_{init}$$

puts the spins in a state whose reduced density matrix is:

$$\rho_{init} = -\sigma_z^A + \sigma_z^B\sigma_z^C - \sigma_y^B\sigma_y^C \ ,$$

or, in matrix form,

$$\rho_{init} = \begin{pmatrix} -1 & 0 \\ 0 & 1 \end{pmatrix}^{(A)} \otimes \begin{pmatrix} 1 & 0 & 0 & 1 \\ 0 & -1 & -1 & 0 \\ 0 & -1 & -1 & 0 \\ 1 & 0 & 0 & 1 \end{pmatrix}^{(BC)} . \tag{3.14}$$

In the pulse sequence notation, each bracket containing an angle represents a rotation of the spins in the superscript around the axis in the subscript by the angle enclosed within the bracket, and the terms containing J_{jk} indicate a delay of the indicated time for the scalar coupling between spins j and k to develop before the next rotation is applied. A representative spectrum of this state is shown in Fig. 3-3.

The density matrix prepared by the above pulse sequence cannot be written in the form of Eq. 3.3 (or Eq. 3.4), and so cannot be transferred by a classical controller. Note that the correlation procedure puts B and C in a mixture of Einstein-Podolsky-Rosen (EPR) entangled states [60, 61, 64-68]. As noted in [67], this state is a separable, *i.e.*, unentangled state; it nonetheless exhibits quantum correlation that cannot be transferred classically. If the same pulse sequence were applied at zero temperature, B and C would be in a pure EPR state and would be strongly entangled. The quantum feedback loop created below transfers any form of quantum correlation, including entanglement.

II. *Coherent sensing*: the controller acquires quantum information from the system. The pulse sequence

$$\rho_{init} \longrightarrow \left[-\frac{\pi}{2}\right]_x^B - \left[\frac{1}{4J_{AB}}\right] - [\pi]_x^C - \left[\frac{1}{4J_{AB}}\right] - \left[\frac{\pi}{2}\right]_y^B \longrightarrow \rho_{sens}$$

flips B if and only if A is in the state $|-\rangle_A$: a C-NOT gate. B becomes coherently correlated with A, *i.e.*, B has now acquired quantum information about A. At this point the spins are in the state

$$\rho_{sens} = -\sigma_z^A - \sigma_z^A \sigma_x^B \sigma_z^C - \sigma_x^B \sigma_y^C \ .$$

See Fig. 3-4.

III. *Coherent control and actuation*: the controller processes the quantum information and feeds it back to the system. The C-NOT pulse sequence

$$\rho_{sens} \longrightarrow \left[\frac{\pi}{2}\right]_x^A - \left[\frac{1}{4J_{AB}}\right] - [\pi]_x^C - \left[\frac{1}{4J_{AB}}\right] - \left[\frac{\pi}{2}\right]_y^A \longrightarrow \rho_{act}$$

first flips A if and only if B is in the state $|-\rangle$. This sequence causes B to coherently process the quantum information acquired in step II and to feed it back to act on A. A and B are

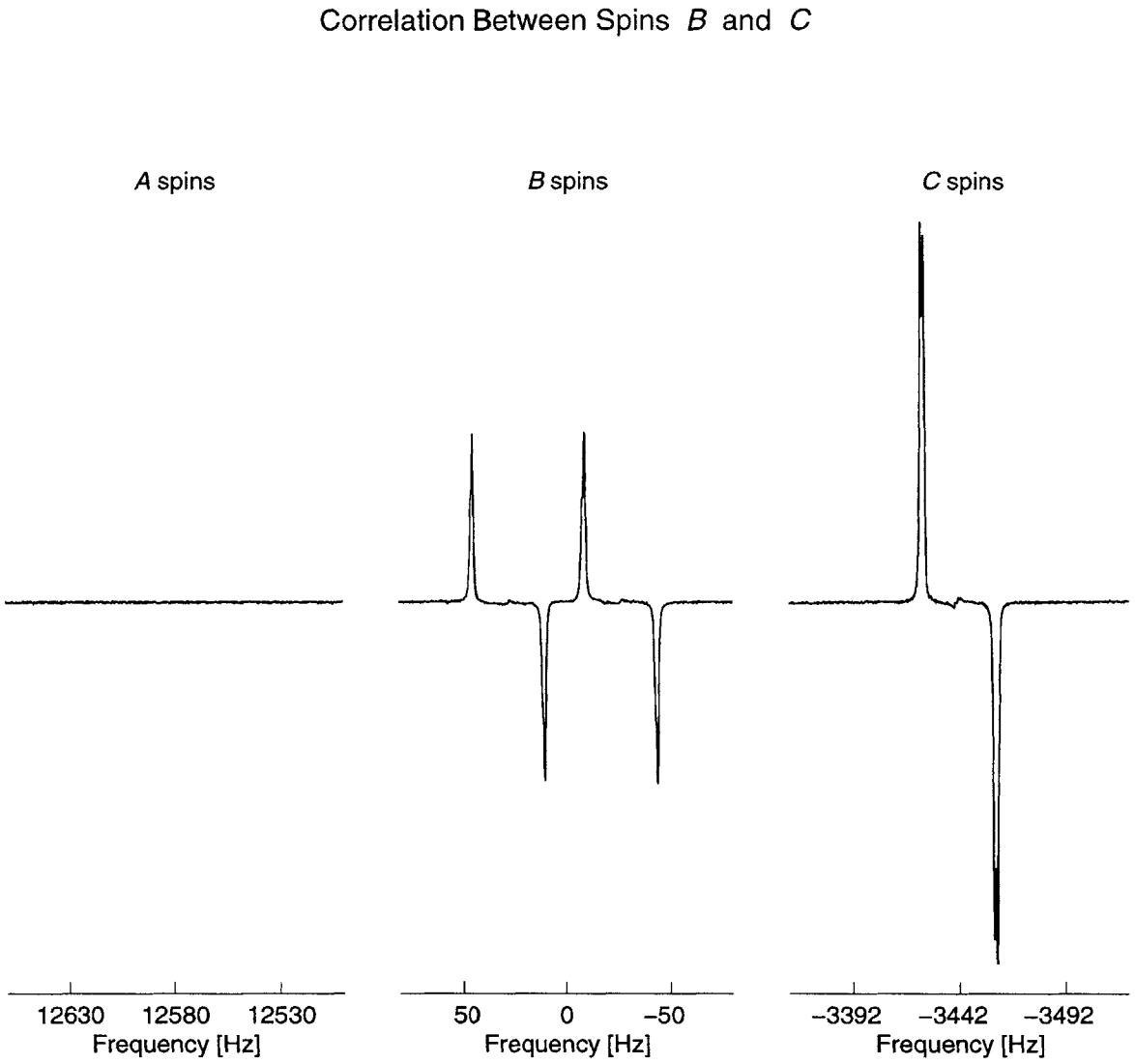

Figure 3-3: **A Quantum Correlation.** The controller spin (B) and an ancilla spin (C) are perfectly correlated. For example, the B spins are $|+\rangle$ whenever the C spins are $|-\rangle$, and are $|-\rangle$ whenever the C spins are $|+\rangle$. Neither B nor C is correlated with A, since half of the B spins (and half of the C spins) are $|+\rangle$ and half are $|-\rangle$ whenever A is $|+\rangle$. The same is true when A is $|-\rangle$. No classical controller can transfer the correlation between B and C to A.

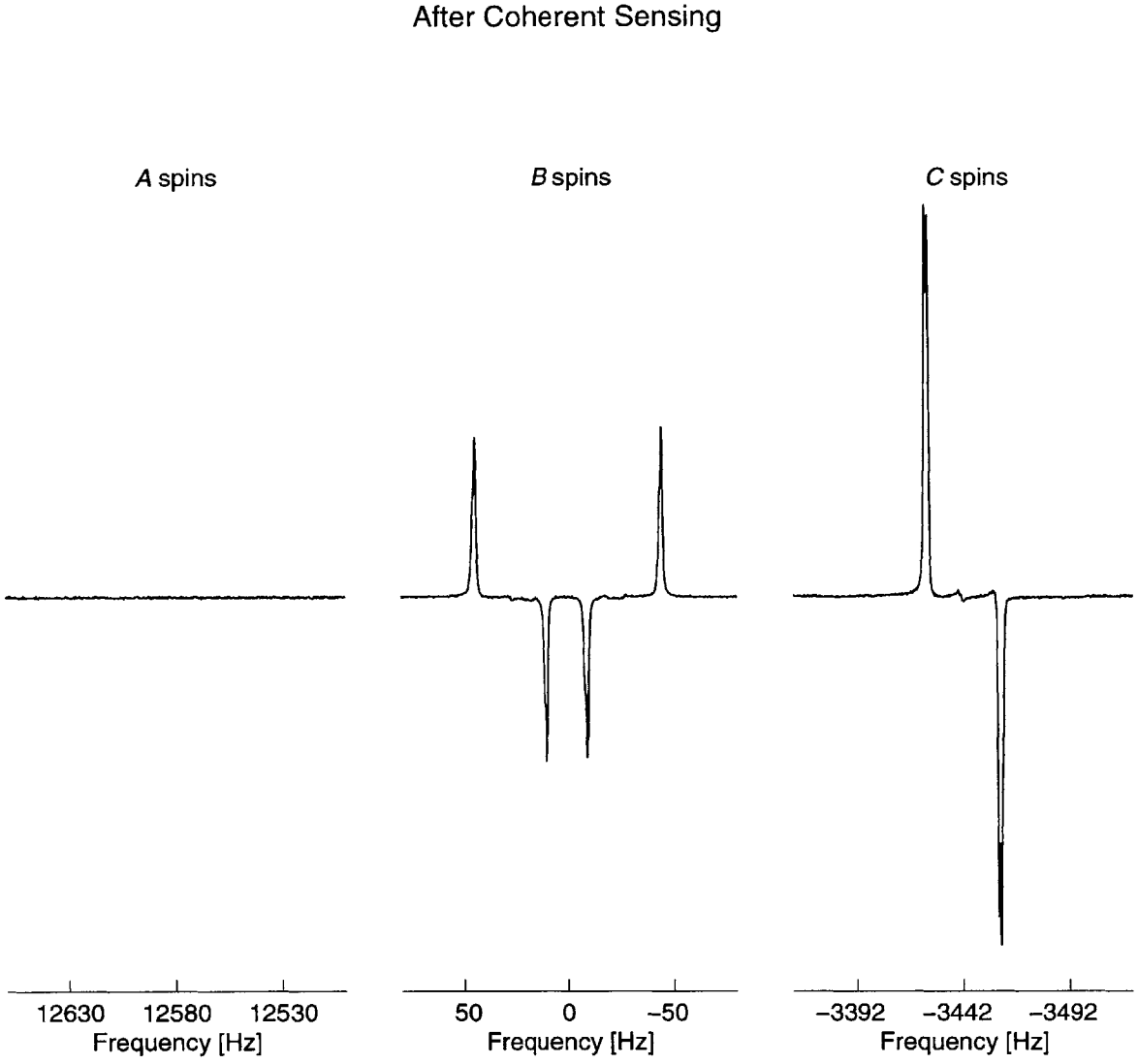

Figure 3-4: **The Controller Acquires Quantum Information.** Instead of making a von Neumann measurement, the purely quantum controller B becomes correlated with the system A. B acquires both amplitude and phase information about the state of A. However, no irreversible measurement is made.

still correlated at this point. A final C-NOT pulse sequence

$$\rho_{act} \longrightarrow \left[\frac{\pi}{2}\right]_x^B - \left[\frac{1}{4J_{AB}}\right] - [\pi]_x^C - \left[\frac{1}{4J_{AB}}\right] - \left[\frac{\pi}{2}\right]_y^B \longrightarrow \rho_f$$

completes the feedback loop, decorrelating A from B and completing the transfer from B to A of B's initial quantum correlation with C. The spins are now in the state

$$\rho_f = -\sigma_z^B + \sigma_z^A\sigma_z^C - \sigma_y^A\sigma_y^C \ ,$$

or, in matrix form,

$$\rho_f = \begin{pmatrix} -1 & 0 \\ 0 & 1 \end{pmatrix}^{(B)} \otimes \begin{pmatrix} 1 & 0 & 0 & 1 \\ 0 & -1 & -1 & 0 \\ 0 & -1 & -1 & 0 \\ 1 & 0 & 0 & 1 \end{pmatrix}^{(AC)} \ . \tag{3.15}$$

A representative spectrometer trace of this state is shown in Fig. 3-5.

3.4.4 Results

As Figs. 3-3 and 3-5 show, the quantum feedback loop operates as expected. The measured initial and final density matrices, as determined via tomography, were experimentally found to be

$$\rho_{init} \propto \begin{pmatrix} -1.0 & 0.01 \\ 0.01 & 1.0 \end{pmatrix}^{(A)} \otimes \begin{pmatrix} 0.99 & -0.04 & -0.12i & 1.0 \\ -0.04 & -0.99 & -1.0 & -0.08i \\ 0.12i & -1.0 & -0.99 & 0.04 \\ 1.0 & 0.08i & 0.04 & 0.99 \end{pmatrix}^{(BC)} \ ,$$

$$\rho_f \propto \begin{pmatrix} -0.96 & 0.12 \\ 0.12 & 0.96 \end{pmatrix}^{(B)} \otimes \begin{pmatrix} 0.92 & 0.03i & -0.05i & 0.97 \\ -0.03i & -1.04 & -0.93 & -0.05i \\ 0.05i & -0.93 & -0.92 & 0.03i \\ 0.97 & 0.05i & -0.03i & 1.04 \end{pmatrix}^{(AC)} \ ,$$

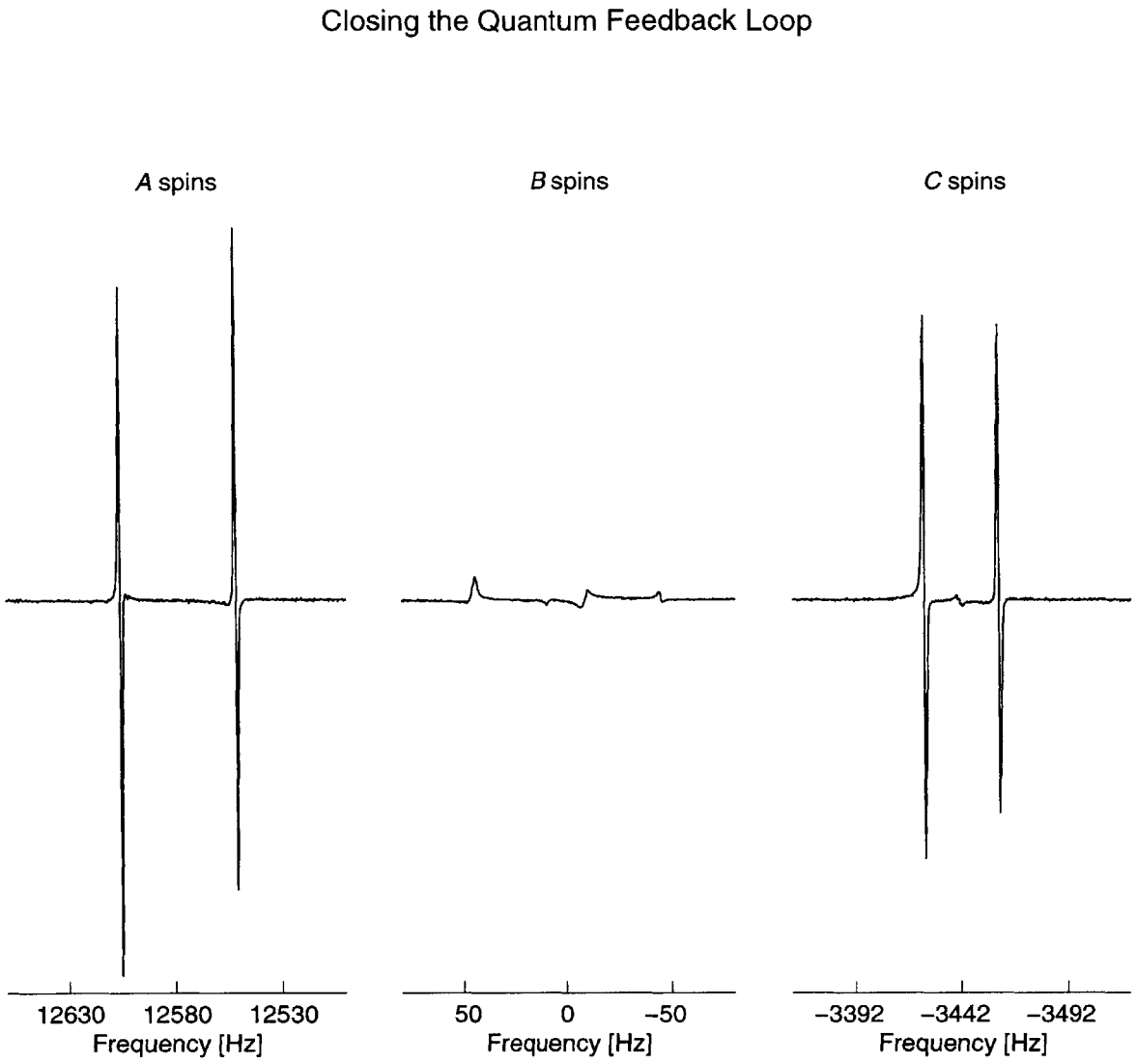

Figure 3-5: **Closing the Feedback Loop.** Allowing the controller B to interact with system A in a coherent and controlled manner has allowed B to transfer its initial correlation with ancilla C to A. At this point, A and C are correlated, although they have no direct interaction between them. In the trace, A is $|-\rangle$ whenever C is $|+\rangle$, and A is $|+\rangle$ whenever C is $|-\rangle$. The same is true of C with respect to A. The B spins, in contrast, end in the same uncorrelated state in which A began.

respectively. The fidelity of the transmission of the quantum correlation, defined for the initial and final reduced density matrices as

$$F(\rho_i, \rho_f) = 1 - \left[\frac{\mathrm{Tr}\,(\rho_f - \rho_i)^2}{\mathrm{Tr}\rho_i^2}\right]^{\frac{1}{2}} \tag{3.16}$$

was 91.5%. Errors were mainly due to imperfect flip angles, especially miscalibration of the refocusing $[\pi]$ pulses, and to signal noise incorporated in the data during numerical analysis. Decoherence caused by the relaxation processes contributed only minor errors since the entire program execution time of 42.3 ms was much smaller than the smallest T_2 for the nuclei (approximately 450 ms for the C spins). The low errors for the transfer of correlation (8.5%) and for the transmission of the initial system state to the final controller state (11.5%) indicates the high degree to which the transformations were unitary.

3.5 Conclusions

The quantum feedback loop accomplishes several tasks that cannot be performed by conventional feedback control of quantum systems. First, it is non-destructive: the initial state of the system spin is not destroyed by sensors but instead transferred to the controller spin. Second, it is deterministic: because no irreversible measurement is made, no probabilistic element is introduced. Third, the transfer of quantum correlation to A could not be accomplished by a classical controller, as any measurement that a classical controller makes on B would destroy some off-diagonal terms in the correlated state $2I_z^B I_z^C - 2I_y^B I_y^C$. To transfer quantum correlation from B to A, A and B must interact directly via an intrinsically quantum-mechanical interaction such as the quantum feedback loop demonstrated here. In addition, the weak interaction between A and C, ($J_{AC} = 1.4$ Hz), precludes any direct transfer of correlation from C to A over the short time scale < 0.05 seconds over which the experiment takes place.

In addition to transfer of quantum correlation, potential applications of coherent quantum feedback control include stabilizing quantum dynamics [78](*e.g.*, to improve frequency standards), quantum trajectory tracking, and quantum error correction [70-73].

As this experiment suggests, the implementation of a quantum feedback loop in NMR is particularly straightforward to accomplish. The concept of fully quantum feedback is not

limited to NMR, however, and coherent quantum feedback loops might also be constructed, albeit with more difficulty, in the context of quantum optics, ion and atom traps, and Bose-Einstein condensates. Essentially any system that allows quantum information processing can be used to construct a coherent quantum feedback loop.

Chapter 4

GHZ: An Open-Loop Control Experiment

4.1 Introduction

The GHZ experiment presented below serves to establish two main objectives: first, to explicitly demonstrate the design and construction of an open-loop quantum mechanical controller; and second, to demonstrate Greenberger-Horne-Zeilinger correlations in an ensemble of quantum mechanical systems.

4.1.1 Quantum mechanics and paradoxes

As noted in the previous chapter, quantum mechanics is well-known to exhibit strange effects. Perhaps the strangest of these effects is the possibility of correlations between quantum-mechanical systems that, under certain measurement scenarios, defy an intuitive explanation of the results when a classical view of physics serves as the basis for that intuition. The original such effect is the Einstein-Podolsky-Rosen (EPR) effect [64, 65]. In the version of this effect due to Bohm and to Bell [66, 79], two particles in an entangled, or quantum-correlated, state exhibit correlations between the results of measurements that cannot be explained under the assumption that those results were predetermined by the states of hidden variables. Specifically, consider two spin-$\frac{1}{2}$ particles in a quantizing magnetic field oriented along the z-axis. The standard product basis for the pure states of such

a system is

$$\{|++\rangle, |+-\rangle, |-+\rangle, |--\rangle\},$$

where $|+\rangle$ and $|-\rangle$ respectively represent the state of a spin: aligned ("up") or anti-aligned ("down") with the external magnetic field. Suppose the two-spin system is prepared in the pure state $|++\rangle$, and subsequently rotated via the unitary operator

$$U_s = e^{-i\frac{\pi}{2}\sigma_y^{(1)}\left(\frac{1}{2}\sigma_x^{(2)}-1\right)}, \tag{4.1}$$

where σ_k is the Pauli spin matrix representation proportional to the angular momentum operator along the k-axis, and the superscript indicates to which spin the operator is applied. Then the resulting state is the singlet state,

$$|\psi_s\rangle = \frac{1}{\sqrt{2}}\left(|+-\rangle - |-+\rangle\right) . \tag{4.2}$$

Such a state is maximally entangled with respect to the product basis since the state of the system can be completely described by the single, inseparable wave function of Eq. 4.2 while the uncertainty in the state of either spin—whether "up" or "down" —is maximal.

It is clear that the singlet state (Eq. 4.2) could in principle be used to verify the non-local effect of quantum mechanics. For example, if a measurement were made of the polarization of the first spin along, say, the x–axis, quantum theory predicts that the wave function for the two-spin system would collapse to either $|+-\rangle$ or $|-+\rangle$, each with probability $\frac{1}{2}$. Then, if a measurement were subsequently made of the polarization of the second spin along the x–axis, quantum mechanics predicts with certainty that the second spin will be anti-aligned with respect to the first spin. Although in this example the x–axis was chosen as the measurement axis, the result (*i.e.*, anti-aligned spins) is independent of this choice; however, it is perhaps counterintuitive that the result is also independent of how temporally close the two measurements are made, regardless of the spatial distance between the two particles. A collection of data on a statistical number of such measurements would reveal that this particular correlation violates Bell's inequalities.

Original attempts to reconcile intuition about local effects with the non-local quantum predictions led some scientists to propose additional variables, called "hidden" variables, to describe the outcomes of quantum measurements [64, 65, 79]. However, in 1964 J. Bell

demonstrated that no classical probability distribution over a finite set of variables could reproduce the quantum-theoretic predictions [66, 80-83].

In the EPR effect, the contradiction with the classical hidden variable picture is statistical: the probabilities for the results of measurements on the quantum systems violate Bell's inequalities, which set limits on the maximum amount of correlation possible between two classical systems. A long series of experiments are required to convincingly establish the existence of the EPR correlations. A more striking contradiction with the local hidden variable picture is obtained in the Greenberger-Horne-Zeilinger (GHZ) effect, in which a single set of measurements on *three* correlated quantum particles gives results that are perfectly correlated in a pattern that is classically impossible [84]. While experimental evidence to support the non-local predictions of quantum theory using EPR-like experiments have been performed using visible photon-correlation experiments [85-91], double-slit scattering experiments [92], and gamma-ray experiments [93-95], the GHZ effect has resisted experimental demonstration until recently.

4.1.2 The Greenberger-Horne-Zeilinger experiment

The following version of the GHZ experiment is due to Mermin [96]. Consider three spin-1/2 particles, labeled A, B, and C, prepared in the state

$$|\psi\rangle = \frac{1}{\sqrt{2}}\left(|+++\rangle \; - \; |---\rangle\right) \; , \tag{4.3}$$

where as above, $|+\rangle$ represents "up" along the z-axis and $|-\rangle$ signifies "down" along the z-axis. Now consider the results of the following products of spin measurements, each made on state $|\psi\rangle$:

(i) particle A along x, particle B along y, and particle C along y. Note that since $\sigma_x^A \sigma_y^B \sigma_y^C |\psi\rangle = +|\psi\rangle$, the product of the results of these measurements should be $+1$, where $+1$ corresponds to the result $|+\rangle$, and -1 corresponds to $|-\rangle$.

(ii) particle A along y, particle B along x, and particle C along y. As in scenario (i), since $\sigma_y^A \sigma_x^B \sigma_y^C |\psi\rangle = +|\psi\rangle$, the product of these results should be $+1$.

(iii) particle A along y, particle B along y, and particle C along x. Again, since $\sigma_y^A \sigma_y^B \sigma_x^C |\psi\rangle = +|\psi\rangle$, the product of these results should also be $+1$.

(iv) particle A along x, particle B along x, and particle C along x. In this case, there

is a significant sign difference: $\sigma_x^A \sigma_x^B \sigma_x^C |\psi\rangle = -|\psi\rangle$, so the product of the results should be -1.

The minus sign in the final scenario is crucial for those who attempt to differentiate between quantum mechanical and classical (*i.e.*, hidden-variable) descriptions of reality. No classical hidden-variable model that assigns a classical variable (such as $+1$ or -1) to the measurement of each individual particle's spin along axes x and y could reproduce the quantum predictions: classically, the product of the four scenarios above for a hidden-variable model must yield $+1$ because each particle is measured along each of the two axes exactly twice.

In addition to demonstrating purely quantum correlations that have no classical analog, the above set of measurements has the potential to verify the hallmark of quantum "weirdness": non-locality. The GHZ experiment—as originally conceived—requires that the measuring apparatuses for the three particles be sufficiently distant from each other so as to eliminate the possibility of local, classical interactions between measurements that might duplicate the quantum mechanical predictions. In NMR experiments, the effective distances between any three spins in a molecule are typically a few angstroms at most; as such, it is practically impossible to demonstrate non-local effects using NMR. However, the NMR experiment below shows how it is possible to create correlations in an ensemble of spins that collectively represent the same quantum GHZ correlations that would be present in a pure 3-spin system in a GHZ state.

4.1.3 Using NMR to demonstrate GHZ correlations

GHZ experiments on pure, 3-particle systems are difficult to realize in the laboratory where the problems associated with faithfully preparing the required state $|\psi\rangle$ and carefully making the necessary measurements pose formidable obstacles. An experiment by Bouwmeester *et al.* exhibits an optical version of the GHZ state for widely separated photons [97]. However, the way in which this experiment was performed made it difficult to exhibit the full set of GHZ correlations. Recent discoveries in the field of quantum information processing using NMR make possible an analog GHZ experiment that validates the GHZ correlations required by a quantum mechanical description of the universe [55, 58, 74]. The idea of using NMR to demonstrate GHZ correlations was proposed in [98], and an effective GHZ state was first created using NMR in [99].

NMR offers a number of advantages in performing tests of few-particle quantum mechanics, including: (1) weak measurements that allow the direct determination of ensemble density matrices; (2) long decoherence times; (3) simple, well-understood Hamiltonians; (4) gradient techniques that allow the construction of effective pure states and the controlled decoherence of samples. These features of NMR make it possible to use quantum systems in mixed states at room temperature to mimic precisely the dynamics of a quantum system in a pure state at low temperature. As a result, NMR is an ideal demonstration system for the predictions of quantum mechanics involving few-variable systems.

Despite the advantages of NMR quantum information processing techniques listed above, it is important to note that demonstrating GHZ correlations using room-temperature NMR differs in significant ways from performing the GHZ experiment as originally envisaged. In particular, because the NMR experiment is inherently local, the NMR demonstration of GHZ correlations cannot rule out nonstandard interactions between classical hidden variables that conspire to exhibit apparently quantum mechanical correlations. In addition, because the NMR experiment is performed on thermal states, though the spins in the experiment mimic the effects of entanglement, they are not in fact entangled: as a result, the NMR experiment cannot rule out local hidden variables. Nonetheless, like the optical experiment reported in [97], the NMR demonstration of GHZ correlations provides unambiguous results that clearly follow the predictions of quantum mechanics. The correspondence of these results from very different physical systems provides confirmation (though not proof) of the underlying quantum nature of physical dynamics and strongly suggest that a full GHZ experiment would lead to the same results.

It is important to keep in mind that although the density matrix for an ensemble in an effective pure state is the same as the density matrix for an ensemble in which some fraction of the systems are in a pure state and the remainder are in a completely mixed state, these two ensembles are not the same. Two different ensembles may have the same density matrix [100]. In particular, when an effective GHZ state is constructed in an ensemble composed of some systems in a pure state and the remainder in a fully mixed state, the systems in a pure state are in fact in GHZ states. In the ensemble constructed here, each of the systems is in a unitarily-transformed version of a thermal state; none are in GHZ states. Nevertheless, since two ensembles with the same density matrix are indistinguishable with respect to measurement, the effective GHZ state constructed is just as effective as an actual

GHZ state for demonstrating the correlations predicted by quantum mechanics.

4.2 Demonstration of Open-loop Control of a Quantum System

As in the previous chapter, the experiment below used the three ^{13}C nuclei in an ensemble of alanine molecules. (See Fig. 3-2). The experiment creates correlations in the ensemble which, when measured, reveal the same correlated pattern that would be present in a pure three-particle GHZ experiment.

4.2.1 Experiment

The experiment works as follows:

(I) *Equilibration.* The sample is allowed to come to thermal equilibrium, in which the density matrix is:

$$\rho_{eq} = \sigma_z^A + \sigma_z^B + \sigma_z^C = \begin{pmatrix} 3 & 0 & 0 & 0 & 0 & 0 & 0 & 0 \\ 0 & 1 & 0 & 0 & 0 & 0 & 0 & 0 \\ 0 & 0 & 1 & 0 & 0 & 0 & 0 & 0 \\ 0 & 0 & 0 & -1 & 0 & 0 & 0 & 0 \\ 0 & 0 & 0 & 0 & 1 & 0 & 0 & 0 \\ 0 & 0 & 0 & 0 & 0 & -1 & 0 & 0 \\ 0 & 0 & 0 & 0 & 0 & 0 & -1 & 0 \\ 0 & 0 & 0 & 0 & 0 & 0 & 0 & -3 \end{pmatrix} \tag{4.4}$$

(II) *Preparation.* The sample is prepared in an incoherent mixture of two pseudo-pure states using the following operations:

$$\begin{aligned} \rho_{eq} \longrightarrow & \left[\frac{\pi}{2}\right]^B_{90^\circ} - \left[\frac{\partial \mathcal{B}_z}{\partial z}\right] \\ & - \left[\frac{\pi}{2}\right]^C_{-90^\circ} - \left[\frac{1}{8J_{BC}}\right] - [\pi]^H_{0^\circ} - \left[\frac{1}{8J_{BC}}\right] - \left[\frac{\pi}{2}\right]^C_{135^\circ} - \left[\frac{\partial \mathcal{B}_z}{\partial y}\right] \\ & - \left[\frac{\pi}{2}\right]^A_{-90^\circ} - \left[\frac{1}{8J_{AB}}\right] - [\pi]^H_{0^\circ} - \left[\frac{1}{8J_{AB}}\right] - \left[\frac{\pi}{2}\right]^A_{135^\circ} - \left[\frac{\partial \mathcal{B}_z}{\partial x}\right] \\ & - \left[\frac{\pi}{2}\right]^B_{0^\circ} - \left[\frac{1}{4J_{AB}}\right] - [\pi]^H_{0^\circ} - \left[\frac{1}{4J_{AB}}\right] - \left[\frac{\pi}{2}\right]^B_{-90^\circ} \longrightarrow \rho_{pp} \ . \end{aligned}$$

As in the previous chapter, each bracketed expression represents one matrix operation: brackets containing angles indicate an rf pulse that selectively rotates the superscripted spin by the specified angle, where the subscripted "phase" designates the axis of rotation in the $x-y$ plane of the co-rotating frame; and brackets containing a coupling constant indicate free evolution of the system under the natural Hamiltonian for the time indicated to allow the pertinent scalar coupling term to correlate spins. Brackets with partial derivatives indicate an applied gradient in the magnetic field along the direction in the denominator; the effect of the gradient pulses is to change the eigenstructure of the density matrix. Brackets with a superscript $(^H)$ represent hard pulses on the hydrogen channel. Selective pulses in this experiment required a pulse length of 2 ms.

The result of the preparation sequence is the density matrix:

$$\begin{aligned}\rho_{pp} &= \frac{1}{4}\sigma_z^A + \frac{1}{4}\sigma_z^B + \frac{1}{4}\sigma_z^C + \frac{1}{4}\sigma_z^A\sigma_z^B\sigma_z^C \\ &= \begin{pmatrix} 1 & 0 & 0 & 0 & 0 & 0 & 0 & 0 \\ 0 & 0 & 0 & 0 & 0 & 0 & 0 & 0 \\ 0 & 0 & 0 & 0 & 0 & 0 & 0 & 0 \\ 0 & 0 & 0 & 0 & 0 & 0 & 0 & 0 \\ 0 & 0 & 0 & 0 & 0 & 0 & 0 & 0 \\ 0 & 0 & 0 & 0 & 0 & 0 & 0 & 0 \\ 0 & 0 & 0 & 0 & 0 & 0 & 0 & 0 \\ 0 & 0 & 0 & 0 & 0 & 0 & 0 & -1 \end{pmatrix},\end{aligned} \tag{4.5}$$

which transforms like a balanced mixture of two pseudo-pure states:

$$\rho_{pp} \propto \frac{1}{2}\left(|+++\rangle\langle+++| \; - \; |---\rangle\langle---|\right) \; .$$

(III) *Rotation.* The density matrix for the sample is now rotated via unitary operator $e^{i\frac{\pi}{4}\sigma_x^A\sigma_x^B\sigma_y^C}$ using the sequence:

$$\begin{aligned}\rho_{pp} \longrightarrow \; & \left[\frac{\pi}{2}\right]^A_{-90^\circ} - \left[\frac{1}{4J_{AB}}\right] - [\pi]^H_{0^\circ} - \left[\frac{1}{4J_{AB}}\right] - \\ & \left[\frac{\pi}{2}\right]^{B,C}_{0^\circ} - \left[\frac{1}{4J_{BC}}\right] - [\pi]^H_{0^\circ} - \left[\frac{1}{4J_{BC}}\right] -\end{aligned}$$

$$\left[\frac{\pi}{2}\right]^{B,C}_{180^\circ} - \left[\frac{1}{4J_{AB}}\right] - [\pi]^{H}_{0^\circ} - \left[\frac{1}{4J_{AB}}\right] - \left[\frac{\pi}{2}\right]^{A}_{-90^\circ} \longrightarrow \rho_{GHZ} \ .$$

The density matrix thus rotated becomes

$$\begin{aligned}
\rho_{GHZ} &= \frac{1}{4}\sigma_x^A\sigma_y^B\sigma_y^C + \frac{1}{4}\sigma_y^A\sigma_x^B\sigma_y^C + \frac{1}{4}\sigma_y^A\sigma_y^B\sigma_x^C - \frac{1}{4}\sigma_x^A\sigma_x^B\sigma_x^C \\
&= \begin{pmatrix}
0 & 0 & 0 & 0 & 0 & 0 & 0 & -1 \\
0 & 0 & 0 & 0 & 0 & 0 & 0 & 0 \\
0 & 0 & 0 & 0 & 0 & 0 & 0 & 0 \\
0 & 0 & 0 & 0 & 0 & 0 & 0 & 0 \\
0 & 0 & 0 & 0 & 0 & 0 & 0 & 0 \\
0 & 0 & 0 & 0 & 0 & 0 & 0 & 0 \\
0 & 0 & 0 & 0 & 0 & 0 & 0 & 0 \\
-1 & 0 & 0 & 0 & 0 & 0 & 0 & 0
\end{pmatrix} .
\end{aligned} \tag{4.6}$$

Note that this matrix has the identical off-diagonal structure as the density matrix formed from the pure state of Eq. 4.3:

$$\rho_{GHZ} \propto \frac{1}{2}\left(-|+++\rangle\langle---| - |---\rangle\langle+++|\right) \ .$$

Thus the NMR sample as prepared above represents the same quantum correlations that would be present in a pure, three-particle GHZ state.

(IV) *Measurement.* An NMR measurement that demonstrates one of the $\left(\sigma_x^A\sigma_y^B\sigma_y^C\right)$, $\left(\sigma_y^A\sigma_x^B\sigma_y^C\right)$, $\left(\sigma_y^A\sigma_y^B\sigma_x^C\right)$, or $\left(\sigma_x^A\sigma_x^B\sigma_x^C\right)$ correlations is now performed by applying rf pulses to the sample to rotate the desired correlation into observable magnetization. Specifically, to measure $\left(\sigma_j^A\sigma_k^B\sigma_l^C\right)$, the pulse sequence

$$\rho_{GHZ} \longrightarrow \left[\frac{\pi}{2}\right]^{A}_{j-90^\circ} - \left[\frac{\pi}{2}\right]^{C}_{l-90^\circ}$$

followed by data acquisition with the absorptive signal phased along k will reveal the magnitude and sign of the desired correlation in the spectrum on resonance with the B spins. Steps (I)$\sim$(III) of the experiment are then identically repeated three times, each with a different measurement sequence (IV).

4.2.2 Results

The results of the four measurements on the sample prepared in state ρ_{GHZ} are shown in Fig. 4-1. For example, to determine the correlations between $\left(\sigma_x^A \sigma_y^B \sigma_y^C\right)$, look at Fig. 4-1(a). The fact that the phase of the first line from the left is (+) confirms the GHZ correlation that when spin A is $|-\rangle$ along x and spin C is $|-\rangle$ along y, spin B is $|+\rangle$ along y. Similarly, the second line (from the left) shows a negative peak, confirming the correlation that when spin A is $|+\rangle$ along x and spin C is $|-\rangle$ along y, spin B is $|-\rangle$ along y. Likewise, the third line, with a negative peak, confirms the GHZ correlation that when spin A is $|-\rangle$ along x and spin C is $|+\rangle$ along y, spin B is $|-\rangle$ along y. Finally, the last line confirms the correlation that when spin A is $|+\rangle$ along x and spin C is $|+\rangle$ along y, spin B is $|+\rangle$ along y. Thus all four lines in Fig. 1(a) confirm that the product of the spin of particle A along x, particle B along y, and particle C along y yields the result $+1$, as in scenario (i) of the GHZ experiment explained above.

Note that Fig. 4-1(b) shows the same four lines in the spectrum for spin B, except that in this case the measurement sequence reveals the correlation that corresponds to $\sigma_y^A \sigma_x^B \sigma_y^C$. As in Fig. 4-1(a), all four lines indicate that the product of the spin of particle A along y, particle B along x, and particle C along y is $+1$, as predicted in scenario (ii) above. Likewise, Fig. 4-1(c) shows the analogous $+1$ result when the product of spin measurements of particle A along y, particle B along y, and particle C along x is computed.

Significantly, Fig. 4-1(d) shows a different spectrum when a measurement of the correlation $\left(\sigma_x^A \sigma_x^B \sigma_x^C\right)$ was made. In this case, when spin A is $|-\rangle$ along x and spin C is $|-\rangle$ along x, spin B is $|-\rangle$ along x, as seen in the first line; when spin A is $|+\rangle$ along x and spin C is $|-\rangle$ along x, spin B is $|+\rangle$ along x; and so forth. In this case, the product of the spin measurements of particle A along x, particle B along x, and particle C along x is *not* $+1$, but rather -1. Taken together, the four spectra in Fig. 4-1 clearly demonstrate the GHZ correlations predicted by quantum mechanics.

Although the NMR experiment demonstrates GHZ correlations, it cannot eliminate local interactions as the cause of those correlations because of the close proximity of the nuclei involved. However, no known interaction in the natural Hamiltonian (Eq. 3.10) could be responsible for the "communication" between the nuclei that caused the GHZ correlations. Specifically, measurement step (IV) required only 4.043 ms to implement; this

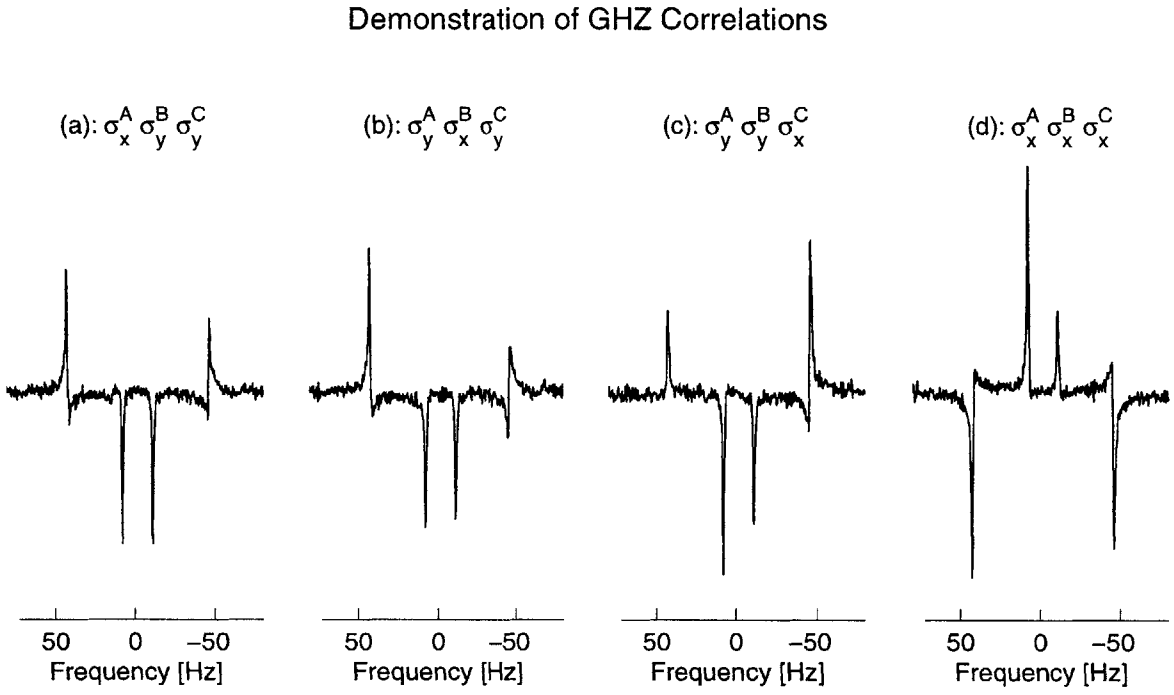

Figure 4-1: **Confirmation of the quantum prediction of GHZ correlations.** The four figures show the spectrum of spin B for each of the measurements. An "up" line indicates the state $|+\rangle$ for spin B, and a "down" line indicates the state $|-\rangle$. Plot (a) confirms the GHZ correlation that the product of measurements of σ_x on the A spins, σ_y on the B spins, and σ_y on the C spins yields the result $+1$. For example, the first line in (a) indicates that when spins A and C give the result (-1) and (-1), respectively, spin B gives the result $+1$; the second line indicates that when spins A and C give the result (-1) and $(+1)$, spin B gives the result -1; *etc.*, so that the product of the results is always $+1$. Similarly, (b) and (c) confirm that the products $\sigma_y^A \sigma_x^B \sigma_y^C$ and $\sigma_y^A \sigma_y^B \sigma_x^C$ also yield the result $+1$. Plot (d), by contrast, shows that the product $\sigma_x^A \sigma_x^B \sigma_x^C$ yields the result -1, in contradiction to the predictions of the classical hidden variable theory.

represents the amount of time *after* the GHZ preparation steps (I)~(III)—common to all four experiments—but before data acquisition, in which the culpable classical local interaction could "inform" the spins of which axes were being measured for which spins and then adjust the phase of the acquisition signal to reveal the quantum mechanical correlations. Since the fastest coupling term in the natural Hamiltonian is slower than 4.043 ms ($1/2J_{AB} = 9.36$ ms), the culpable "classical demon," if it exists, would have to be a non-standard interaction.

In addition, the NMR experiment cannot completely rule out classical hidden variables. The effective pure state used to demonstrate GHZ correlations is in fact a mixed state of an ensemble in which individual members are unitarily transformed from a thermal state. It can be shown that such states can be described by non-negative discrete Wigner functions [101]. Accordingly, the results of the experiment could be "explained" by a hypothetical ensemble of classical systems each of which possesses a definite state for its hidden variables. As in the case of local interactions in the previous paragraph, however, to be consistent with the measured properties of the states above (Eqs. 4.4, 4.5, 4.6), the preparation of such an ensemble from the thermal ensemble with which the experiment begins would require a conspiracy of non-standard interactions.

4.3 Conclusions

This chapter reported on an experiment that displays GHZ correlations using nuclear magnetic resonance. Creation of the GHZ correlations relied on the use of geometric control ideas by implementing available transformations in order to guide the initial state at thermal equilibrium to the final state in which the off-diagonal elements of the ensemble density matrix displayed the same quantum correlations as a pure, three-particle GHZ state. Although the NMR experiment performed cannot entirely rule out classical local hidden variables, it nonetheless provides an unambiguous demonstration of the apparently paradoxical GHZ correlations and puts significant constraints on the set of viable hidden variable theories. Since the measured density matrix contains the same correlations as would be present in a pure 3-particle GHZ state, the experiment underscores the ability of quantum information processing using NMR to demonstrate quantum-mechanical predictions.

Appendix A

Satellite Attitude Model Using Two Single-Gimbal Control Moment Gyroscopes

This appendix shows the derivation of the state-space model for the attitude control of a satellite using two single-gimbal gyroscopes. In general, each body needs 6 independent equations to describe its orientation in space: three rotation angles and three angular speed values. Thus, in general, 18 independent equations of motion are needed to describe the attitude state of a satellite with two gyroscopes. In the model presented below, this number is reduced to 10 independent equations by the introduction of holonomic constraints.

The orientation of the platform is conveniently expressed using the so-called "3-2-1" Euler angles, which, unlike spherical coordinates, avoids the singularity at the origin. Imagine an orthonormal axis system $(\mathbf{x}, \mathbf{y}, \mathbf{z})$, attached to the satellite, that instantaneously coincides with an inertial reference frame. The Euler angles are given by the following procedure:

1. Rotate around $\mathbf{z}$ (in the right-hand sense) by an amount ψ, where $-\pi < \psi \leq \pi$; label the new axis directions with respect to the inertial reference frame as $(\mathbf{x}', \mathbf{y}', \mathbf{z}')$.

2. Rotate around $\mathbf{y}'$ by an amount θ, where $-\frac{\pi}{2} < \theta \leq \frac{\pi}{2}$; label the new axis directions with respect to the inertial frame $(\mathbf{x}'', \mathbf{y}'', \mathbf{z}'')$.

3. Rotate around $\mathbf{x}''$ by an amount ϕ, where $-\pi < \phi \leq \pi$.

The attitude of the satellite can then be given by the triplet (ψ, θ, ϕ).

In the system described herein, the satellite frame of reference is spanned by the axis system $(\mathbf{e}_1, \mathbf{e}_2, \mathbf{e}_3)$, chosen to coincide with the principal moments of inertia (I_1, I_2, I_3) for that body. Similarly, the axis systems for the gyroscopes (called "a" and "b" for convenience) are chosen along the principal moments of inertia for the gyroscopes, respectively, as $(\mathbf{a}_1, \mathbf{a}_2, \mathbf{a}_3)$ and $(\mathbf{b}_1, \mathbf{b}_2, \mathbf{b}_3)$. Letting $(\omega_1, \omega_2, \omega_3)$ denote the components of the satellite's angular velocity vector as expressed in the rotating satellite frame, the kinematic equations for the three Euler angles are:

$$\dot{\psi} = \left(\frac{\sin\phi}{\cos\theta}\right)\omega_2 + \left(\frac{\cos\phi}{\cos\theta}\right)\omega_3 \tag{A.1}$$

$$\dot{\theta} = (\cos\phi)\,\omega_2 - (\sin\phi)\,\omega_3 \tag{A.2}$$

$$\dot{\phi} = \omega_1 + (\sin\phi\tan\theta)\,\omega_2 + (\cos\phi\tan\theta)\,\omega_3\ . \tag{A.3}$$

The orientation of the gyroscopes is developed in the consideration of the constraints (below).

The development of the dynamic equations of motion begins with Euler's equations for a rotating body; in general,

$$I_x\,\dot{\omega}_x = (I_y - I_z)\,\omega_y\,\omega_z + \boldsymbol{\tau}_{\text{ext}}\cdot\mathbf{x} \tag{A.4}$$

$$I_y\,\dot{\omega}_y = (I_z - I_x)\,\omega_x\,\omega_z + \boldsymbol{\tau}_{\text{ext}}\cdot\mathbf{y} \tag{A.5}$$

$$I_z\,\dot{\omega}_z = (I_x - I_y)\,\omega_x\,\omega_y + \boldsymbol{\tau}_{\text{ext}}\cdot\mathbf{z}\ , \tag{A.6}$$

where the axis system $(\mathbf{x}, \mathbf{y}, \mathbf{z})$ are unit vectors along the three orthogonal principal moments of inertia in the body reference frame, and the (I_x, I_y, I_z) are the rotational inertias around the respective axes. In addition, $\boldsymbol{\tau}_{\text{ext}}$ designates all external torques on the body.

The gimbal axes are arbitrarily set $\frac{\pi}{2}$ apart for convenience (although any angle that is not an integer multiple of π will suffice). The specific orientation is represented in Fig. A-1. In addition, the gyroscopes are modeled as thin solid disks with the $\mathbf{a}_3$ and $\mathbf{b}_3$ chosen along the axisymmetric directions for the gyroscopes, so that

$$I_a \equiv I_{a,3} = 2I_{a,2} = 2I_{a,1} \tag{A.7}$$

$$I_b \equiv I_{b,3} = 2I_{b,2} = 2I_{b,1}\ . \tag{A.8}$$

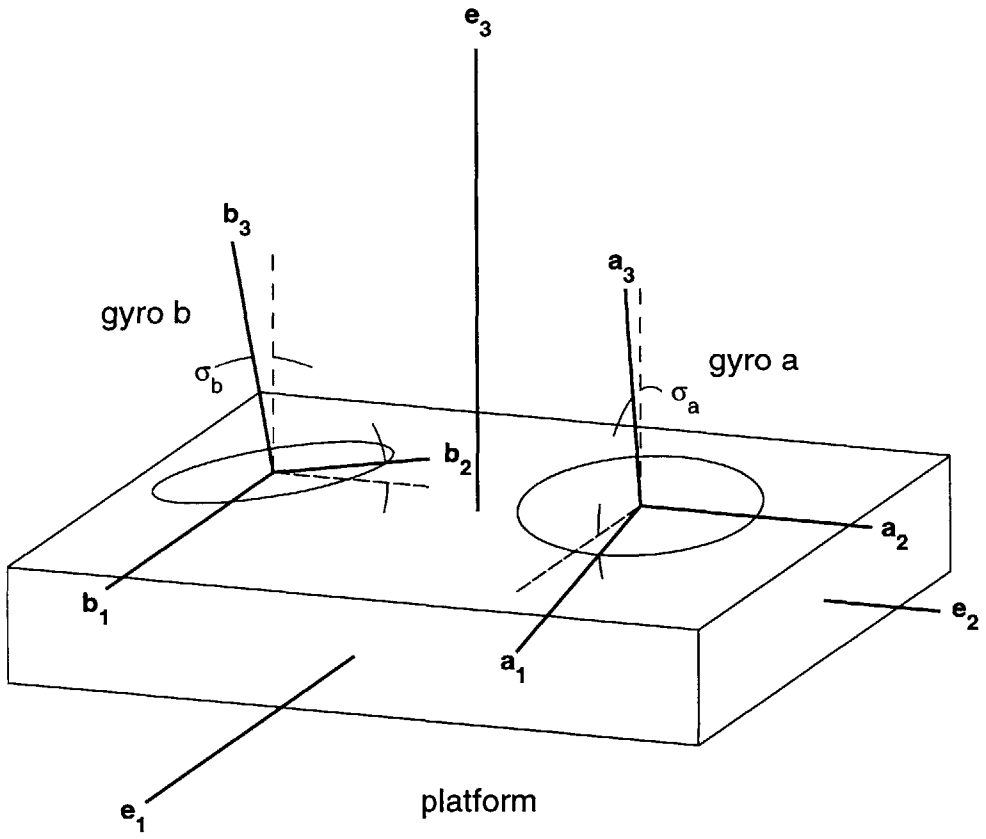

Figure A-1: **Satellite with 2 Control Moment Gyroscopes.** The axis system $(\mathbf{e}_1, \mathbf{e}_2, \mathbf{e}_3)$ is chosen along the three principal axes of inertia for the satellite platform. Single-gimbal gyroscope "a" has $\mathbf{a}_2$ as the gimbal axis, pointing along $\mathbf{e}_2$, around which torque τ_a is applied; $\mathbf{a}_3$ points along the axis of symmetry for the gyroscope, making an angle of σ_a with the $\mathbf{e}_3$ axis. Similarly, gyroscope "b" has $\mathbf{b}_1$ as the gimbal axis, fixed along $\mathbf{e}_1$, around which torque τ_b is applied; $\mathbf{b}_3$ points along the axis of symmetry for the gyroscope, making an angle of σ_b with the $\mathbf{e}_3$ axis.

The dynamic equations of motion are thus:

$$I_1\,\dot{\omega}_1 = (I_2 - I_3)\,\omega_2\,\omega_3 - (\boldsymbol{\tau}_{a,p}\cdot\mathbf{e}_1) - (\boldsymbol{\tau}_{b,p}\cdot\mathbf{e}_1) \tag{A.9}$$

$$I_2\,\dot{\omega}_2 = (I_3 - I_1)\,\omega_1\,\omega_3 - (\boldsymbol{\tau}_{a,p}\cdot\mathbf{e}_2) - (\boldsymbol{\tau}_{b,p}\cdot\mathbf{e}_2) \tag{A.10}$$

$$I_3\,\dot{\omega}_3 = (I_1 - I_2)\,\omega_1\,\omega_2 - (\boldsymbol{\tau}_{a,p}\cdot\mathbf{e}_3) - (\boldsymbol{\tau}_{b,p}\cdot\mathbf{e}_3) \tag{A.11}$$

$$\frac{1}{2}I_a\,\dot{\omega}_{a,1} = -\frac{1}{2}I_a\,\omega_{a,2}\,\omega_{a,3} + (\boldsymbol{\tau}_{a,p}\cdot\mathbf{a}_1) \tag{A.12}$$

$$\frac{1}{2}I_a\,\dot{\omega}_{a,2} = \frac{1}{2}I_a\,\omega_{a,1}\,\omega_{a,3} + (\boldsymbol{\tau}_{a,p}\cdot\mathbf{a}_2) \tag{A.13}$$

$$I_a\,\dot{\omega}_{a,3} = (\boldsymbol{\tau}_{a,p}\cdot\mathbf{a}_3) \tag{A.14}$$

$$\frac{1}{2}I_b\,\dot{\omega}_{b,1} = -\frac{1}{2}I_b\,\omega_{b,2}\,\omega_{b,3} + (\boldsymbol{\tau}_{b,p}\cdot\mathbf{b}_1) \tag{A.15}$$

$$\frac{1}{2}I_b\,\dot{\omega}_{b,2} = \frac{1}{2}I_b\,\omega_{b,1}\,\omega_{b,3} + (\boldsymbol{\tau}_{b,p}\cdot\mathbf{b}_2) \tag{A.16}$$

$$I_b\,\dot{\omega}_{b,3} = (\boldsymbol{\tau}_{b,p}\cdot\mathbf{b}_3)\ . \tag{A.17}$$

In this notation, a subscript "p" indicates the platform or satellite, and "a" and "b" signify the respective gyroscopes. The symbol $\boldsymbol{\tau}_{a,p}$ represents the torque applied to gyroscope "a" due to the action of "p", etc.

The constraints are as follows:

1. Gyroscope "a" is constrained by its mounts to move with the satellite such that the gimbal axis $\mathbf{a}_2$ always coincides with $\mathbf{e}_2$. It is convenient to introduce angle σ_a as the angle between the axes systems of gyroscope "a" and the satellite, as shown in Fig. A-1. Then the constraint implies:

$$\mathbf{a}_1 = (\cos\sigma_a)\,\mathbf{e}_1 - (\sin\sigma_a)\,\mathbf{e}_3 \tag{A.18}$$

$$\mathbf{a}_2 = \mathbf{e}_2 \tag{A.19}$$

$$\mathbf{a}_3 = (\sin\sigma_a)\,\mathbf{e}_1 + (\cos\sigma_a)\,\mathbf{e}_3\ . \tag{A.20}$$

2. Gyroscope "b" is similarly constrained (see Fig. A-1), with reference angle σ_b with respect to the satellite:

$$\mathbf{b}_1 = \mathbf{e}_1 \tag{A.21}$$

$$\mathbf{b}_2 = (\cos\sigma_b)\,\mathbf{e}_2 + (\sin\sigma_b)\,\mathbf{e}_3 \tag{A.22}$$

$$\mathbf{b}_3 = -(\sin\sigma_b)\,\mathbf{e}_2 + (\cos\sigma_b)\,\mathbf{e}_3\ . \tag{A.23}$$

3. In addition to the angle constraint above, gyroscope "a" must have $\omega_{a,1} = \boldsymbol{\omega}_p \cdot \mathbf{a}_1$; in other words,

$$\omega_{a,1} = \omega_1 \cos\sigma_a - \omega_3 \sin\sigma_a \ . \tag{A.24}$$

This constraint can be differentiated to produce

$$\dot{\omega}_{a,1} = \dot{\omega}_1 \cos\sigma_a - \dot{\omega}_3 \sin\sigma_a - \omega_1 \dot{\sigma}_a \sin\sigma_a - \omega_3 \dot{\sigma}_a \cos\sigma_a \ . \tag{A.25}$$

4. As with gyroscope "a", gyroscope "b" has $\omega_{b,2} = \boldsymbol{\omega}_p \cdot \mathbf{b}_2$, implying:

$$\omega_{b,2} = \omega_2 \cos\sigma_b + \omega_3 \sin\sigma_b \tag{A.26}$$

$$\dot{\omega}_{b,2} = \dot{\omega}_2 \cos\sigma_b + \dot{\omega}_3 \sin\sigma_b - \omega_2 \dot{\sigma}_b \sin\sigma_b + \omega_3 \dot{\sigma}_b \cos\sigma_b \ . \tag{A.27}$$

5. The gyroscope mounts are assumed frictionless: no torque is referred to either gyroscope along its main spinning axis. One constraint is

$$\boldsymbol{\tau}_{a,p} \cdot \mathbf{a}_3 = 0 \ ; \tag{A.28}$$

6. similarly,

$$\boldsymbol{\tau}_{b,p} \cdot \mathbf{b}_3 = 0 \ . \tag{A.29}$$

7. Constraint 5 implies $\dot{\omega}_{a,3} = 0$, which can be integrated immediately to yield one of the states. This particular state variable is uninteresting because of the assumed uniformity of the gyroscope anyway. For simplicity, let $\omega_a \equiv \omega_{a,3}$.

8. Constraint 6 implies $\dot{\omega}_{b,3} = 0$, and like constraint 7, can be used to immediately eliminate one of the states that describes the angular orientation of gyroscope "b". For simplicity, let $\omega_b \equiv \omega_{b,3}$.

Having introduced σ_a and σ_b, it is convenient to relate $\omega_{a,2}$ and $\omega_{b,1}$, respectively, to these relative angles. Referring again to Fig. A-1, we have:

$$\omega_{a,2} = \omega_2 + \dot{\sigma}_a \tag{A.30}$$

$$\omega_{b,1} = \omega_1 + \dot{\sigma}_b \ , \tag{A.31}$$

which can both be trivially differentiated to produce

$$\dot{\omega}_{a,2} = \dot{\omega}_2 + \ddot{\sigma}_a \tag{A.32}$$

$$\dot{\omega}_{b,1} = \dot{\omega}_1 + \ddot{\sigma}_b \ . \tag{A.33}$$

The kinematic expressions for the gyroscope orientations is now relatively simple; it is natural to use σ_a and σ_b as the states that describe the orientation of the gyroscopes:

$$\frac{d}{dt}(\sigma_a) = \dot{\sigma}_a \tag{A.34}$$

$$\frac{d}{dt}(\sigma_b) = \dot{\sigma}_b \,. \tag{A.35}$$

Finally, the inputs to the gyroscopes are the torques along the gimbal axes:

$$\tau_a \equiv \boldsymbol{\tau}_{a,p} \cdot \mathbf{e}_2 \tag{A.36}$$

$$\tau_b \equiv \boldsymbol{\tau}_{b,p} \cdot \mathbf{e}_1 \,. \tag{A.37}$$

The constraints reduce the number of dynamic equations to five, which, when the equivalent torque terms have been eliminated, may be solved for derivatives of interest $(\dot{\omega}_1, \dot{\omega}_2, \dot{\omega}_3, \ddot{\sigma}_a, \ddot{\sigma}_b)$ to give:

$$\begin{aligned}
I_1 \dot{\omega}_1 = {} & \frac{1}{8}\frac{r_a r_b}{R}\frac{I_a}{I_3} I_b \omega_b \sin(2\sigma_a)\sin\sigma_b\,(\omega_1 + f_b\dot{\sigma}_b) \\
& - \frac{1}{2} r_a \left[1 - \frac{1}{2}\frac{r_a}{R}\frac{I_a}{I_3}\sin^2\sigma_a\right] I_a \omega_a \cos\sigma_a\,(\omega_2 + f_a\dot{\sigma}_a) \\
& + \frac{1}{4}\frac{r_a}{R}\frac{(I_1 - I_2)\,I_a}{I_3}\sin(2\sigma_a)\;\omega_1\omega_2 - \frac{1}{16}\frac{r_a r_b}{R}\frac{(I_3 - I_1)\,I_a I_b}{I_2 I_3}\sin(2\sigma_a)\sin(2\sigma_b)\;\omega_1\omega_3 \\
& + r_a\left[1 + \frac{1}{16}\frac{r_a}{R}\frac{I_a^2}{I_1 I_3}\sin^2(2\sigma_a)\right](I_2 - I_3)\;\omega_2\omega_3 \\
& + \frac{1}{16}\frac{r_a r_b}{R}\frac{I_a I_b}{I_2 I_3}\sin(2\sigma_a)\sin(2\sigma_b)\;\tau_a \\
& - r_a\left[1 + \frac{1}{16}\frac{r_a}{R}\frac{I_a^2}{I_1 I_3}\sin^2(2\sigma_a)\right]\tau_b
\end{aligned} \tag{A.38}$$

$$\begin{aligned}
I_2 \dot{\omega}_2 = {} & \frac{1}{2} r_b \left[1 - \frac{1}{2}\frac{r_b}{R}\frac{I_b}{I_3}\sin^2\sigma_b\right] I_b \omega_b \cos\sigma_b\,(\omega_1 + f_b\dot{\sigma}_b) \\
& - \frac{1}{8}\frac{r_a r_b}{R}\frac{I_b}{I_3} I_a \omega_a \sin\sigma_a \sin(2\sigma_b)\;(\omega_2 + f_a\dot{\sigma}_a) \\
& - \frac{1}{4}\frac{r_b}{R}\frac{(I_1 - I_2)\,I_b}{I_3}\sin(2\sigma_b)\;\omega_1\omega_2 + r_b\left[1 + \frac{1}{16}\frac{r_b}{R}\frac{I_b^2}{I_2 I_3}\sin^2(2\sigma_b)\right](I_3 - I_1)\;\omega_1\omega_3 \\
& - \frac{1}{16}\frac{r_a r_b}{R}\frac{(I_2 - I_3)\,I_a I_b}{I_1 I_3}\sin(2\sigma_a)\sin(2\sigma_b)\;\omega_2\omega_3 \\
& - r_b\left[1 + \frac{1}{16}\frac{r_b}{R}\frac{I_b^2}{I_2 I_3}\sin^2(2\sigma_b)\right]\tau_a \\
& + \frac{1}{16}\frac{r_a r_b}{R}\frac{I_a I_b}{I_1 I_3}\sin(2\sigma_a)\sin(2\sigma_b)\;\tau_b
\end{aligned} \tag{A.39}$$

$$I_3 \dot{\omega}_3 = \frac{1}{2}\frac{r_b}{R} I_b \omega_b \sin\sigma_b\,(\omega_1 + f_b\dot{\sigma}_b) + \frac{1}{2}\frac{r_a}{R} I_a \omega_a \sin\sigma_a\,(\omega_2 + f_a\dot{\sigma}_a)$$

$$
\begin{aligned}
&+\frac{1}{R}\left(I_1-I_2\right)\,\omega_1\omega_2-\frac{1}{4}\frac{r_b}{R}\frac{\left(I_3-I_1\right)I_b}{I_2}\sin\left(2\sigma_b\right)\omega_1\omega_3\\
&+\frac{1}{4}\frac{r_a}{R}\frac{\left(I_2-I_3\right)I_a}{I_1}\sin\left(2\sigma_a\right)\omega_2\,\omega_3\\
&+\frac{1}{4}\frac{r_b}{R}\frac{I_b}{I_2}\sin\left(2\sigma_b\right)\tau_a-\frac{1}{4}\frac{r_a}{R}\frac{I_a}{I_1}\sin\left(2\sigma_a\right)\tau_b \qquad \text{(A.40)}\\
\ddot{\sigma}_a \;=\;&-\frac{1}{2}r_b\left[1-\frac{1}{2}\frac{r_b}{R}\frac{I_b}{I_3}\sin^2\sigma_b\right]\frac{I_b}{I_2}\,\omega_b\cos\sigma_b\,\left(\omega_1+f_b\,\dot{\sigma}_b\right)+\omega_a\cos\sigma_a\,\omega_1\\
&+\frac{1}{8}\frac{r_ar_b}{R}\frac{I_aI_b}{I_2I_3}\,\omega_a\sin\sigma_a\sin\left(2\sigma_b\right)\,\left(\omega_2+f_a\,\dot{\sigma}_a\right)-\omega_a\sin\sigma_a\,\omega_3\\
&+\frac{1}{4}\frac{r_b}{R}\frac{\left(I_1-I_2\right)I_b}{I_2I_3}\sin\left(2\sigma_b\right)\,\omega_1\omega_2-r_b\left[1+\frac{1}{16}\frac{r_b}{R}\frac{I_b^2}{I_2I_3}\sin^2\left(2\sigma_b\right)\right]\frac{\left(I_3-I_1\right)}{I_2}\,\omega_1\omega_3\\
&+\frac{1}{16}\frac{r_ar_b}{R}\frac{\left(I_2-I_3\right)I_aI_b}{I_1I_2I_3}\sin\left(2\sigma_a\right)\sin\left(2\sigma_b\right)\,\omega_2\,\omega_3\\
&+2\left\{1+\frac{1}{2}r_b\frac{I_a}{I_2}\left[1+\frac{1}{16}\frac{r_b}{R}\frac{I_b^2}{I_2I_3}\sin^2\left(2\sigma_b\right)\right]\right\}\frac{1}{I_a}\,\tau_a\\
&-\frac{1}{16}\frac{r_ar_b}{R}\frac{I_aI_b}{I_1I_2I_3}\sin\left(2\sigma_a\right)\sin\left(2\sigma_b\right)\,\tau_b \qquad \text{(A.41)}\\
\ddot{\sigma}_b \;=\;&-\frac{1}{8}\frac{r_ar_b}{R}\frac{I_aI_b}{I_1I_3}\,\omega_b\sin\left(2\sigma_a\right)\sin\sigma_b\,\left(\omega_1+f_b\,\dot{\sigma}_b\right)-\omega_b\cos\sigma_b\,\omega_2\\
&+\frac{1}{2}r_a\left[1-\frac{1}{2}\frac{r_a}{R}\frac{I_a}{I_3}\sin^2\sigma_a\right]\frac{I_a}{I_1}\,\omega_a\cos\sigma_a\,\left(\omega_2+f_a\,\dot{\sigma}_a\right)-\omega_b\sin\sigma_b\,\omega_3\\
&-\frac{1}{4}\frac{r_a}{R}\frac{\left(I_1-I_2\right)I_a}{I_1I_3}\sin\left(2\sigma_a\right)\,\omega_1\omega_2+\frac{1}{16}\frac{r_ar_b}{R}\frac{\left(I_3-I_1\right)I_aI_b}{I_1I_2I_3}\sin\left(2\sigma_a\right)\sin\left(2\sigma_b\right)\,\omega_1\omega_3\\
&-r_a\left[1+\frac{1}{16}\frac{r_a}{R}\frac{I_a^2}{I_1I_3}\sin^2\left(2\sigma_a\right)\right]\frac{\left(I_2-I_3\right)}{I_1}\,\omega_2\,\omega_3\\
&-\frac{1}{16}\frac{r_ar_b}{R}\frac{I_aI_b}{I_1I_2I_3}\sin\left(2\sigma_a\right)\sin\left(2\sigma_b\right)\,\tau_a\\
&+2\left\{1+\frac{1}{2}r_a\frac{I_b}{I_1}\left[1+\frac{1}{16}\frac{r_a}{R}\frac{I_a^2}{I_1I_3}\sin^2\left(2\sigma_a\right)\right]\right\}\frac{1}{I_b}\,\tau_b\;, \qquad \text{(A.42)}
\end{aligned}
$$

where we have used

$$
\begin{aligned}
r_a \;&\equiv\; r_a(\sigma_a)=\frac{1}{1+\frac{1}{2}\frac{I_a}{I_1}\cos^2\sigma_a}\;, &\text{(A.43)}\\
r_b \;&\equiv\; r_b(\sigma_b)=\frac{1}{1+\frac{1}{2}\frac{I_b}{I_2}\cos^2\sigma_b}\;, &\text{(A.44)}\\
R \;&\equiv\; R(\sigma_a,\sigma_b)=1+\frac{1}{2}r_a\left(\frac{I_a}{I_3}\right)\sin^2\sigma_a+\frac{1}{2}r_b\left(\frac{I_b}{I_3}\right)\sin^2\sigma_b\;, &\text{(A.45)}
\end{aligned}
$$

and

$$
\begin{aligned}
f_a \;&\equiv\; f_a(\omega_1,\omega_3,\sigma_a)=1-\frac{\omega_1}{\omega_a}\sin\sigma_a-\frac{\omega_3}{\omega_a}\cos\sigma_a\;, &\text{(A.46)}\\
f_b \;&\equiv\; f_b(\omega_2,\omega_3,\sigma_b)=1+\frac{\omega_2}{\omega_b}\sin\sigma_b-\frac{\omega_3}{\omega_b}\cos\sigma_b\;. &\text{(A.47)}
\end{aligned}
$$

To make the equations more manageable, introduce the following assumptions:

1. The rotational inertia of the platform around any axis is much larger than that of either of the gyroscopes:

$$I_k \gg I_a \quad \text{and} \quad I_k \gg I_b \quad \text{for all} \quad k = 1,\ 2,\ 3\ ; \tag{A.48}$$

   thus, r_a, r_b, R, and all bracketed expressions in Eq. A.38$\sim$A.42, are very close to 1.

2. The angular speed of the gyroscopes is always (*i.e.*, at all times t) much larger than the the angular speed of the platform around any axis:

$$\omega_k \ll \omega_a \quad \text{and} \quad \omega_k \ll \omega_b \quad \text{for all} \quad k = 1,\ 2,\ 3\ ; \tag{A.49}$$

   in other words, $f_a \approx 1$ and $f_b \approx 1$.

In addition, let the two gyroscopes be identical, with the gyroscopes spinning in opposite directions when the state vector (see Eq. A.71) is at the origin; *i.e.*

$$\omega_g \equiv \omega_a = -\omega_b \tag{A.50}$$

$$I_g \equiv I_a = I_b\ ; \tag{A.51}$$

this eliminates unnecessary complexity while still demonstrating the important features of the system. Finally, it is convenient to non-dimensionalize the dynamic equations; we therefore introduce:

$$\nu_1 = \frac{I_1\,\omega_1}{(I_g\,\omega_g)} \tag{A.52}$$

$$\nu_2 = \frac{I_2\,\omega_2}{(I_g\,\omega_g)} \tag{A.53}$$

$$\nu_3 = \frac{I_3\,\omega_3}{(I_g\,\omega_g)} \tag{A.54}$$

$$\nu_a = \frac{\dot{\sigma}_a}{\omega_g} \tag{A.55}$$

$$\nu_b = \frac{\dot{\sigma}_b}{\omega_g} \tag{A.56}$$

$$u_a = \frac{\tau_a}{I_g\omega_g^2} \tag{A.57}$$

$$u_b = \frac{\tau_b}{I_g\omega_g^2}\ . \tag{A.58}$$

The kinematic equations of motion (Equations A.1, A.2, A.3, A.34, and A.35) can be written

$$\dot{\psi} = \Omega_{1,2} \frac{\sin(\phi)}{\cos(\theta)} \nu_2 + \Omega_{1,3} \frac{\cos(\phi)}{\cos(\theta)} \nu_3 \tag{A.59}$$

$$\dot{\theta} = \Omega_{2,2} \cos(\phi) \nu_2 - \Omega_{2,3} \sin(\phi) \nu_3 \tag{A.60}$$

$$\dot{\phi} = \Omega_{3,1} \nu_1 + \Omega_{3,2} \sin(\phi) \tan(\theta) \nu_2 + \Omega_{3,3} \cos(\phi) \tan(\theta) \nu_3 \tag{A.61}$$

$$\dot{\sigma}_a = \Omega_{4,4} \nu_a \tag{A.62}$$

$$\dot{\sigma}_b = \Omega_{5,5} \nu_b \tag{A.63}$$

where the $\Omega_{j,k}$ are elements, indexed by (j, k), of a (10×8) array Ω that contains only the constants $(I_1, I_2, I_3, I_g, \omega_g)$; see Eq. A.69.

With these simplifying assumptions, the dynamic equations reduce to:

$$\begin{aligned}
\dot{\nu}_1 \approx & -\Omega_{6,1} \sin(2\sigma_a) \sin(\sigma_b) \nu_1 - \Omega_{6,2} \cos(\sigma_a) \nu_2 \\
& - \Omega_{6,4} \cos(\sigma_a) \nu_a - \Omega_{6,5} \sin(2\sigma_a) \sin(\sigma_b) \nu_b \\
& + \Omega_{6,6} \sin(2\sigma_a) \nu_1 \nu_2 - \Omega_{6,7} \sin(2\sigma_a) \sin(2\sigma_b) \nu_1 \nu_3 + \Omega_{6,8} \nu_2 \nu_3 \\
& + C_{6,1} \sin(2\sigma_a) \sin(\sigma_b) u_a - C_{6,2} u_b
\end{aligned} \tag{A.64}$$

$$\begin{aligned}
\dot{\nu}_2 \approx & -\Omega_{7,1} \cos(\sigma_b) \nu_1 - \Omega_{7,2} \sin(\sigma_a) \sin(2\sigma_b) \nu_2 \\
& - \Omega_{7,4} \sin(\sigma_a) \sin(2\sigma_b) \nu_a - \Omega_{7,5} \cos(\sigma_b) \nu_b \\
& - \Omega_{7,6} \sin(2\sigma_b) \nu_1 \nu_2 + \Omega_{7,7} \nu_1 \nu_3 - \Omega_{7,8} \sin(2\sigma_a) \sin(2\sigma_b) \nu_2 \nu_3 \\
& - C_{7,1} u_a + C_{7,2} \sin(2\sigma_a) \sin(2\sigma_b) u_b
\end{aligned} \tag{A.65}$$

$$\begin{aligned}
\dot{\nu}_3 \approx & -\Omega_{8,1} \sin(\sigma_b) \nu_1 + \Omega_{8,2} \sin(\sigma_a) \nu_2 + \Omega_{8,4} \sin(\sigma_a) \nu_a - \Omega_{8,5} \sin(\sigma_b) \nu_b \\
& + \Omega_{8,6} \nu_1 \nu_2 - \Omega_{8,7} \sin(2\sigma_b) \nu_1 \nu_3 + \Omega_{8,8} \sin(2\sigma_a) \nu_2 \nu_3 \\
& + C_{8,1} \sin(2\sigma_b) u_a - C_{8,2} \sin(2\sigma_a) u_b
\end{aligned} \tag{A.66}$$

$$\begin{aligned}
\dot{\nu}_a \approx & \Omega_{9,1} \left[\cos(\sigma_a) + \frac{1}{2} \left(\frac{I_g}{I_2} \right) \cos(\sigma_b) \right] \nu_1 + \Omega_{9,2} \sin(\sigma_a) \sin(2\sigma_b) \nu_2 - \Omega_{9,3} \sin(\sigma_a) \nu_3 \\
& + \Omega_{9,4} \sin(\sigma_a) \sin(2\sigma_b) \nu_a + \Omega_{9,5} \cos(\sigma_b) \nu_b \\
& + \Omega_{9,6} \sin(2\sigma_b) \nu_1 \nu_2 - \Omega_{9,7} \nu_1 \nu_3 + \Omega_{9,8} \sin(2\sigma_a) \sin(2\sigma_b) \nu_2 \nu_3 \\
& + C_{9,1} u_a - C_{9,2} \sin(2\sigma_a) \sin(2\sigma_b) u_b
\end{aligned} \tag{A.67}$$

$$\begin{aligned}
\dot{\nu}_b \approx & \Omega_{10,1} \sin(2\sigma_a) \sin(\sigma_b) \nu_1 + \Omega_{10,2} \left[\frac{1}{2} \left(\frac{I_g}{I_1} \right) \cos(\sigma_a) + \cos(\sigma_b) \right] \nu_2 + \Omega_{10,3} \sin(\sigma_b) \nu_3 \\
& + \Omega_{10,4} \cos(\sigma_a) \nu_a + \Omega_{10,5} \sin(2\sigma_a) \sin(\sigma_b) \nu_b \\
& - \Omega_{10,6} \sin(2\sigma_a) \nu_1 \nu_2 + \Omega_{10,7} \sin(2\sigma_a) \sin(2\sigma_b) \nu_1 \nu_3 - \Omega_{10,8} \nu_2 \nu_3 \\
& - C_{10,1} \sin(2\sigma_a) \sin(2\sigma_b) u_a + C_{10,2} u_b \ ,
\end{aligned} \tag{A.68}$$

where Ω is given by

$$\Omega = \omega_g \begin{pmatrix} 0 & \frac{I_g}{I_2} & \frac{I_g}{I_3} & 0 & 0 & 0 & 0 & 0 \\ 0 & \frac{I_g}{I_2} & \frac{I_g}{I_3} & 0 & 0 & 0 & 0 & 0 \\ \frac{I_g}{I_1} & \frac{I_g}{I_2} & \frac{I_g}{I_3} & 0 & 0 & 0 & 0 & 0 \\ 0 & 0 & 0 & 1 & 0 & 0 & 0 & 0 \\ 0 & 0 & 0 & 0 & 1 & 0 & 0 & 0 \\ \frac{1}{8}\frac{I_g^2}{I_1 I_3} & \frac{1}{2}\frac{I_g}{I_2} & 0 & \frac{1}{2} & \frac{1}{8}\frac{I_g}{I_3} & \frac{1}{4}\frac{(I_1-I_2)I_g^2}{I_1 I_2 I_3} & \frac{1}{16}\frac{(I_3-I_1)I_g^3}{I_1 I_2 I_3^2} & \frac{(I_2-I_3)I_g}{I_2 I_3} \\ \frac{1}{2}\frac{I_g}{I_1} & \frac{1}{8}\frac{I_g^2}{I_2 I_3} & 0 & \frac{1}{8}\frac{I_g}{I_3} & \frac{1}{2} & \frac{1}{4}\frac{(I_1-I_2)I_g^2}{I_1 I_2 I_3} & \frac{(I_3-I_1)I_g}{I_1 I_3} & \frac{1}{16}\frac{(I_2-I_3)I_g^3}{I_1 I_2 I_3^2} \\ \frac{1}{2}\frac{I_g}{I_1} & \frac{1}{2}\frac{I_g}{I_2} & 0 & \frac{1}{2} & \frac{1}{2} & \frac{(I_1-I_2)I_g}{I_1 I_2} & \frac{1}{4}\frac{(I_3-I_1)I_g^2}{I_1 I_2 I_3} & \frac{1}{4}\frac{(I_2-I_3)I_g^2}{I_1 I_2 I_3} \\ \frac{I_g}{I_1} & \frac{1}{8}\frac{I_g^3}{I_2^2 I_3} & \frac{I_g}{I_3} & \frac{1}{8}\frac{I_g^2}{I_2 I_3} & \frac{1}{2}\frac{I_g}{I_2} & \frac{1}{4}\frac{(I_1-I_2)I_g^3}{I_1 I_2^2 I_3} & \frac{(I_3-I_1)I_g}{I_1 I_2 I_3} & \frac{1}{16}\frac{(I_2-I_3)I_g^4}{I_1 I_2^2 I_3^2} \\ \frac{1}{8}\frac{I_g^3}{I_1^2 I_3} & \frac{I_g}{I_2} & \frac{I_g}{I_3} & \frac{1}{2}\frac{I_g}{I_1} & \frac{1}{8}\frac{I_g^2}{I_1 I_3} & \frac{1}{4}\frac{(I_1-I_2)I_g^3}{I_1^2 I_2 I_3} & \frac{1}{16}\frac{(I_3-I_1)I_g^4}{I_1^2 I_2 I_3^2} & \frac{(I_2-I_3)I_g^2}{I_1 I_2 I_3} \end{pmatrix}, \tag{A.69}$$

and where the $\mathbf{C}$ matrix is

$$\mathbf{C} = \omega_g \begin{pmatrix} 0 & 0 \\ 0 & 0 \\ 0 & 0 \\ 0 & 0 \\ 0 & 0 \\ \frac{1}{16}\frac{I_g^2}{I_2 I_3} & 1 \\ 1 & \frac{1}{16}\frac{I_g^2}{I_1 I_3} \\ \frac{1}{4}\frac{I_g}{I_2} & \frac{1}{4}\frac{I_g}{I_1} \\ 2 & \frac{1}{16}\frac{I_g^3}{I_1 I_2 I_3} \\ \frac{1}{16}\frac{I_g^3}{I_1 I_2 I_3} & 2 \end{pmatrix}. \tag{A.70}$$

Equations (A.59), (A.60), (A.61), (A.62), (A.63), (A.64), (A.65), (A.66), (A.67), (A.68) constitute the state space model given in the text. The states are contained in the vector $\mathbf{x}$, where

$$\mathbf{x} = [\psi\ \theta\ \phi\ \sigma_a\ \sigma_b\ \nu_1\ \nu_2\ \nu_3\ \nu_a\ \nu_b]^T\ . \tag{A.71}$$

In this case, of the 18 equations needed to describe the full state of the satellite and gyroscopes, there are eight holonomic constraints, leading to ten equations of motion. The ten equations are further constrained by three non-holonomic constraints, namely, the three equations that express conservation of angular momentum.

For the simulation, it is convenient to express the state-space model as

$$\dot{\mathbf{x}} = \mathbf{A}\left(\sigma_a,\, \sigma_b\right) \begin{bmatrix} \nu_1 \\ \nu_2 \\ \nu_3 \\ \nu_a \\ \nu_b \\ \nu_1\nu_2 \\ \nu_1\nu_3 \\ \nu_2\nu_3 \end{bmatrix} + \mathbf{B}\left(\sigma_a,\, \sigma_b\right) \begin{bmatrix} u_a \\ u_b \end{bmatrix}, \tag{A.72}$$

where $\mathbf{A}$ is a (10×8) array containing the constants in the Ω matrix and the pertinent trigonometric functions of σ_a and σ_b, and where $\mathbf{B}$ is a (10×2) array, likewise containing the $\mathbf{C}$ matrix of constants and the pertinent trigonometric functions of σ_a and σ_b. Note that the system can be written

$$\dot{\mathbf{x}} = \mathbf{f}\left(\mathbf{x}\right) + \sum_k u_k\, \mathbf{g}_k\ . \tag{A.73}$$

References

[1] W. Chow. Über System von Linearen Partiellen Differentialgleichungen ester Ordinung. *Math. Ann.*, 117:98–105, 1939.

[2] K. Chen. Integration of paths, geometric invariants and a generalized Baker-Hausdorff formula. *Ann. Math.*, 65:163–178, 1957.

[3] R. Brockett. Volterra series and geometric control theory. *Automatica*, 12:167–176, 1976.

[4] A. Bloch. Estimation, principal components and Hamiltonian systems. *Systems & Control Letters*, 6:103–108, 1985.

[5] H. Hermes. Control systems which generate decomposable Lie algebras. *J. Diff. Eq.*, 44:166–187, 1982.

[6] H. Sussmann. Lie brackets, real analyticity and geometric control. In Brockett et al. [43], pages 1–116.

[7] V. Jurdjevic. Polynomial control systems. *Proc. 22nd IEEE CDC*, pages 904–906, 1983.

[8] H. Hermes. *On the accessibility problem in control theory*, pages 325–332. International Symposium on Nonlinear Differential Equations and Nonlinear Mechanics. Academic Press, New York, 1951.

[9] H. Sussmann and V. Jurdjevic. Controllability of nonlinear systems. *J. Diff. Eq.*, 12:95–116, 1972.

[10] H. Sussmann. A general theorem on local controllability. *SIAM J. Contr. and Opt.*, 25:158–194, 1987.

[11] R. Murray, Z. Li, and S. Sastry. *A Mathematical Introduction to Robotic Manipulation.* CRC Press, Boca Raton, Florida, 1994.

[12] Z. Li and J. Canny, editors. *Nonholonomic Motion Planning.* Kluwer, Boston, 1993.

[13] A. Isidori. *Nonlinear Control Systems.* Springer-Verlag, London, third edition, 1995.

[14] A. Blaquiere, S. Diner, and G. Lochak, editors. *Proc. Fourth International Seminar on Mathematical Theory of Dynamical Systems and Microphysics, Udine*, New York, September 4-13, 1985 1987. Springer-Verlag.

[15] A. Blaquiere, editor. *Proc. Bellman Continuum Workshop, Sophia Antipolis*, New York, June 13-14, 1988 1989. Springer-Verlag.

[16] A. Butkovskiy and Y. Samoilenko. *Control of Quantum-Mechanical Processes and Systems.* Kluwer Academic, Dordrecht, 1990.

[17] V. Ramakrishna, M. Salapaka, M. Dahleh, H. Rabitz, and A. Peirce. Controllability of molecular systems. *Phys. Rev. A*, 51:960–966, 1995.

[18] W. Warren, H. Rabitz, and M. Dahleh. Coherent control of quantum dynamics: the dream is alive. *Science*, 259:1581–1589, 1993.

[19] M. Dahleh, A. Peirce, and H. Rabitz. Optimal control of uncertain quantum systems. *Phys. Rev. A*, 42:1065–1079, 1990.

[20] A. Peirce, M. Dahleh, and H. Rabitz. Optimal control of quantum-mechanical systems: existence, numerical approximation, and applications. *Phys. Rev. A*, 37:4950–4964, 1988.

[21] J. Waugh. *Advances in Magnetic Resonance.* Academic, New York, 1965.

[22] H. Goldstein. *Classical Mechanics.* Addison-Wesley, Cambridge (MA), 1950.

[23] D. Luenberger. *Introduction to Dynamic Systems: Theory, Models, and Applications.* Wiley, New York, 1979.

[24] G. Lafferriere. A general strategy for computing steering controls of systems without drift. *IEEE Decision and Control*, 2:1115–1120, 1991.

[25] H. Nijmeijer and A. Van der Schaft. *Nonlinear Dynamical Control Systems.* Springer-Verlag, New York, 1990.

[26] R. Brockett. Nonlinear systems and differential geometry. *Proc. of the IEEE*, 64:61–72, 1976.

[27] R. Penrose and W. Rindler. *Spinors and Space-time.* Cambridge University Press, Cambridge, 1984.

[28] A. Bloch, P. Krishnaprasad, J. Marsden, and G. Sanchez de Alvarez. Stabilization of rigid body dynamics by internal and external torques. *Automatica*, 28:745–756, 1992.

[29] J. Wen. The attitude control problem. *IEEE Trans. Automatic Control*, 36:1148–1162, 1991.

[30] P. Crouch. Spacecraft attitude control and stabilization: Applications of geometric control theory to rigid body models. *IEEE Trans. Automatic Control*, 29:321–331, 1984.

[31] C. Byrnes and A. Isidori. On the attitude stabilization of rigid spacecraft. *Automatica*, 27:87–95, 1991.

[32] T. Dwyer. Exact nonlinear control of spacecraft slewing maneuvers with internal momentum transfer. *J. Guidance, Control, and Dynamics*, 9:240–247, 1986.

[33] S. Vadali. Variable-structure control of spacecraft large-angle maneuvers. *J. Guidance, Control, and Dynamics*, 9:235–239, 1986.

[34] H. Krishnan, M. Reyhanoglu, and H. McClamroch. Attitude stabilization of a rigid spacecraft using two control torques: A nonlinear control approach based on the spacecraft attitude dynamics. *Automatica*, 30:1023–1027, 1994.

[35] G. Margulies and J. Aubrun. Geometric theory of single-gimbal control moment gyro systems. *J. Astronautical Sciences*, 26:159–191, 1978.

[36] H. Wiseman and G. Milburn. Quantum theory of optical feedback via homodyne detection. *Phys. Rev. Lett.*, 70:548–551, 1993.

[37] G. Huang, T. Tarn, and J. Clark. On the controllability of quantum-mechanical systems. *J. Math. Phys.*, 24:2608–2618, 1983.

[38] H. Ezawa and Y. Murayama, editors. *Quantum Control and Measurement.* North-Holland, Amsterdam, 1993.

[39] V. Ramakrishna, M. Salapaka, M. Dahleh, H. Rabitz, and A. Peirce. Controllability of molecular systems. *Phys. Rev. A*, 51:960–966, 1995.

[40] H. Wiseman and G. Milburn. Squeezing via feedback. *Phys. Rev. A*, 49:1350–1366, 1994.

[41] H. Wiseman. Quantum theory of continuous feedback. *Phys. Rev. A*, 49:2133–2150, 1994.

[42] M. Keller and G. Mahler. Nanostructures, entanglement and the physics of quantum control. *J. Mod. Opt.*, 41:2537–2555, 1994.

[43] R. Brockett, R. Millman, and H. Sussmann, editors. *Differential Geometric Control Theory.* Birkhauser, Boston, 1983.

[44] R. Judson and H. Rabitz. Teaching lasers to control molecules. *Phys. Rev. Lett.*, 68:1500–1503, 1992.

[45] C. Monroe, D. Meekhof, B. King, W. Itano, and D. Wineland. Demonstration of a fundamental quantum logic gate. *Phys. Rev. Lett.*, 75:4714–4717, 1995.

[46] C. Chiu, E. Sudarshan, and B. Misra. Time evolution of unstable quantum states and a resolution of Zeno's paradox. *Phys. Rev. D*, 16:520–529, 1977.

[47] A. Peres. Zeno paradox in quantum theory. *Am. J. Phys.*, 48:931–932, 1980.

[48] V. Braginsky, Y. Yorontsov, and K. Thorne. Quantum nondemolition measurements. *Science*, 209:547–557, 1980.

[49] C. Caves, K. Thorne, R. Drever, V. Sandberg, and M. Zimmerman. On the measurement of a weak classical force coupled to a quantum mechanical oscillator. *Rev. Mod. Phys.*, 52:341–392, 1980.

[50] D. DiVincenzo. Quantum computation. *Science*, 270:255–261, 1995.

[51] S. Lloyd. Quantum-mechanical computers. *Sci. Am.*, 273:44–50, 1995.

[52] S. Lloyd. A potentially realizable quantum computer. *Science*, 261:1569–1571, 1993.

[53] R. Landauer. Dissipation and noise immunity in computation and communication. *Nature*, 335:779–784, 1988.

[54] R. Landauer. The physical nature of information. *Phys. Lett. A*, 217:188–193, 1996.

[55] D. Cory, A. Fahmi, and T. Havel. Ensemble quantum computing by nuclear magnetic resonance spectroscopy. *Proc. Natl. Acad. Sci.*, 94:1634–1639, 1997.

[56] C. Slichter. *Principles of Magnetic Resonance.* Springer-Verlag, New York, 1990.

[57] O. Ernst, G. Bodenhausen, and A. Wokaun. *Principles of Nuclear Magnetic Resonance in One and Two Dimensions.* Oxford University Press, Oxford, 1987.

[58] N. Gershenfeld and I. Chuang. Bulk spin-resonance quantum computation. *Science*, 275:350–356, 1997.

[59] R. Feynman. Quantum mechanical computers. *Opt. News*, 11:11–20, 1985.

[60] A. Barenco, D. Deutsch, and A. Ekert. Conditional quantum dynamics and logic gates. *Phys. Rev. Lett.*, 74:4083–4086, 1995.

[61] M. Zukowski, A. Zeilinger, M. Horne, and A. Ekert. "Event-ready detectors": Bell experiment via enganglement swapping. *Phys. Rev. Lett.*, 71:4287–4290, 1993.

[62] W. Wootters and W. Zurek. A single quantum cannot be cloned. *Nature*, 299:802–803, 1982.

[63] D. Dieks. Communication by EPR devices. *Phys. Lett.*, 92A:271–272, 1982.

[64] A. Einstein, B. Podolsky, and N. Rosen. Can quantum-mechanical description of reality be considered complete? *Phys. Rev.*, 47:777–780, 1935.

[65] D. Bohm. *Quantum Theory.* Prentice-Hall, Englewood Cliffs, New Jersey, 1951.

[66] J. Bell. On the Einstein Podolsky Rosen paradox. *Physics*, 1:195–200, 1964.

[67] C. Bennett, D. DiVincenzo, J. Smolin, and W. Wootters. Mixed-state entanglement and quantum error correction. *Phys. Rev. A*, 54:3824–3851, 1996.

[68] J. Schlienz and G. Mahler. Description of entanglement. *Phys. Rev. A*, 52:4396–4404, 1995.

[69] C. Bennett. Quantum information and computation. *Physics Today*, 48:24–30, 1995.

[70] P. Shor. Scheme for reducing decoherence in quantum computer memory. *Phys. Rev. A*, 52:R2493–R2496, 1995.

[71] A. Calderbank and P. Shor. Good quantum error-correcting codes exist. *Phys. Rev. A*, 54:1098–1105, 1996.

[72] A. Steane. Error-correcting codes in quantum theory. *Phys. Rev. Lett.*, 77:793–797, 1996.

[73] R. Laflamme, C. Miquel, J. Paz, and W. Zurek. Perfect quantum error correcting code. *Phys. Rev. Lett.*, 77:198–201, 1996.

[74] D. Cory, M. Price, and T. Havel. Nuclear magnetic resonance: an experimentally accessible paradigm for quantum computing. *Physica D*, 120:82–101, 1998.

[75] D. Cory, A. Fahmy, and T. Havel. Nuclear magnetic resonance spectroscopy: An experimentally accessible paradigm for quantum computing. In T. Toffoli, M. Biafore, and J. Leão, editors, *PhysComp96*, pages 87–91. Proc. of the Fourth Workshop on Physics and Computation, New England Complex Systems Institute, 1996.

[76] S. Lloyd. Quantum controllers for quantum systems. quant-ph/9703042, 1997.

[77] S. Somaroo, D. Cory, and T. Havel. Expressing the operations of quantum computing in multiparticle geometric algebra. *Phys. Rev. A*, 240:1–7, 1998.

[78] S. Lloyd and J. Slotine. Analog quantum error correction. *Phys. Rev. Lett.*, 80:4088–4091, 1998.

[79] D. Bohm. A suggested interpretation of the quantum theory in terms of "hidden" variables, i and ii. *Phys. Rev.*, 85:166–179, 1952.

[80] J. Bell. On the problem of hidden variables in quantum mechanics. *Rev. Mod. Phys.*, 38:447–452, 1966.

[81] H. Clauser, M. Horne, R. Holt, and A. Shimony. Proposed experiment to test local hidden-variable theories. *Phys. Rev. Lett.*, 23:880–884, 1969.

[82] P. Eberhard. Bell's theorem without hidden variables. *Nuovo Cimento*, 38B:75–80, 1977.

[83] P. Eberhard. Bell's theorem and the different concepts of locality. *Nuovo Cimento*, 46B:392–419, 1978.

[84] D. Greenberger, M. Horne, A. Shimony, and A. Zeilinger. Bell's theorem without inequalities. *Am. J. Phys.*, 58:1131–1143, 1990.

[85] S. Freedman and J. Clauser. Experimental test of local hidden-variable theories. *Phys. Rev. Lett.*, 28:938–941, 1972.

[86] J. Clauser. Measurement of the circular-polarization correlation in photons from an atomic cascade. *Nuovo Cimento*, 33B:740–746, 1976.

[87] E. Fry and R. Thompson. Experimental test of local hidden-variable theories. *Phys. Rev. Lett.*, 37:465–468, 1976.

[88] A. Aspect, P. Grangier, and G. Roger. Experimental tests of realistic local theories via Bell's theorem. *Phys. Rev. Lett.*, 47:460–463, 1981.

[89] A. Aspect, P. Grangier, and G. Roger. Experimental realization of Einstein-Podolsky-Rosen-Bohm gedankenexperiment: a new violation of Bell's inequalities. *Phys. Rev. Lett.*, 49:91–94, 1982.

[90] A. Aspect, J. Dalibard, and G. Roger. Experimental test of bell's inequalities using time-varying analyzers. *Phys. Rev. Lett.*, 49:1804–1807, 1982.

[91] W. Perrie, A. Duncan, H. Beyer, and H. Kleinpoppen. Polarization correlation of the two photons emitted by metastable deuterium: a test of Bell's inequality. *Phys. Rev. Lett.*, 54:1790–1793, 1985.

[92] M. Lamehi-Rachti and W. Mittig. Quantum mechanics and hidden variables: a test of Bell's inequality by the measurement of the spin correlation in low-energy proton-proton scattering. *Phys. Rev. D*, 14:2543–2555, 1976.

[93] L. Kasday, J. Ullman, and C. Wu. Angular correlation of Compton-scattered annihilation photons and hidden variables. *Nuovo Cimento*, 25B:633–661, 1975.

[94] A. Wilson, J. Lowe, and D. Butt. Measurement of the relative planes of polarization of annihilation quanta as a function of separation distance. *J. Phys. G*, 2(9):613–624, 1976.

[95] M. Bruno, M. d'Agostino, and C. Maroni. Measurement of linear polarization of positron annihilation photons. *Nuovo Cimento*, 40B:143–152, 1977.

[96] N. Mermin. Quantum mysteries revisited. *Am. J. Phys.*, 58:731–734, 1990.

[97] D. Bouwmeester, J. Pan, M. Daniell, H. Weinfurter, and A. Zeilinger. Observation of three-photon Greenberger-Horne-Zeilinger entanglement. *Phys. Rev. Lett.*, 82:1345–1349, 1999.

[98] S. Lloyd. Microscopic analogs of the Greenberger-Horne-Zeilinger experiment. *Phys. Rev. A*, 57:R1473–R1476, 1998.

[99] R. Laflamme, E. Knill, W. Zurek, P. Catasti, and S. Mariappan. NMR GHZ. *Phil. Trans. Roy. Soc. Lond.*, A356:1941–1948, 1998.

[100] A. Peres. *Quantum Theory: Concepts and Methods.* Kluwer Academic, Dordrecht, 1993.

[101] S. Braunstein, C. Caves, R. Jozsa, N. Linden, S. Popescu, and R. Schack. Separability of very noisy mixes states and implications for NMR quantum computing. quant-ph/9810082, 1998.

5930-36